12-2010

ANALYSIS OF β8 INTEGRIN IN NEUROGENESIS AND NEUROVASCULAR HOMEOSTASIS

Aaron K. Mobley

ANALYSIS OF β8 INTEGRIN IN NEUROGENESIS AND NEUROVASCULAR HOMEOSTASIS

By

Aaron Kyle Mobley, B.S.

APPROVED:

_____
Joseph H. McCarty, Ph.D.
Supervisory Professor

_____
Gary E. Gallick, Ph.D.

_____
Oliver Bögler, Ph.D.

_____
Jaroslaw Aronowski, Ph.D.

_____
Vidya Gopalakrishnan, Ph.D.

APPROVED:

_____
Dean, The University of Texas
Graduate School of Biomedical Sciences

ANALYSIS OF β8 INTEGRIN IN NEUROGENESIS AND NEUROVASCULAR HOMEOSTASIS

A

DISSERTATION

Presented to the Faculty of

The University of Texas

Health Science Center at Houston

and

The University of Texas

M.D. Anderson Cancer Center

Graduate School of Biomedical Sciences

In Partial Fulfillment

of the Requirements

for the Degree of

DOCTOR OF PHILOSOPHY

by

Aaron Kyle Mobley, BS

Houston, Texas

December, 2010

DEDICATION

I would like to dedicate this dissertation
to my parents, Charles and Vicki Mobley,
who have always stood behind me in my endeavors,
both educational and personal, and knew I would succeed.

To my sisters; Shannon, Tyffanne and Amber,
and my brother, Ian
for their friendship and support throughout the years
from childhood to adulthood.

ACKNOWLEDGEMENTS

It is with immense gratitude that I acknowledge my mentor, Dr. Joseph McCarty. His support throughout my PhD training has helped me to become a better scientist. His guidance has helped me to develop better critical thinking, technical, scientific presentation and writing skills and for that I thank you.

I would also like to thank the many people here in Houston who have helped me throughout my career as a graduate student. First, I thank all the people of the Cancer Biology Program, the Graduate School of Biomedical Sciences for their guidance along the way. Also, the Smith Research Foundation for their funding during my time at MD Anderson.

I am very thankful for the members of my advisory, examining and supervisory committees for offering their advice to help me to create a focused project and keep me moving along in my research. Thank you to: Drs. Gary Gallick, Jaroslaw Aronowski, Vidya Gopalakrishnan, Oliver Bogler, Dennis Hughes and Karen Hirschi, I greatly appreciate you taking time from your busy schedules to advance my scientific development. Additionally, I would like to thank Mr. Joseph Douglas and Mrs. Donna Reynolds for their expertise in immunohistochemistry. Without their insight and troubleshooting efforts I could not have completed many of the experiments in this dissertation. I also thank Mr. Kenneth Dunner, for his help with all electron microscopy experiments.

I am also very thankful to the members of the McCarty lab both past and present including: Mohammad Hossain, Steve Reyes, Jae-kyung Shin, Jessica Jung and Drs. Brent Hayek, Adam Hsu and Roman Schinder for their support in the lab. I would also like to thank everyone in the Cancer Biology Department and the Smith Research Building.

A very special thanks goes to Jeremy Tchaicha, who has been with me throughout my entire graduate school career. Thank you for always being there for me when I needed help in the lab with experiments or with thoughts and ideas about my project. I also thank you for being there for me in good times and bad times in my personal life, you will never know how grateful I am to you for that.

ANALYSIS OF β8 INTEGRIN IN NEUROGENESIS AND NEUROVASCULAR HOMEOSTASIS

Publication No. _____

Aaron Kyle Mobley, BS

Supervisory Professor: Joseph McCarty, PhD

Neurogenesis in the adult mouse brain occurs within the subventricular zone (SVZ) of the lateral ventricle. In the SVZ, neural stem cells (NSC) reside in a specialized microenvironment, or vascular niche, consisting of blood vessels and their basement membranes. Most NSCs in the SVZ differentiate into progenitor cells, which further differentiate to generate neuroblasts, which then migrate from the SVZ to the olfactory bulbs (OB) along the rostral migratory stream (RMS). ECM-mediated adhesion and signaling within the vascular niche likely contribute to proper NSC self-renewal, survival, differentiation and neuroblast motility. The mechanisms that control these events are poorly understood. Previous studies from our group and others have shown that loss of the ECM receptor, αvβ8 integrin, in NSCs in the embryonic mouse brain leads to severe developmental vascular defects and premature death. Here, the functions of αvβ8 integrin in the adult brain have been examined using mice that have been genetically manipulated to lack a functional β8 integrin gene. This study reveals that loss of β8 integrin leads to

widespread defects in homeostasis of the neurovascular unit, including increased intracerebral blood vessels with enhanced perivascular astrogliosis. Additionally, β8 integrin dependent defects in NSC proliferation, survival, and differentiation, as well as neuroblast migration in the RMS were observed both *in vivo* and *in vitro*. The defects correlated, in part, with diminished integrin-mediated activation of TGFβ, an ECM ligand of β8 integrin. Collectively, these data identify important adhesion and signaling functions for β8 integrin in the regulation of neural stem and progenitor cells in the SVZ as well as in neuroblast migration along the RMS in the adult brain.

Table of Contents

List of Figures

CHAPTER 1: Introduction and Background

Chapter 3: Specific Aim 1

LIST OF TABLES

List of Abbreviations

CNS- Central Nervous System

NVU- Neurovascular Unit

BBB- Blood Brain Barrier

ECM- Extracellular Matrix

GFAP- Glial Fibrillary Acidic Protein

NSC- Neural Stem Cells

SGZ- Subgranular Zone

DG- Dentate Gyrus

PSA-NCAM- Polysialated Neural Cell Adhesion Molecule

SVZ- Subventricular Zone

DCX- Doublecortin

RMS- Rostral Migratory Stream

OB- Olfactory Bulb

LAP- Latent Associated Peptide

CB-Cerebellum

CHAPTER 1:

Introduction and Background

The Neurovascular Unit

Within the vertebrate central nervous system (CNS) there are many different cell types including neuronal and glial cells, as well as the vascular endothelial cells and pericytes that comprise the brain vasculature. Taken together, these cells and their basement membranes make up the neurovascular unit (NVU) (1) (Figure 1). The dynamic interactions between the cells of the NVU and the extracellular matrix proteins within their basement membranes regulate CNS development as well as many homeostatic events, such as neurogenesis, blood brain barrier permeability, cerebral blood flow, and synaptic activity (2-4).

Intimate associations between neural cells and vascular cells begin in the early stages of embryonic brain development. Angiogenic blood vessels migrate into the embryonic brain along a scaffold of neuroepithelial and radial glial cells (5, 6). In the neonatal CNS, blood vessel-derived cues regulate differentiation of glial precursors in the cerebral cortex (7, 8). Additionally, in the adult brain, interactions at the NVU are necessary for proper neurogenesis (1). Neural stem cells are closely associated with blood vessels, and their association regulates stem cell fate and behavior (9-11). Furthermore, soluble growth factors from NSCs and blood vessels influence neural and vascular behaviors in the avian higher vocal center (12). CNS

neural cells provide signals that influence blood vessel growth, survival and blood-brain-barrier (BBB) integrity (13, 14).

Abnormal interactions within the NVU can lead to several CNS pathologies, including birth defects, Alzheimer's disease, stroke and cancer (15). An ischemic or hemorrhagic insult during brain development can lead to porencephaly, hydrocephaly, mental retardation and cerebral palsy (16, 17). Dementia and Alzheimer's disease studies have shown impaired amyloid-beta clearance through disruption of LRP1 functions, as well as increased influx into the brain through the RAGE receptor, both of which direct amyloid-beta transport across the BBB (18). Other studies have shown that endothelial cells can directly release neurotoxins, including apolipoprotein-E and activated thrombin, that kill neurons (19, 20). Disruption of the neurovascular unit and the BBB has been implicated in stroke, characterized by hemorrhage and vascular occlusion. Upon ischemic infarct, the integrity of the basement membrane is compromised and loss of matrix-associated receptors has also been noted (21, 22). Furthermore, brain cancers are characterized by blood vessels that exhibit abnormal NVU cytoarchitecture and BBB functions. Also, brain tumor-initiating cells lie within a neurovascular niche that promotes tumor growth and invasion (23-25).

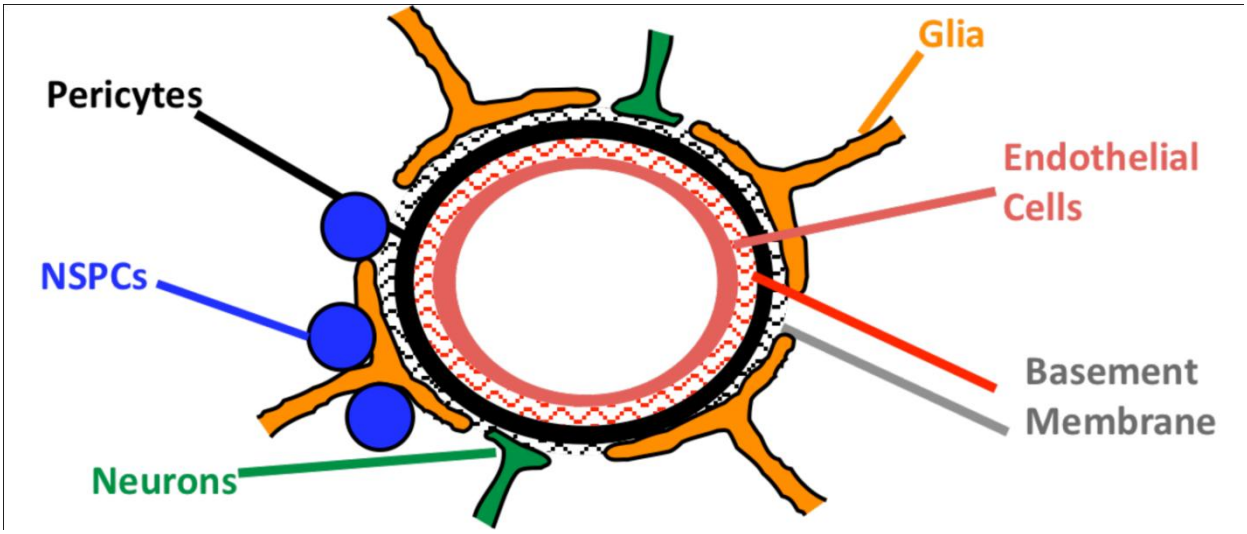

Figure 1: The Neurovascular Unit

The vasculature in the CNS shows unique cellular associations. Astrocytic and neuronal endfeet closely associate with the cerebral blood vessels through direct contact with the basement membrane secreted by the vascular endothelial cells and pericytes. In specific regions of the brain, neural stem and progenitor cells are intimately associated with the vasculature as well. The interactions between these cell types regulate many functions within the CNS. This figure was adapted from McCarty JH, 2005 (1).

Neural Stem Cells

Stem cells are defined by their specialized ability to self renew, produce progenitor cells and differentiate into multiple lineages (26). These characteristics of stem cells must be tightly regulated for proper development and organization in the tissue. It is clear that the specialized nature of stem cells is dependent upon signals from the surrounding cells, basement membrane and extracellular matrix (ECM) proteins. This dependence upon signals from the surrounding microenvironment, originally discovered in hematopoietic stem cells, has led these areas to be termed a ‘stem cell niche’. Schofield et al. (26) originally described a stem cell niche with the following characteristics: 1) stem cells held in a fixed anatomical location; 2) control of the proliferation and self renewal of the stem cells; 3) restrictions on stem cell differentiation; and 4) maintains a fixed number of stem cells in the niche (26).

During brain development, neuroepithelial cells found in the ventricular zone are responsible for generating most neuronal and glial cells (27). Upon thickening of the developing brain, some neuroepithelial cells elongate and change into radial glia cells. Radial glia are thought to be glial cell progenitors because they express many glial markers including, glial fibrillary acidic protein (GFAP) and the glutamate transporter GLAST (27, 28). Radial glia cell bodies remain in the ventricular zone and extend long processes to the pial surface of the brain and continue to maintain contact with both the ventricular and pial surfaces throughout development (27). The radial glia cells act as a scaffold upon which differentiating neurons migrate. Radial glia cell processes continue to extend upon expansion of the cortex to maintain direct contact with the pial surface. After neuronal migration is complete, a

sub-population of radial glia cells convert into SVZ astrocytes, and remain in an undifferentiated state within the adult brain (5, 29).

The adult CNS maintains two regions where neural stem cells (NSCs) reside; the subgranular zone (SGZ) of the hippocampal dentate gyrus and the subventricular zone (SVZ) of the lateral ventricle, both of which generate neurons and glia. The stem cells found in these regions show remarkable similarities to astrocytes, including expression of GFAP, a widely used astrocyte marker (30). Both of these locations are associated with a specialized neurovascular unit termed the vascular niche (1). Outside of these two regions, neurogenesis is very restricted unless affected by a pathological stimulation. After a pathological stimulation, such as a tumor or stroke, neuroblasts from known neurogenic regions migrate to regions that are normally non-neurogenic (31). While very little is understood about how NSCs adhere and communicate with the ECM components of the neurovascular niche, the identification and organization of the two niches has been studied greatly.

Subgranular Zone of the Dentate Gyrus

New granule neurons for the hippocampal dentate gyrus are generated from within the subgranular zone (SGZ) of the dentate gyrus (DG) (32). The SGZ is a region of the hippocampus found between the dentate gyrus and the hilus. The SGZ is very organized around the vasculature. The SGZ contains several different cells types including specialized astrocytes, which act as the precursors, immature neuronal precursors, termed Type D cells, newly formed neurons and the endothelial cells of the associated vasculature (32). The specialized astrocytes,

termed Type B cells within both neurogenic regions, extend a process spanning from underneath the dentate gyrus to the granule cell layer. Type B cells give rise to Type D cells, neuronal committed progenitor cells that express Poly-Sialated Neural Cell Adhesion Molecule (PSA-NCAM) a marker of neuronal differentiation (9). Type D cells then continue to differentiate into granule neurons (type G cells) (Figure 2B). The newly formed granule neurons migrate a very short distance to the granule cell layer and extend an axon into the CA3 region of the hippocampus (9).

New neurons have been shown to be involved in learning and memory in the hippocampus. Animal studies using mice in enriched environments, where mice are allowed to exercise and play with toys, versus ordinary cages revealed increased neurogenesis as evidenced by increased proliferation of DG cells (33). Many environmental factors have been shown to affect SGZ neurogenesis including stress, seizures and drug abuse (32). In artificially-induced epileptic seizures, mice displayed an increase in hippocampal neurogenesis; however the new neurons were aberrantly incorporated into neuronal networks (34). Studies of prolonged usage of morphine caused a significant reduction in neurogenesis of the rat hippocampus, which may be responsible for cognitive defects in chronic drug users (35).

Subventricular Zone of the Lateral Ventricle

The other neurogenic region in the adult brain, the subventricular zone (SVZ), contains five main cell types: SVZ astrocytes, transit amplifying cells, neuroblasts, vascular endothelial cells, pericytes and ependymal cells (36). Cellular markers and appearance at the ultrastructural level were used to identify these cell types. SVZ astrocytes (type B cells), like the SGZ astrocytes, act as the precursors. B cells express GFAP have light cytoplasm, irregularly shaped nuclei, and extend a single cilium into the ventricle (37). Type B cells show stem cell properties including self-renewal and are multipotential, giving rise to both neurons and glia. Neuroblasts (type A cells) are identified by their dark cytoplasm and elongated nuclei, as well as expression of doublecortin (DCX) and PSA-NCAM (37). Type A cells form chains, which are ensheathed in type B cells (38). Transit amplifying cells (type C cells) are found in clusters around the neuroblasts and are marked by their large, spherical, deeply invaginated nuclei and their high rates of proliferation (37). Ependymal cells are found lining the ventricle and exhibit very light cytoplasm and round nuclei and a lack of proliferation (37) (Figure 2A).

Figure 2: The Adult Neurovascular Niches

In the adult brain there are two main regions of neurogenesis; the subventricular zone (SVZ) of the lateral ventricle and the subgranular zone (SGZ) of the dentate gyrus. **(A)** The subventricular zone has is made up of neuroblasts (type A cells), neuronal progenitors, surrounded by neural stem cells (B cells), and transit amplifying cells (type C cells), which are highly proliferative progenitor cells. These cells are found just beneath the ependymal cell layer (E cells) all of the cell types within the SVZ are very closely associated with a specialized vasculature with areas of direct contact between the NSCs and endothelial basement membrane. **(B)** The SGZ consists of neural stem cells (type B cells) closely associated with the vasculature. NSCs go on to differentiate into immature proliferative cells (type D cells), which further differentiate into granule neurons (type G cells), which integrate into the hippocampal neuron network. **(C)** Neuroblasts from the subventricular zone (SVZ) migrate along a defined pathway termed the rostral migratory stream (RMS) to the olfactory bulb (OB) where they fully differentiate into interneurons. Adapted from Doestch, 2003 (39).

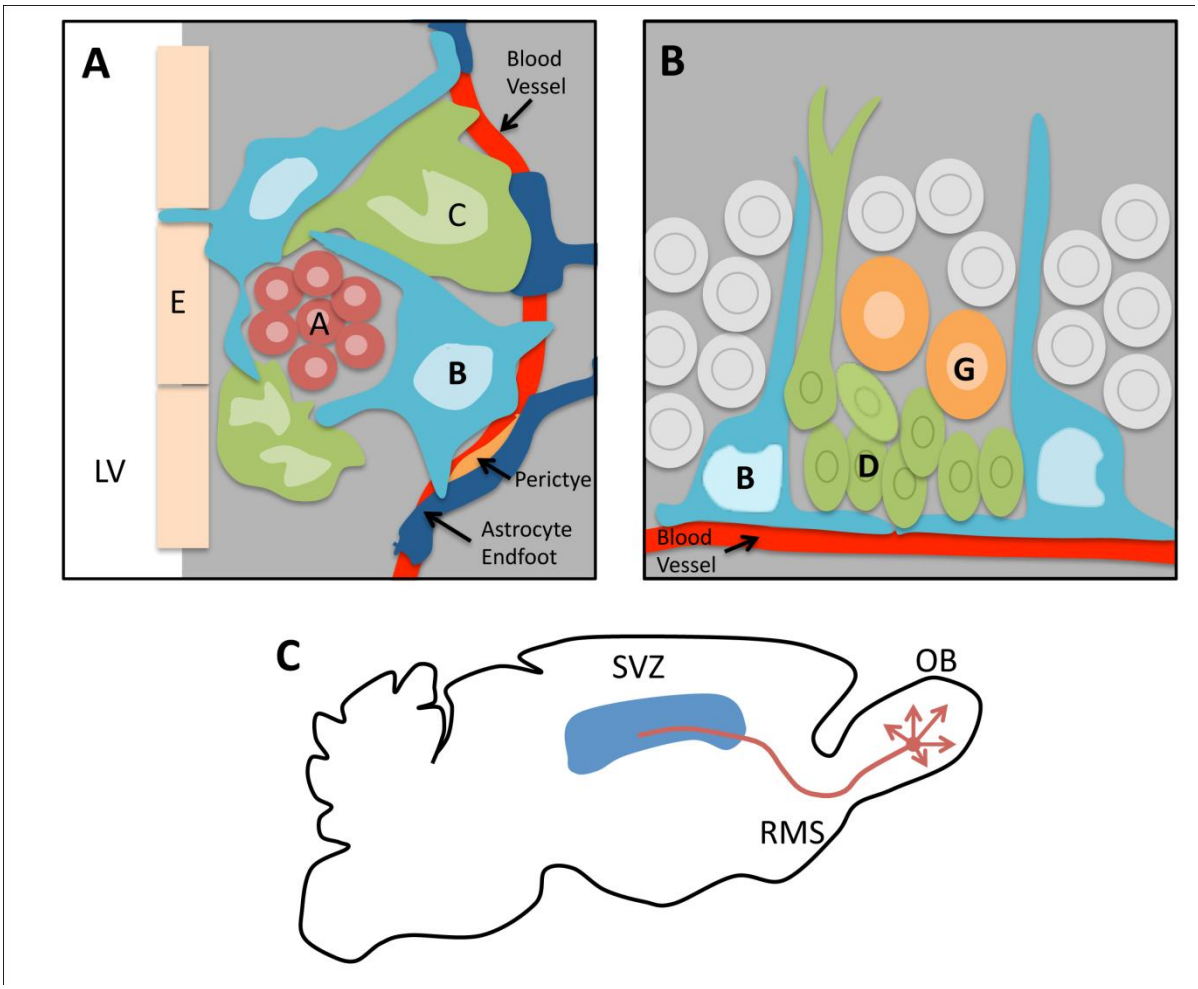
A
Blood
Vessel
C
E
A
B
LV
Pericyte
Astrocyte
Endfoot
B
G
B
D
Blood
Vessel
C
SVZ
OB
RMS

Figure 2

Role of Vasculature in Stem Cell Niche

In the healthy postnatal brain most of the vasculature is quiescent, however, in neurogenic regions there are angiogenic capillaries (40). While it has been noted that NSCs closely associate with the proliferating vasculature, the importance of this association has not been studied until recently (9). In the adult brain there has been a link shown between angiogenesis and neurogenesis. Studies of songbird neurogenesis reveal that upon induction of angiogenesis in the brain, there is increased migration of newly developed neurons in the high vocal center, a neurogenic region in the songbird brain (12). Also, in the mammalian hippocampus, new neurons are generated in close association with angiogenic vessels (9). Furthermore, *in vitro* studies co-culturing endothelial cells and NSCs show that diffusible signals from endothelial cells enhance NSC self-renewal (41).

The SVZ contains a vascular plexus and NSCs and are adjacent to the vessels of this unique plexus (42). Blood vessels and NSCs maintain direct contact within the SVZ at regions of the vessels where there is minimal astrocyte or pericyte coverage and enhanced blood brain barrier permeability (42). This direct association is exclusive to the SVZ and has not been noted elsewhere in the brain including other neurogenic regions (42). NSCs in the SVZ are also affected by circulating diffusible signals from the endothelial cells, to which they have direct access (41). The role of these diffusible molecules as well as adhesive receptors appears to be important for maintaining proper architecture and regulation of the SVZ neurogenic niche.

Neuroblast Migration and the RMS

Cell migration from the SVZ is accomplished by neuroblasts. Cells leaving the SVZ migrate tangentially along a well-defined rostral migratory stream (RMS) toward the olfactory bulb (OB) (Figure 2C). Cells arriving in the OB differentiate into interneurons and integrate into neuronal circuitry. These new neurons are thought to function in odor recognition and short-term odor memory (43). There are four major cell types identified in the RMS; neuroblasts, GFAP-positive astrocytes, microglia and endothelial cells from the vasculature (38). The major cell type is the neuroblast, which forms organized chains that polarize in the direction of migration. Migration of neuroblasts along the RMS is different from migration during development because there are no radial glia or axonal processes upon which the neuroblasts migrate. The other major cell type in the RMS is the astrocyte, which form a tube surrounding the neuroblasts, termed the glial tube, and may act as a scaffold for migration (44). Astrocytes surrounding the neuroblasts maintain coverage from the wall of the lateral ventricle all the way to the core of the OB. The glial tube's function is unknown, but does not appear to be absolutely required for neuroblast migration *in vitro*, however, factors secreted by these cells do show an enhancement of migration (45). Astrocytes may be acting as a boundary for the neuroblasts to migrate within or may physically prevent the neuroblasts from leaving the RMS, or may provide directions for the neuroblasts through growth factor secretion (46). The ECM plays a large role in RMS migration; it is also possible that cues could come from the closely associated vasculature to regulate migration (47, 48). Indeed, blood vessels align parallel to the RMS and are closely associated with

migrating neuroblasts (49). Upon arrival in the OB, neuroblasts migrate radially as individual cells and fully differentiate into granule and glomerular layers as inhibitory interneurons (38, 50).

Integrins

Cells within the neurovascular niche, including NSCs, express varying levels and types of cell surface adhesion molecules, which include many members of the integrin family of proteins (51). Integrins are heterodimeric cell surface receptors and are the primary receptors for cell-cell adhesions and adhesion to ECM ligands (52). The ligand-binding site is found in the head domain of the α subunit of the heterodimer in the extracellular portion of the protein. The cytoplasmic tails of most integrins are short sequences of approximately 50 amino acids (53). While α subunit cytoplasmic tails show great diversity, there is remarkable homology in the β subunits. Most β subunits contain at least one NPXY motif, which is important for its intracellular signaling capabilities (53). Integrin signaling events control multiple cellular activities including proliferation, migration and differentiation (52, 54). Signaling through integrins can take place by two different mechanisms, inside-out or outside-in. Inside-out signaling regulates the integrins affinity for its ligand. Intracellular signaling causes phosphorylation on the cytoplasmic tail of the β subunit, which then allows for ligand binding on the extracellular binding domain. Outside-in signaling starts with ligand binding, causing a conformational change in which the cytoplasmic tails separate, allowing activation of signaling events inside the cell (55).

In vertebrates there are 18 genes encoding α subunits and 8 genes encoding β subunits, which combine to form 24 different αβ heterodimers (Figure 3). Integrins can be divided into several subfamilies based upon their ligand specificity and evolutionary characteristics. These groups include laminin-binding, and RGD recognizing integrins, which are considered ancient and highly conserved throughout all metazoans from sponges to humans (56). The other, more recently evolved groups include collagen binding and leukocyte integrins, which have only been found in chordates and vertebrates, respectively (55).

Laminin binding integrins consist of α1β1, α2β1, α3β1, α6β1, α7β1, and α6β4. This family can be further divided into smaller subgroups based upon where they bind to the laminin molecule. One cluster binds to the long arm of laminin, this group includes α3β1, α6β1 and α7β1. The second, group (α1β1 and α2β1), which contain an I domain, binds to the cross region of laminin (57). RGD recognizing integrins, including α5β1, αvβ1, αvβ3, αvβ5, αvβ6, αvβ8, and αIIbβ3, recognize a tripeptide sequence consisting of the amino acids arginine-glycine-aspartic acid (RGD), which is expressed on the ligands. The RGD sequence is found in a variety of different ECM ligands including; vitronectin, fibronectin, osteopontin, and many others. RGD integrins are expressed on various cell types and are involved in many physiological events including angiogenesis, apoptosis, and bone resorption and they appear to play a major role in development (58).

The collagen binding and leukocyte integrins' α-subunits all share a common I-domain. Collagen binding integrins include α1β1, α2β1, α3β1, α10β1, and α11β1. These integrins recognize a short peptide sequence (GFOGER), similar to the RGD

sequence, which is found in the triple helical collagen-I molecule (59). Functional studies of collagen binding integrins show the involvement of α2β1 integrin in the activation and aggregation of platelets (60). αLβ2, αMβ2, αXβ2, and αDβ2 make up the subgroup of leukocyte integrins. These integrins, all containing the β2 subunit, are involved in immune response. Defects in β2 integrins in humans have been attributed to impaired tissue remodeling, wound healing, as well as increased susceptibility to bacterial infections (61).

Several integrins are expressed in the cells of the neurovascular unit and within the neural stem cell vascular niche. The vascular endothelial cells express α1β1 and α6β1, both laminin receptors. Upon a pathological insult, such as ischemia, the levels of these integrins are dramatically decreased. Astrocytes express several integrins as well, including α6β1 and α6β4 on the endfeet, which directly associate with the vascular basement membrane and regulates astrocyte-ECM adhesion in the NVU. Loss of α6β4 following stroke correlates with increased BBB permeability. Furthermore, αvβ3 integrin is expressed on both the neural and vascular cells of NVU and is greatly upregulated following ischemic stroke. Upon inhibition, using a αvβ3 selective inhibitor, after artificial stroke in a rat middle cerebral artery occlusion (MCAO) model, animals showed decreased BBB breakdown and edema as well as improved neurological function (62). Many integrins are specifically expressed in NSCs as well, including several β1 integrins as well as αvβ5 and αvβ8 integrin (51). β1 integrin has been used as a cell surface marker for isolation and purification of NSCs from the more differentiated

neuroblasts (51). While the expression of many integrins on the surface of NSCs has been noted, their functional role has not been well characterized.

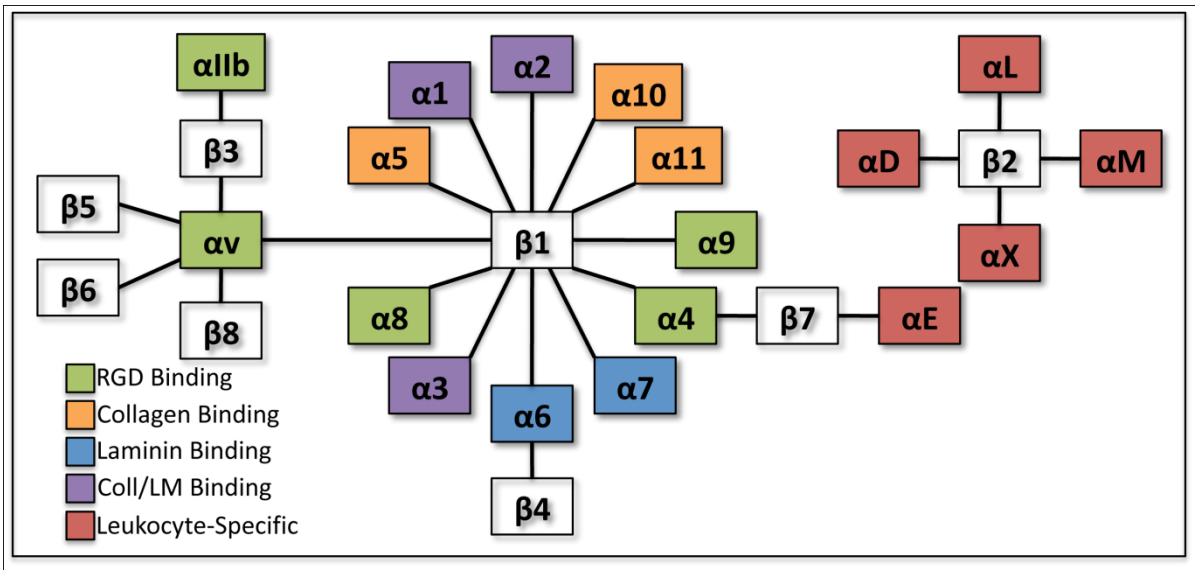

Figure 3: Integrins

In mammals 18 α and 8 β subunits combine to form a possible 24 distinct αβ heterodimers. The individual heterodimers can be classified into four different groups based upon their ligand specificity. Those groups include RGD (green), collagen (orange, purple), and laminin (blue, purple) binding integrins as well as leukocyte specific (red) integrins.

αv Integrin Subfamily

The αv integrin subfamily contains five different heterodimers: αvβ1, αvβ3, αvβ5, αvβ6 and αvβ8. Even though all of these integrins recognize the RGD peptide sequence, they bind to a diverse array of ligands. These integrins are widely expressed throughout the body, however the expression of each is tightly regulated. Developmental expression includes neural crest cells (63), radial glial cells, muscle (64), epithelial (65) and endothelial cells (66). Taken together, the many ligands and tight regulation of expression suggest many roles for αv integrins.

To study the function of integrins *in vivo*, gene knockout mouse models have been created for nearly all of the integrin subunits, including all of the members of the αv subfamily (52). Ablation of the αv integrin gene results in lethality; however, most development progresses almost normally and some mice are born alive. Mice homozygous for the αv null allele die at two different timepoints. The first developmental defect begins between embryonic days 9.5 and 10.5 (E9.5-E10.5), showing delayed growth as well as pericardial edema. The majority of αv null embryos at E10.5 are dead and resorped, while a small percentage appears to be developing normally. The latter population survives through development and results in viable αv null offspring; however, these mice develop intracranial hemorrhage and a cleft palate, which results in lethality shortly after birth. Intracerebral hemorrhage first appears around E12.5 within the ganglionic eminence of the telencephalon (Figure 4A). The hemorrhage spreads to the diencephalon and into the cortical hemispheres as development progresses. Histological examination of αv null mice after E12.5 revealed dilated vessels in the

forebrain as well as cavitation in the ganglionic eminence. Clearly, the αv subfamily of integrins is very important for proper formation of the CNS vasculature (67).

Deletion of the αv gene shows a drastic phenotype, but because all five of the αv binding β-subunits are deleted it is impossible to tell which specific integrin is responsible for the vascular phenotype. Genetic knockout mouse models have been described for all five of the β subunits that associate with αv. Mice genetically null for the β1 subunit, which can bind with αv as well as 11 other α subunits, show a dramatic phenotype as well. These mice develop normally up until the blastocyst stage but die shortly after implantation in the uterus at day E6.5. In the β1 null blastocysts implanted in the uterine wall, there is no indication of the inner cell mass cells, the cells that become the embryo. However, the trophoblast cells, the cells that develop into the placenta, were still present. This suggests that the inner cell mass cells are dying sooner than the trophoblast cells (68). Inactivation of the β3, β5 or β6 integrin genes in mice produce mice that are viable and fertile. β3 null mice develop hemorrhage in the skin and the gastrointestinal tract after birth, these defects have been attributed to β3 integrin's binding with αIIb, as knockout mice for αIIb show an identical phenotype (69, 70). β5 null mice show no obvious developmental defects (71) but exhibit age-related retinal dysfunction (72). β6 integrin, which is expressed only in epithelial cells, shows inflammation in the skin and the lungs upon deletion in mice (73). β8 null mice appear to develop normally until E10.5, after which about half of them exhibit poorly vascularized yolk sacs. Some have no heartbeat, while others show an enlarged pericardiac cavity. The other 50% of β8 null mice appear normal at E10.5. By E11.5 half of the remaining

null mice begin to be absorbed and deteriorate, while the rest of them still appear normal. Interestingly, by E12.5 an intracerebral hemorrhage identical to that seen in the complete αv null model appears and gets progressively worse towards birth (Figure 4B, D). These mice are viable, but die shortly after birth (74). Based on knockout models of all five αv-binding β subunits, the loss of only one integrin, αvβ8, is responsible for the neurovascular defects seen in the brain.

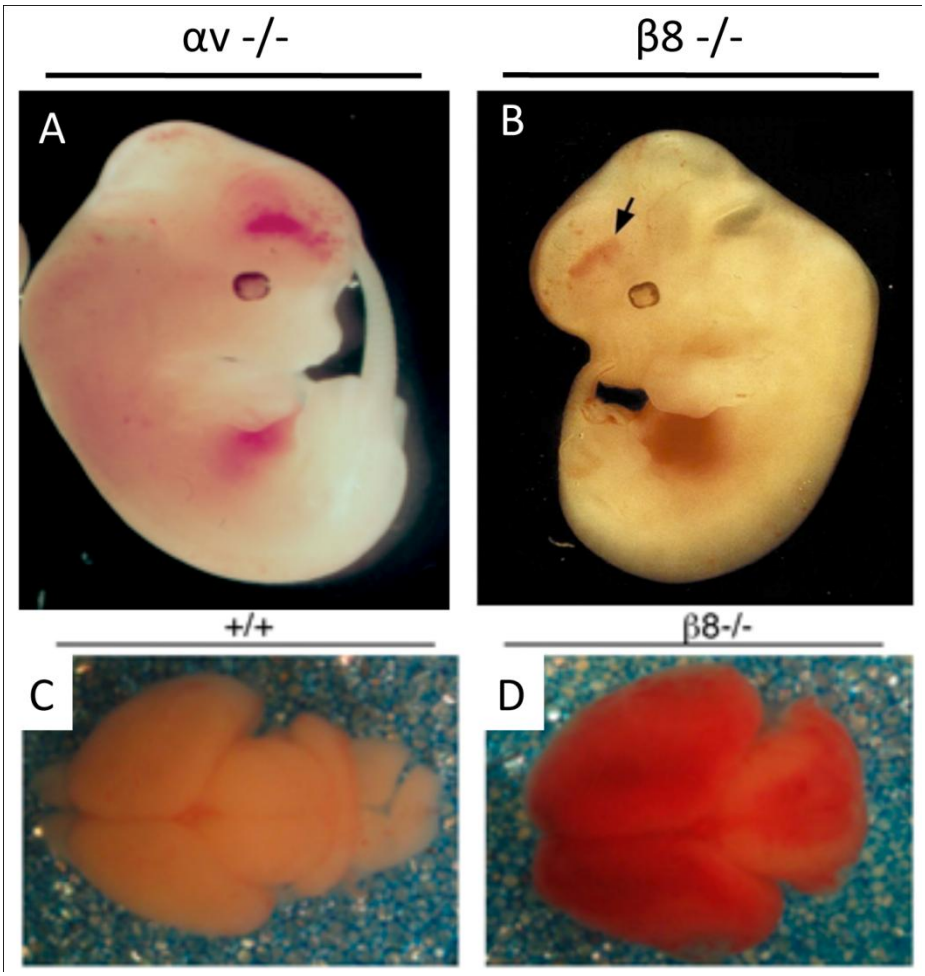

Figure 4: CNS Specific Vascular Pathologies During Development in αv and β8 Knockout Mice.

(A,B) Complete αv or β8 null mice develop intracerebral hemorrhage beginning at embryonic day 12.5 (E12.5). This hemorrhage gets progressively worse towards birth and is readily evident at postnatal day 0 (P0). **(C, D)** Wild type and β8 knockout brains at P0. Notice the severe hemorrhage seen throughout the brain in the β8 knockout.

αvβ8 Integrin

β8 integrin is only known to bind to the αv subunit (75). αvβ8 integrin's expression is very limited. The mRNA for β8 is seen in only the ovary, uterus, kidney, placenta and brain, with the highest levels being seen in the brain, suggesting a brain specific function (75). β8 protein is highly expressed in the brain but in very specific regions. Through immunohistochemical analysis, β8 is highly expressed in the CA3 region, and the molecular and granule layers of the dentate gyrus in the hippocampus. β8 is also expressed mildly in the cerebellum, olfactory bulb and the cerebral cortex (76). The main cell types expressing β8 are neurons and astrocytes, no expression is seen in oligodendrocytes (77).

The β8 cDNA sequence shows divergence from other β integrin subunits. Within the extracellular domain of β8, there is very little conservation with other β subunits, with only 6 of the 56 cysteine residues that are normally conserved (75). Also, the cytoplasmic domain, which is 65 amino acids in length, appears to be unique among β subunits. Conserved sequences in other integrin β subunits are important for mediating cytoskeletal interactions with the signals leading to cell adhesion, and inside out signaling (78). For example, the NPXY tetrapeptide motif, which recruits talin to the β cytoplasmic tails of most integrins, is absent from β8 (79). β8 integrin does not mediate adhesion like the others do, likely due to lack of these conserved regions (75). Yeast two-hybrid technology was used to identify one specific cytoplasmic domain interaction that is unique to β8 integrin, the ability to bind to Band 4.1B, a member of the Band 4.1 protein family. This family of proteins is a member of the FERM domain family, which are recruited for many integrin

signaling events (52). Band 4.1B contains 3 major regions a FERM domain, spectrin/actin binding domain (SABD) and the C-terminal domain (CTD). The interaction between Band 4.1B and β8 integrin was determined to be at the CTD. This interaction is thought to affect either the activation status of β8 integrin or regulate various signaling cascades (79). Extracellular ligands for αvβ8 integrin include vitronectin (80), collagen IV (81), and LAP-TGFβ1 (82, 83) all of which are found associated with the vascular basement membrane.

TGFβ is secreted in an inactive state, bound to the extracellular matrix in a large latent complex, consisting of TGFβ, the latent associated peptide (LAP) and the latent TGFβ binding protein. For bioactiavtion, TGFβ must be liberated from this complex (84). Several different activation methods exist including; proteaslytic cleavage by plasmin (85), MMP2 and MMP9 (86), thrombospondin-1 interacting with LAP portion binding to a short peptide sequence (RFK) (87), and through integrin αvβ6 (88) and αvβ8 (82) binding to a short RGD peptide sequence. Munger and colleagues (89) recently revealed the importance of integrin-mediated activation of TGFβ. Using a mouse knock-in strategy the RGD peptide sequence in the LAP portion of TGFβ1, required for integrin binding and activation, was mutated to an RGE sequence (90). Upon mutation, αvβ6 and αvβ8 were unable to activate TGFβ1 and these mice developed a phenotype including vasculogenic defects and multi-organ nflammation, similar to the complete TGFβ1 knockout mouse model (91). Furthermore, when TGFβ1 RGE/RGE mice were crossed to complete TGFβ3 null mice, they develop intracerebral hemorrhage similar to that seen in complete αv

and β8 null mice (92). These data indicate that αvβ8 integrin-mediated activation of TGFβ is a very important activation method for TGFβ.

Conditional Knockout Strategies

Deletion of αv or β8 integrins in transgenic mice leads to perinatal lethality. Severe intracerebral hemorrhage and hydrocephaly in both models, along with a cleft palate in the αv null mice likely lead to this early death (67, 74). To study the role of αvβ8 integrin specifically in the adult neurovascular unit, the use of conditional cre-lox technology was required to prevent the neonatal lethality. Thus, αv was deleted in nestin positive CNS stem and progenitor cells but not in any other cell types or organs. All of the αv mutant mice generated developed intracerebral hemorrhage that was grossly noticeable at birth. A GFAP-cre transgenic model, deleting αv on astrocytes and neural stem and progenitor cells, revealed intracerebral hemorrhage in the neonatal brain as well. However, in both models, while present, the hemorrhage was much less severe than the hemorrhage observed in the complete αv null mice. Also, the palate developed normally and the conditional mutants survived beyond the perinatal period (93). On the contrary, deletion of αv integrin expression on vascular endothelial cells, using Tie2-Cre, showed no intracerebral hemorrhage or any other obvious neurovascular defects, however they did develop colitis (93). Interestingly, conditional deletion of the β8 gene using the nestin-cre transgene showed a similar intracerebral hemorrhage, and mice survived beyond the perinatal period (94) (Table 1). Taken together, these

data reveal αvβ8 integrin expression on CNS neural cells is necessary for proper neurovascular unit development.

Microscopic analysis of brains from nestin-cre αv conditional mutant mice at P5, showed cerebral blood vessels separated from the neural tissue. Vessels appeared tortuous and disorganized, unlike the vessels in control mice, which appeared normal. Also, mutant brains had irregularly high levels of GFAP-positive astrocytes, which could represent a potential repair mechanism (93). Similarly, in confocal microscopy studies of nestin-cre β8 conditional mutant mice brains at P0 astroglial processes associated with blood vessels appeared disorganized (94). Radial glial cells, which give rise to neurons and glial cells, and are thought to transform into adult NSCs (27), were also examined in the β8 conditional mutants. E14.5 mutant brain analysis unveiled disorganization within the ganglionic eminences, the origin site of the hemorrhage (94).

Gene Deletion Strategy	Cell Types with Deletion	Resulting Phenotype
αv -/-	All Cells, Complete KO	Cerebral Hemorrhage
Nestin-Cre; αv flox/flox	CNS Neurons, Glia, NSPCs	Cerebral Hemorrhage
Tie2-Cre; αv flox/flox	Vascular Endothelial Cells	NO Cerebral Hemorrhage
β8 -/-	All Cells, Complete KO	Cerebral Hemorrhage
Nestin-Cre; β8 flox/flox	CNS Neurons, Glia, NSPCs	Cerebral Hemorrhage
Tie2-Cre; β8 flox/flox	Vascular Endothelial Cells	NO Cerebral Hemorrhage

Table 1: Results of Complete and Conditional Knockout Strategies for αv and β8 Integrin

Conditional deletion of either αv or β8 on glia or progenitor cells is associated with the development of hemorrhage, while deletion of αv or β8 on endothelial cells show no obvious defects.

Examination of the adult brain in both the αv and β8 nestin-cre conditional mutants six to ten weeks postnatally showed no sign of pathological hemorrhage (93, 94). Unexpectedly, the vascular defects observed perinatally in both models were repaired. Further analysis of nestin-cre αv conditional mutants showed that the loss of αv on neural cells results in behavioral abnormalities in the adult mouse. Two to three months postnatally, mutants show hind limb coordination defects, as well as involuntary tail wriggling and ataxia. By 6 months, mutant mice develop seizures and worsening hind limb paraparesis as well as urinary dysfunction (93). Complete β8 integrin knockout mice were backcrossed to an ICR genetic background. β8 null mice from this backcross do not show perinatal lethality initially reported for the strain. These mice survive for several months and develop a severe neurological phenotype similar to that seen in the nestin-cre conditional αv and β8 mutants (89).

The Cre transgene does not lead to complete gene deletion. The resolution of hemorrhage in the adult brain of Nestin-Cre conditional mutants was originally thought to be a result of this. However, with recent findings demonstrating that complete β8 null mice show resolution of hemorrhage as well, this idea was negated. Current thinking is that β8 integrin, expressed on neural cells is only important in regions of active angiogenesis, similar to those seen during embryonic brain development. As stated previously, angiogenesis in the adult brain is rarely seen after postnatal day 30 (40). However, in the neurogenic regions of the adult brain, there is still ongoing angiogenesis and NSCs are closely associated with the

angiogenic vessels (2, 9). Therefore, it seems likely that β8 integrin in NSCs promotes interactions with blood vessels in the neurovascular niche.

The following findings show an important role for αvβ8 integrin in the adult neural stem cell niche: 1) αvβ8 integrin is highly expressed on NSCs but not on the vascular cells in the brain; 2) ablation of murine αvβ8 integrin in embryonic NSCs leads to neurovascular pathologies; and 3) adult mice null for αvβ8 integrin develop age related neurological defects and die prematurely. This dissertation will test the importance of αvβ8 integrin within the neurovascular niche and evaluate its involvement is essential for NSC growth, self-renewal, survival and migration to the olfactory bulb.

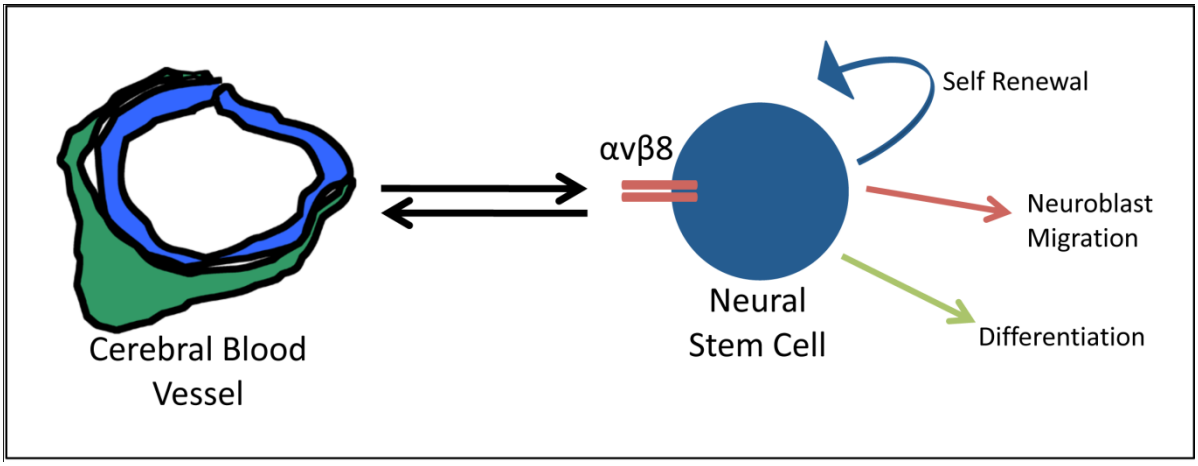

Figure 5: Working Model for β8 Integrins Involvement in the Adult NSC Vascular Niche.

αvβ8 integrin is highly expressed on the surface of neural stem cells (NSC). NSCs are closely associated with the vasculature in the neurovascular niche. Signals coming from the vasculature are thought to regulate the functions of the neural stem cells (i.e., self-renewal, differentiation as well as neuroblast migration) and maintain homeostasis. We believe that these signals are relayed through αvβ8 integrin and in this dissertation we test the importance of expression and function of αvβ8 on the NSCs.

Specific Aims

Neural stem cells (NSCs) reside in fixed locations in the adult brain termed the NSC vascular niche. The NSC niche is comprised mainly of NSCs, blood vessels, and various ECM proteins. Within this niche, NSCs interact with nearby cells and ECM proteins, which control their self-renewal and differentiation properties, however the signaling mechanisms in the niche have not been well characterized. Integrins are cell surface receptors for ECM proteins, and are expressed on NSCs. αvβ8 integrin is highly expressed in NSCs, however its role in their regulation is poorly understood. **I hypothesize that αvβ8 integrin is essential for proper communication between NSCs and cells of the vascular niche, and that disruption of normal αvβ8 integrin function leads to decreased self-renewal and abnormal differentiation and migration of neural progenitor cells.** To test this hypothesis the following specific aims were developed:

Specific Aim 1: Elucidate the involvement of αvβ8 integrin in the regulation of NSC self-renewal, proliferation and differentiation using whole body β8 null mice as well as inducible β8 knockout mouse strategies.

Specific Aim 2: Determine αvβ8 integrin's role in neuroblast migration using complete β8 knockout mice and conditional, cell specific β8 knockout strategies.

CHAPTER 2:

Materials and Methods

Experimental Mice and Breeding Strategies

β8+/- mice were acquired from the Mutant Mouse Regional Resource Center (MMRRC), and were backcrossed with CD1 mice (purchased from Jackson Laboratories) for 3 generations. β8+/- males and β8+/- females were crossed to generate β8+/+ and β8-/- progeny, used as control and mutants for all experiments.

β8 flox/flox mice were acquired from the Mutant Mouse Regional Resource Center. Rosa (R26R) and Nestin-Cre (N-Cre) mice were obtained from Jackson Laboratories. The tamoxifen inducible mouse strain, GLAST-CreERT2, was a kind gift from the Magdalena Götz Lab. Rosa mice were used to confirm Cre activity in both the GLAST-CreERT2 strains. Control and mutant littermates were generated by first crossing a GLAST-CreERT2 homozygous male with a β8+/- female. Progeny from this cross were all GLAST-CreERT2 positive and either wild type or heterozygous null for the β8 gene. Next, GLAST-CreERT2; β8+/- males were backcrossed with GLAST-CreERT2 homozygous female to generate offspring that are GLAST-CreERT2 homozygous; β8+/-. Finally, a GLAST-CreERT2; β8+/- male was crossed with a β8 flox/flox female. Progeny from this cross were 50% GLAST-CreERT2; β8 flox/+ and 50% GLAST-CreERT2; β8 flox/-. These mice were used as controls and mutants for all experiments. Generation of Nestin-Cre; β8 flox/+ controls and Nestin-Cre; β8 flox/- mutants, as well as generation of GLAST-

CreERT2; Rosa and Nestin-Cre; Rosa mice were accomplished using a similar mating scheme.

Doublecortin-GFP mice developed by GENSAT to analyze doublecortin expression in the brain, were acquired the MMRRC. Hemizygous DCX-GFP/+ mice were bred with β8+/- mice to generate offspring that were 25% DCX-GFP/+; β8+/+, 25% DCX-GFP/+; β8+/-, 25% +/+; β8+/+, and 25% +/+; β8+/-. A male mouse that was DCX-GFP/+; β8+/-, was then crossed to β8+/- females to generate control (DCX-GFP/+; β8+/+) and mutant (DCX-GFP/+; β8+/-) mice.

Mouse Genotyping

Mouse genotypes were confirmed with genomic PCR. DNA was extracted from ear snips by digesting the tissue in STE with 100μg/ml proteinase-K (USB Scientific, Cleveland, OH) overnight at 55°C. Precipitation of DNA was accomplished by mixing the digested tissue with an equal volume of 100% Ethanol. DNA was extracted and dissolved in TE buffer at 37°C for 30 minutes. PCR conditions are described by manufacturer of TAKARA Taq polymerase. The primer sequences are as follows;

β8 PCR: DW74: 5'-ATT ATC TGG TTG ATG TGT CAG C-3', DW94: 5'-GGA GGC ATA CAG TCT AAA TTG T-3', DW56: 5'-AGA GGC CAC TTG TGT AGC GCC AAG-3' AND JW153: 5'-AGA GAG GAA CAA ATA TCC TTC CC-3'. The PCR generates a wild type band of 330bp and mutant band of 450bp (74). The PCR was run with the following conditions: 95°C for 5 minutes, 1 time. 95°C for 45 seconds, 58°C for 30 seconds, 72°C for 1 minute, 30 times. 72°C for 10 minutes, 1 time. Cool to 4°C.

β8 flox PCR: Forward: 5′-GAG ATG CAA GAG TGT TTA CC-3′ and Reverse: 5′-CAC TTT AGT ATG CTA ATG ATG G-3′. The wild type band is seen at 250bp and the floxed allele band is seen at 370bp (94). Thermocycling conditions: 95°C for 5 minutes, 1 time. 95°C for 45 seconds, 64°C for 45 seconds, 72°C for 1 minute, 30 times. 72°C for 10 minutes, 1 time. Cool to 4°C.

GLAST-CreERT2 PCR: GLAST F8: 5′-GAG GCA CTT GGC TAG GCT CTG AGG A-3′, GLAST R3: 5′-GAG GAG ATC CTG ACC GAT CAG TTG G-3′, and CER1: 5′-GGT GTA CGG TCA GTA AAT TGG ACA T-3′. PCR products for this reaction include a 700bp control band, present in wild type mice, and a 400bp Cre band present only in Cre-positive mice (28). Program conditions are: 95°C for 5 minutes, 1 time. 95°C for 30 seconds, 56°C for 30 seconds, 72°C for 1 minute, 30 times. 72°C for 10 minutes extension time

Nestin-Cre PCR: Forward: 5′-ACC AGC CAG CTA TCA ACT C-3′ and 5′-TAT ACG CGT GCT AGC GAA GAT CTC CAT CTT CCA GCA G-3′. The amplification product for a Cre positive mouse is approximately 200bp. If there is no Cre transgene there will be no band present (95). Program conditions are: 95°C for 5 minutes, 1 time. 95°C for 30 seconds, 56°C for 30 seconds, 72°C for 1 minute, 30 times. 72°C for 10 minutes, 1 time. Cool to 4°C.

DCX-GFP PCR: DCX F: 5'- TTC ACA GGC AGC AGA TTG CAG C-3' and DCX R: 5'- TAG CGG CTG AAG CAC TGC A -3'. PCR amplification will yield a product of 388bp. PCR conditions are: 95°C for 5 minutes, 1 time. 94°C for 1 minute, 66°C for 1 minute, 72°C for 1 minute, 35 times. 72°C for 7 minutes, 1 time. Cool to 4°C.

Tamoxifen Administration

To induce gene deletion in GLAST-CreERT2 mutant (Cre/+; β8 fl/-) and control (Cre/+; β8 fl/+) mice, we performed a series of intraparitoneal injections with Tamoxifen. Lyophilized tamoxifen (Sigma) was dissolved at 10mg/ml in 90% sunflower seed oil and 10% ethanol. Negative control injections consisted of only the sunflower seed oil/ethanol mixture. 1mg of tamoxifen was injected intraparitoneally twice daily for 5 consecutive days. Cohorts of at least 3 control and at least 3 mutants were used for all experiments. Mice were sacrificed and analyzed for gene deletion 30 days after the last injection.

LacZ/X-gal Staining

Cre expression in tamoxifen inducible (GLAST-CreERT2) and Nestin-Cre mouse models was verified by mating the Cre strains with Rosa reporter mice. Mice were then injected with tamoxifen twice daily for 5 days. 30 days after the last injection, mice were cardiac perfused with 4% paraformaldehyde (PFA) in PBS and brains were removed and fixed for an additional hour in 4% PFA/PBS. Next, brains were sliced either coronally or sagitally and washed 4 times with PBS, followed by two washes in X-gal buffer. Brain slices were incubated overnight at 33°C in X-gal buffer containing 1mg/ml X-gal. The next day the samples were washed 3 times with PBS and post-fixed in 4% PFA/PBS for 2 hours. Brain slices were then imaged under a dissecting microscope followed by processing for paraffin or OCT embedding and sectioning.

Alternatively, the LacZ/X-gal enzymatic product emits fluorescence when excited with a 633nm laser (using the Cy5 analysis settings) on a confocal microscope. This fluorescent product can be combined with other immunofluorescent antibody stains to determine cell specificity of Cre activity.

Bromodeoxyuridine Incorporation Analysis

BrdU (BD Pharmingen) was injected at 65ug/g body weight into mice once daily for two consecutive days. After another 24 hours, mice were cardiac perfused with 4% PFA/PBS, the brains were removed and post-fixed overnight. The next day the brains were cryopreserved with sucrose steps consisting of 10% and 20% sucrose in PBS at 4°C, then embedded in OCT compound. The MDACC histology core then prepared sections. Genomic DNA was denatured with 2N HCl for 1 hour at 37°C then neutralized in 0.1M Sodium Borate solution for 30 minutes at room temperature, followed by normal immunofluorescent staining protocol with anti-BrdU (Accurate Biochemicals).

For BrdU studies in NSCs, BrdU was added to the culture media at 1mM for 1 hour. The cells are then fixed in 4% PFA for 10 min at 4°C, permeabilized with 0.5% NP40 in PBS solution for 10 min at room temperature, denatured in 2N HCl for 1 hour at 37°C, then neutralized with 0.1M sodium borate buffer for 30 minutes at room temperature. This was followed by immunofluorescence with anti-BrdU. BrdU incorporation was analyzed by counting total cell nuclei and calculating percentage of total BrdU positive cells.

Tunel Assay

TUNEL fluorescence was performed on PFA fixed paraffin embedded sections to analyze cell death, using the DeadEnd Fluorometric Tunel System (Promega) following manufacturers protocol. Analysis was performed by counting total number of TUNEL-positive cells within the subventricular zone of wild type and knockout mice.

Biotin perfusions

Post-natal day 60 (P60) control and mutant animals were sacrificed with a lethal injection of Avertin (250 mg/kg) and a 20 gauge needle was inserted into the left ventricle of the heart. Animals were first perfused with 20 ml of PBS to flush the circulation so that no residual cells or serum proteins were labeled with reactive biotin. Animals were then perfused for five minutes continuously with 1 mg/ml EZLink-NHS-Biotin (Pierce Chemicals, Inc.) dissolved in PBS (approximately 7.5 ml in total per animal). Animals were then perfused with 4% PFA-PBS fixative to preserve brain morphology. Brains were removed and coronally sliced into 1 mm segments followed by cryopreservation in 30% sucrose-PBS, embedded in OCT, and cut in 7 µm sections. Frozen brain sections were rehydrated in PBS and blocked with 10% goat serum in PBS and visualized using streptavidin conjugated to Alexa Fluor 488 fluorophore (Molecular Probes).

Whole Mount Staining

Adult mice were anesthetized and brains were removed. The SVZ was microdissected and fixed for 1 hour in 4% PFA/PBS. Tissue was washed three times with PBS, followed by overnight blocking in 10% goat serum (diluted in PBS)

at 4°C. Samples were washed 3 times in PBS containing 1% triton-x 100 (Sigma) (PBS-triton) 1 hour each wash. Next, primary antibody was added and samples were incubated at 4°C with gentle rotation. The following antibodies were used: anti-CD31 (BD Biosciences), anti-GFAP (Millipore), and anti-DCX (Cell Signaling). After 3 days of incubation, samples were washed 3 times with PBS-triton for 1 hour each wash, followed by secondary antibody addition. Secondary antibodies used were: goat anti-rat Cy3, goat anti-mouse Cy5 and goat anti-rabbit Cy5. After 48 hours, samples were again washed 3 times in PBS-triton for 1 hour each wash followed by a 1 hour incubation in Sytox Green (Invitrogen). Washes were repeated 3 times and samples were placed in 100% glycerol overnight at 4°C. Then, samples were moved to 50% glycerol until the samples sunk. Samples were mounted in 50% glycerol on microscope slides and covered with an imaging chamber (Grace Biolabs). Imaging was performed using a Zeiss LSM 510 laser-scanning microscope equipped with an argon laser (458/477/488/514 nm, 30 mW), HeNe lasers (543 nm, 1mW and 633 nm, 5 mW).

Immunohistochemistry

Adult mice were anesthetized and fixed with cardiac perfusion of 4% paraformaldehyde (PFA). Brains were removed and post fixed overnight in 4% PFA and processed for standard paraffin embedding. Sections were deparaffinized using sequential xylene and alcohol steps, followed by rehydration in PBS. Antigen retrieval was performed using 1x Target Retrieval Solution pH9 according to

manufacturer's recommendation (DAKO). Sections were blocked in 10% serum of the species the secondary antibody was produced in for 30 minutes. Next, primary antibodies, diluted in 10% serum, were added to the sections and incubated overnight at 4°C. Sections were washed twice with PBS containing 0.1% Tween-20 followed by one wash with PBS, five minutes for each wash. Endogenous peroxidases were then blocked using 0.3% hydrogen peroxide in PBS for 10 minutes, followed by three PBS washing steps. Next, biotin-conjugated secondary antibody was added to the sections and incubated for one hour at room temperature, followed by two washes in PBS+0.1% Tween-20 and one wash in PBS. Vectastain ABC kit (Vector Labs) was then added to the sections for 30 minutes at room temperature. Washing steps were repeated, followed by incubation for 5-10 minutes in DAB chromagen (Vector Labs). Finally counterstaining was done using Hematoxylin according to the manufacturers protocol (Vector Labs), followed by dehydration, mounting and coverslipping. For immunofluorescent staining, fluorescent-conjugated secondary antibody was added after the primary antibody washing steps, and incubated for one hour at room temperature. The washing steps were repeated and the sections were mounted with Vectashield (Vector Labs) and coverslipped. Alternatively, brains were removed from adult mice, after asphyxiation with carbon dioxide, with no fixation and embedded in OCT (Sakura) and frozen on dry ice. Fresh frozen sections were then cut from these OCT blocks and immunostained using the same procedure as paraffin embedded sections.

Immunocytochemistry was performed on cells adherent to substrate-coated glass coverslips. Cells were fixed in 4% PFA/PBS for 10 minutes, then permeabilized in PBS containing 0.5% TritonX-100 for 10 minutes. Next, coverslips were removed and blocked with 10% goat serum for 30 minutes, followed by primary antibody incubation overnight. Coverslips were washed 3 times and incubated with fluorescent-conjugated secondary antibody for 1 hour and 3 more washes were performed. Finally, coverslips were inverted and placed onto a slide with Vectashield mounting medium.

Brightfield and fluorescent analysis of samples was performed using a Zeiss Axio Imager Z1 Microscope. Confocal fluorescence images were collected using a Zeiss LSM 510 laser-scanning microscope equipped with an argon laser (458/477/488/514 nm, 30 mW), HeNe lasers (543 nm, 1mW and 633 nm, 5 mW).

Brain and NSC Lysates and Immunoblotting

Lysates were prepared in RIPA Buffer (10mM Tris, pH7.4, 1%NP40, 0.5% Deoxycholate, 0.1% SDS, 150mM NaCl and 1mM EDTA) and protein concentration was determined using BCA assay (Thermo Scientific). 20µg of Protein was mixed with 2x sample buffer and heated then resolved on 7.5% or 10% SDS-PAGE and then immunoblotted.

Biotinylation and Immunoprecipitation

NSCs in suspension were centrifuged and rinsed once with PBS. Next, cells were resuspended in PBS containing 0.1mg/ml EZlink-NHS Biotin (Pierce Chemicals, Inc.) and incubated for 30 minutes at 37°C. Cells were then spun down and rinsed 2x with TBS. Cells were resuspended in RIPA lysis buffer and lysates were placed on a tumbler for 15 minutes followed by a 15 minute centrifugation to pellet the insoluble fraction. Next, lysate concentration was determined using BCA assay. Equal concentrations of all lysates were diluted to 1ml total volume in RIPA buffer and pre-cleared by adding 50µl of secondary antibody-conjugated to agarose beads and tumbling for 30 minutes at 4°C. Lysates were spun down at 1000rpm for 1 minute to pellet the secondary antibody, soluble portion was removed and transferred to a new tube primary antibody was added. Antibodies used were: anti-αv (2µl, generated using a synthetic peptide (CKRVRPPQEEQEREQLQPHENGEGTSEA) corresponding to a region of the chicken αv cytoplasmic tail), anti-α5 (2µl, Emfret Analytics), anti-α6 (2µl, Millipore) and anti-β8 (2µl, previously described (79)). Lysates were tumbled overnight at 4°C in primary antibody. 50µl secondary antibody was added and samples were tumbled for 1 hour. Then, lysates were centrifuged and the soluble portion was removed and the pellets were washed with RIPA buffer 3 times. Pellets were resuspended in 20µl of 2x Sample Buffer (BioRad) and heated for 5 minutes at 100°C. Samples were loaded in 7.5% SDS-PAGE followed by transfer to PVDF membrane (Immobilon). Membranes were blocked in 3% BSA for 30 minutes followed by 3 washes with TBS-T and then incubated in Vectastain ABC kit diluted

in 3% BSA for 30 minutes followed by three more washes with TBS-T. Membranes were then incubated with standard ECL reagents (Amersham) and imaged.

Antibodies

The following antibodies were used for immunohistochemistry: anti-GFAP, anti-PSANCAM, anti-α6, anti-β1 and anti-Doublecortin (Millipore); anti-Nestin (Neuromics); anti-Ki67 (Abcam); anti-CD34 (Genetex); anti-CD31 (BD Biosciences); anti-Laminin and anti-MAP2 (Sigma Aldrich); and BrdU (Accurate Biochemicals); anti-Tuj1 (Covance). Secondary antibodies used for fluorescence were Alexa-conjugated goat anti-rabbit, goat anti-mouse, and goat anti-chicken from molecular probes. For chromogen analysis secondary antibodies used were swine anti-rabbit-HRP and horse anti-mouse-HRP purchased from DAKO.

Antibodies used for western blot analysis include: anti-Actin and anti-MAP2 (Sigma Aldrich); anti-α3 integrin, anti-β1 integrin, anti-β5 integrin, anti-β3 integrin, anti-GFAP and anti-PSANCAM (Millipore); anti-GFP (Abcam); anti-α5 integrin (Emfret Analytics); anti-Tuj1 and anti-Nestin (Covance); anti-Occludin, anti-Claudin5 (Zymed); anti-DCX, anti-pSMAD2, anti-pSMAD3, anti-SMAD2,3, anti-pSMAD1,5,8, anti-pAKT, anti-AKT, anti-pTAK1, anti-phospho-p38 and anti pERK (Cell Signaling). Anti-αv integrin was generated using a synthetic peptide (CKRVRPPQEEQEREQLQPHENGEGTSEA) corresponding to a region of the chicken αv cytoplasmic tail. Anti-β8 integrin antibody was previously described (79).

Live Cell Sorting

Live cell sorting was performed using a Vantage Turbo-Sort-SE cell sorter

(BD Biosciences). Live cell sorting was performed to isolate GFP-positive cells after SVZ isolation (same isolation as Neurosphere) from DCX-GFP+ mice. A GFP- mouse SVZ was isolated and sorted in a similar manner for a negative control. All flow cytometry was performed in the Flow Cytometry and Cellular Imaging Core Facility.

Neural Stem Cell Cultures

Neural stem cells were isolated from adult SVZ as described previously (96). Briefly, mice were asphyxiated and brains were isolated. Olfactory bulbs were removed, followed by coronal slicing of the brain at the optic chiasm, the caudal portion of the brain was discarded. The medial aspect of the ventricle was removed and the lateral portion was carefully microdissected and moved to a new petri dish with PBS. Tissue was then minced with a sterile razor blade, followed by digestion in tissue dissociation media (TDM). (The recipe for TDM is as follows: add 476 mg of HEPES, 40 mg of EDTA, 50 mg of trypsin, and 1 ml of 0.1% DNase I to 200 ml of Ca^{2+}/Mg^{2+} Hanks' balanced salt solution (HBSS). Mix well, filter sterilize, and then aliquot (3 ml/aliquot) and store at −20°.) Tissue was incubated for 10 minutes in TDM followed by dissociation with a sterile glass polished pipet. Finally, cells were plated at a density of 3500 cells/cm^2. Cells were cultured in a specified media made of DMEM/F12 (Mediatech Inc, Manassas, VA), 20ng/ml EGF and 20ng/ml FGF (Biosource, Camarillo, CA), 1x B27 supplement (Gibco, Grand Island, NY) and 1unit/ml Penn/Strep (Sigma Aldrich). After 7-10 days, neurospheres were passaged by passing through a 23-gauge needle into a single cell suspension and then replated in fresh media.

NSC Proliferation Assay

Neurospheres were dissociated using 23g needle and then counted using a hemocytometer. $5x10^5$ cells were plated in a T-25 flask containing 6 ml of NSC Media. After 7 days the spheres were dissociated again and total cell numbers were counted. Again, $5x10^5$ cells were replated. This method was repeated serially for 10 passages. For analyses, the starting cell numbers ($5x10^5$ cells) were subtracted from the total cell numbers for each passage.

NSC Secondary Sphere Formation Assay

Single spheres of similar sizes were mechanically dissociated and plated in one well of a 24 well plate. After 7 days the number of newly formed secondary spheres were counted and then single spheres were taken and dissociated and plated again. This method was carried out every 7 days until no secondary spheres formed. Alternatively, this assay was carried out in the presence or absence of recombinant TGFβ (10ng/ml) or anti-TGFβ (5μg/ml) (both from R&D Systems).

NSC Differentiation Assay

Wild type and β8-/- neurospheres were plated on laminin-coated coverslips and allowed to adhere. 10% fetal bovine serum (FBS, Hyclone) was added to complete NSC growth media and cells were incubated for 5 days to allow for differentiation. Next, neurospheres were fixed on coverslips in 4% PFA and stained with anti-Tuj1 and anti-GFAP antibodies, to show differentiation into neurons or

astrocytes, respectively. The percentage of cells differentiating into each lineage was then quantified by counting total nuclei and number of cells stained with each marker.

Luciferase Reporter Assay

For initial analysis of αvβ8 TGFβ activation, HEK293T cells were plated into poly-lysine-coated six-well plates at 4×10^5 cells per well and allowed to attach overnight. Cells were then transfected with a β8V5 plasmid and PAI1-luciferase plasmid (97) using Effectene reagents (Qiagen). After 24 hours, transfection media was removed and media with or without 10ng/ml LAP-TGFβ1 was added. HEK293T cells transfected with only PAI1-luciferase were used as a negative control. After 24 hours, cell lysates were made and luciferase substrates were added according to Enhanced Luciferase Assay kit instructions (BD Biosciences). Lysates were plated in duplicate wells in a 96-well plate and luciferase activities were determined using a Lumistar Galaxy Luminometer (BMG Lab Technologies).

For neurosphere TGFβ activation assay, HEK293T cells were plated into poly-lysine-coated six-well plates at 4×10^5 cells per well and allowed to attach overnight. Cells were then transfected with a PAI1-luciferase plasmid (97) using Effectene reagents (Qiagen). After 24 hours the transfection medium was removed and serum free medium was added for an additional 24 hours. Meanwhile, 100 wild type or $\beta8^{-/-}$ adult neurospheres of similar diameters (~75 μm) were added to six-well dishes containing 2 ml of neurosphere growth medium. LAP-TGFβ1 (SLC, R&D Systems) at 10 ng/ml (or PBS as a negative control) was added to the neurospheres. After 16 hours conditioned medium was collected, passed through a

sterile 0.2μm filter, and added to transfected HEK293T cells (see above) for 16 hours. As a control to confirm PAI1-luciferase plasmid transfection, bioactive TGFβ1 (R&D Systems) was added at 5 ng/ml to transfected HEK293T cells and incubated for 4 hours. Cell lysates were prepared and luciferase activity was analyzed as detailed above.

Neurosphere Migration Assay

Single neurospheres were allowed to adhere to laminin coated coverslips, one per coverslip and incubated at 37°C. Images were taken every 4 hours for 48 hours on Olympus IX-81 microscope. Analysis of cell migration was performed using Image J software (NIH). Total sphere area at set timepoints was calculated and normalized to the original sphere size. Alternatively, migration assays were performed using the following antibodies; anti-αv integrin (5μg/ml), anti-β1 integrin (5μg/ml, R&D Systems), anti-TGFβ1,2,3 (5μg/ml, R&D Systems). Additionally, human recombinant active TGFβ (R&D Systems) was added at 10ng/ml. Neurospheres were pre-incubated with the antibody or cytokine for 30 minutes prior to adhesion to laminin-coated coverslips. Antibody or cytokine was also added to the media during the assay at the concentrations indicated above.

Timelapse Microscopy

Timelapse microscopy studies were done using an Olympus IX-81 inverted light microscope equipped with a temperature and CO_2 regulated chamber and Slidebook software. Images were captured every 4 hours for a total of 48 hours.

Transmission Electron Microscopy

Adult mice were anesthetized then cardiac perfused with PBS followed by perfusion with Karnovsky's Fixative (Polysciences Inc.). Brains were then removed and postfixed overnight. Samples were then dissected from the SVZ and Cortex. Samples were fixed with a solution containing 3%glutaraldehyde plus 2% paraformaldehyde in 0.1M-cacodylate buffer, pH 7.3, for 1 hour. After fixation, the samples were washed and treated with 0.1% Millipore-filtered cacodylate buffered tannic acid, postfixed with 1% buffered osmium tetroxide for 30 min, and stained en bloc with 1% Millipore-filtered uranyl acetate. The samples were dehydrated in increasing concentrations of ethanol, infiltrated, and embedded in Poly-bed 812 medium. The samples were polymerized in a 60C oven for 2 days. Ultrathin sections were cut in a Leica Ultracut microtome (Leica), stained with uranyl acetate and lead citrate in a Leica EM Stainer, and examined in a JEM 1010 transmission electron microscope (JEOL, USA, Inc.) at an accelerating voltage of 80kV. Digital images were obtained using AMT Imaging System (Advanced Microscopy Techniques Corp).

RNA and cDNA Synthesis

RNA was isolated from neurospheres using TRIZOL reagent (Invitrogen). cDNA was then made from 5ug RNA using Superscript III reverse transcriptase (Invitrogen) following manufacturers protocol.

rtPCR

rtPCR was performed on synthesized cDNA using Hotstar Taq protocol (Qiagen, Valencia, CA). Primers used include: p53 forward 5'-GAT GAC TGC CAT

GGA GGA GT-3' and reverse 5'-CTC GGG TGG CTC ATA AGG TA-3'; BMI-1 forward 5'-CAG CAA TGA CTG TGA TGC-3' and reverse 5'-CTC CAG CAT TCG TCA GTC-3'; BLBP forward 5'-GAT GAG TAC ATG AAA CTC TGG-3' and reverse 5'-ACA GCG AAC AGC AAC GAT ATC C-3'; Musashi-1 forward 5'-TGC AAG ATG TTC ATC GGA GG-3' and reverse 5'-GTC GAA CAT CAG CAT GGC ATC ATC C-3'; Podoplanin forward 5'-TGA TAT TGT GAC CCC AGG-3' and reverse 5'-TTG TCT GCG TTT CAT CC-3'; and Sox2 forward 5'-GGA GAA CCC CAA GAT GC-3' and reverse 5'-CTC GTA GCT GTC CAT GCG-3'.

Statistical Analysis

Student's t-test was used to determine statistically significant differences. Analysis of variance (ANOVA) was used to determine differences in self-renewal between wild type and mutant NSCs. WIlcoxan rank sum test was used to analyze Kaplan-Meier survival results.

CHAPTER 3:

Specific Aim 1

Introduction

NSCs reside in at least two specific regions in the adult mouse brain: the subgranular zone (SGZ) of the dentate gyrus and the subventricular zone (SVZ) of the lateral ventricle (98, 99). NSC behaviors in the SVZ are regulated by intracellular gene regulatory pathways (100) as well as many extracellular cues from the local microenvironment (39, 101). NSCs have direct access to soluble growth factors, and extracellular matrix (ECM) cues from within the vascular basement membrane, owing to their close association with the cerebral vasculature in the neurovascular niche. Access to these cues is important for regulation of stem cell behaviors, including self-renewal, proliferation, survival and differentiation (102). Many growth factors and their receptors have been well characterized in the NSC niche (103-106). However, adhesion and signaling pathways used by NSCs in response to ECM cues remain mostly uncharacterized.

Integrins are cell surface receptors for ECM proteins. Many integrins are expressed in post-natal astrocytes and NSCs (51, 93), although the function integrins play in the adult neurovascular niche remains mostly unknown. Our group and others have shown that one integrin, αvβ8 integrin, is required for normal neurovascular development (74, 107). Although αvβ8 is a receptor for many ECM ligands (81), recent studies indicate that cerebral blood vessel development regulation occurs mainly through integrin-mediated activation of latent TGFβ. TGFβ

is found in the vascular basement membrane bound to an inactive latent peptide (LAP-TGFβ), which it must be liberated from to become active (84). αvβ8 adhesion to LAP-TGFβ1 or LAP-TGFβ3 mediates the bioactivation of TGFβ and, upon activation, intracellular signaling ensues (83, 92). The importance of integrin-mediated TGFβ activation has been shown through mutating the integrin-binding RGD motif to an RGE motif in TGFβ1, thereby inhibiting the ability to bind integrins. Mice with this mutation die prematurely and show a phenotype that is similar to the complete TGFβ1 knockout mice (90). Additionally, when mice harboring the TGFβ1 RGD to RGE mutation are combined with complete TGFβ3 null mice, they develop a brain-specific neurovascular pathology nearly identical to the phenotype observed in complete αv or β8 knockout mice (92).

These gaps in knowledge of the role of αvβ8 integrin in the adult brain, and more specifically in the adult neurovascular niche, led me to study the role αvβ8 plays in the adult brain. I hypothesized that αvβ8 integrin is involved in the regulation of adult neural stem cell self-renewal, proliferation and differentiation. I tested this hypothesis using whole body β8 null mice as well as tamoxifen-inducible β8 knockout mouse models.

Results:

Post-Natal Viability of Complete β8-/- Mice Depends on Genetic Background

Prior reports indicate that αv and β8 null mice, originally developed on a CD57BL6/129S4 mixed genetic background die, either embryonically due to placental defects or shortly after birth due to severe intracerebral hemorrhage and/or cleft palate (67, 74). β8 heterozygous (β8+/-) mice on the CD57BL6/129S4 background were backcrossed to the ICR/CD1 outbred strain for two generations. β8+/- progeny were then interbred to produce β8+/+, β8+/-, and β8-/- mice. Interestingly, nearly all of the β8-/- progeny were born in near predicted mendalian ratios (26 of a total of 123 mice, 21%). Mutant mice continued to display intracerebral hemorrhage, and were initially identified by this characteristic, while wild type and heterozygous mice displayed a normal phenotype at birth and no pathologies in adulthood.

Approximately 90% (23 out of 26 mice analyzed) of β8-/- mice survive beyond the first postnatal week (Figure 6A), but displayed an obvious phenotype and were readily distinguishable from control mice. Mutants were significantly smaller than their littermates as they reached adulthood (Figure 6B) and showed an abnormal posture (Figure 6D). Approximately 50% of null mice survived to about P21-P30, while the remaining mutant mice survived for as long as five months (Figure 6A). As β8-/- mice progress in age they develop more severe neurological phenotypes such as hind limb paresis and an abnormal gait (Figure 6E). Spatial analysis of β8 integrin protein expression through western blot of lysates from several brain regions including, the subventricular zone (SVZ), olfactory bulb (OB),

dentate gyrus (DG), and cerebellum (CB) reveal that β8 integrin was expressed at similar levels throughout all regions analyzed in wild type lysates. No expression was seen in β8-/- brain lysates (Figure 6F). The phenotypes seen in the adult β8-/- mice are similar to those observed for nestin-cre conditional αv and β8 integrin adult mice (93, 94). These results indicate that the neurological defects observed in the complete β8-/- mouse model are due to the loss of β8 integrin expression in the CNS and that the loss contributes to its early death.

Figure 6: β8 Null Mice on CD-1 Genetic Background Survive to Adulthood, But Die Prematurely Due to Severe Neurological Phenotype.

(A) Kaplan-Meier survival analysis with wild type (+/+) and β8 -/- mice. Approximately 50% of β8 -/- mice die by P30. All of the remaining β8 -/- mice die by five months of age. **(B)** Weight analysis of one-month and two-month old wild type and β8 -/- mice. Mutant mice weigh significantly less than wild type mice at both timepoints. **(C,D)** Pictures of four-month old wild type (C) and β8 -/- (D) mice. β8 -/- mice develop severe hunched posture and hind limb paresis. **(E)** Footprint analysis of three-month old wild type (upper panel) and β8 -/- mice (lower panel). Hind paws were painted blue and fore paws were painted red. Note the β8 -/- mouse drags its limbs. **(F)** Western blot analysis of wild type and β8 -/- mouse regional brain lysates probed with anti-β8 polyclonal antibody (top panel) and actin loading control (bottom panel). Note that β8 integrin is expressed in all regions analyzed in wild type lysates, but not detected at all in β8 -/- lysates.

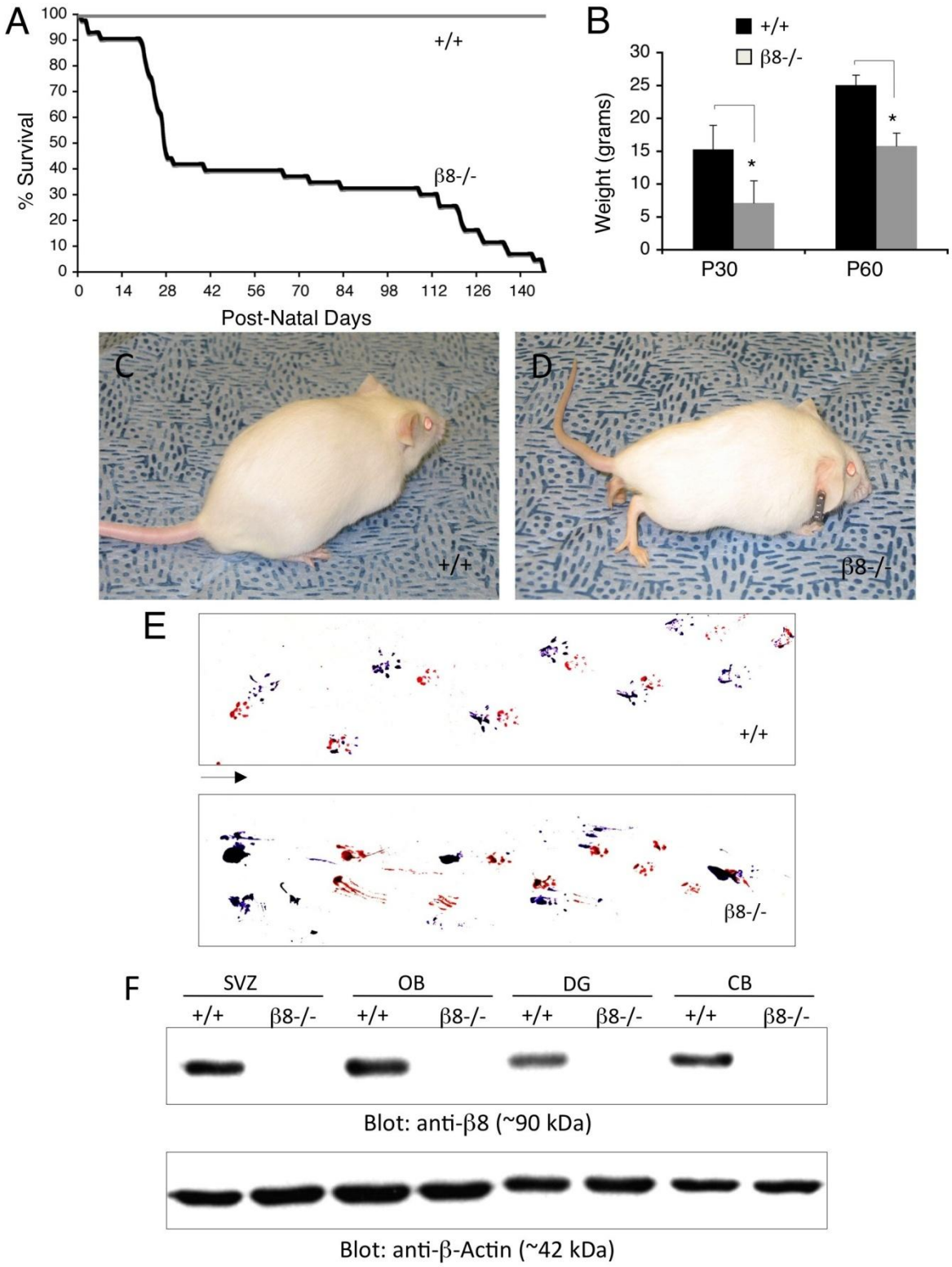
A
100
90
80
70
60
50
40
30
20
10
0
% Survival
+/+
β8-/-
0
14
28
42
56
70
84
98
112
126
140
Post-Natal Days
B
+/+
β8-/-
30
25
20
15
10
5
0
Weight (grams)
*
*
P30
P60
C
+/+
D
β8-/-
E
+/+
β8-/-
F
SVZ
OB
DG
CB
+/+
β8-/-
+/+
β8-/-
+/+
β8-/-
+/+
β8-/-
Blot: anti-β8 (~90 kDa)
Blot: anti-β-Actin (~42 kDa)

Figure 6

Neurovascular Unit Defects in Adult β8-/- Mice

Analysis of brain sections from adult β8-/- mice showed no sign of the intracerebral hemorrhage. The resolution of hemorrhage was also seen in conditional αv and β8 integrin knockout mouse models (93, 94). Next, blood vessel density in adult wild type and mutant brains was quantified in the cortex. Brain sections were immunostained with an anti-laminin antibody (Figure 7A, B) to show the vascular basement membrane. β8 null brains showed an approximately two-fold increase in blood vessel number when compared to wild type mice (Figure 7C). To determine if the increase in vasculature was due to increased endothelial cell proliferation control and mutant mice were injected with BrdU, and brain sections were analyzed for colocalization of anti-BrdU and anti-laminin antibodies (data not shown). No increase in proliferation was noted in mutant endothelial cells when compared to control brain sections.

Anti-GFAP immunostaining of wild type and β8-/- mice revealed an increase in GFAP positive reactive astrocytes throughout the mutant brain (Figure 7D, E). Quantitation of GFAP positive cells showed a nearly five-fold increase in the β8-/- brain (Figure 7F). BrdU analysis for proliferating cells did not show any sign of double positive GFAP/BrdU cells, indicating that the increase in astrocytes was not due to increased astrocytic proliferation (data not shown). Double immunofluorescent staining with anti-laminin and anti-GFAP indicated that many of the astrocytes made direct contact with the vasculature (Figure 7 D, E Arrows). Electron microscopy was used to examine the ultrastructure of cerebral blood vessels in wild type and mutant mice (Figure 7G, H). Increased astrocytic endfoot

coverage was evident in the β8-/- mice (arrows in Figure 7H). Astrocytic endfoot coverage was quantified by counting the percentage of vessels with more than one GFAP-positive astrocyte contacting them. This analysis revealed that in mutant mice almost 90% of vessels have multiple astrocytic contacts, whereas in wild type mice only about 30% have multiple astrocytic contacts (Figure 7I).

Figure 7: β8 -/- Mice Show Neurovascular Pathologies.

(A,B) Wild type (A) and β8 -/- (B) P60 mouse cortical sections were immunostained with anti-laminin to show cerebral blood vessels. **(C)** Quantification of cerebral blood vessels from anti-laminin immunostain. β8-/- mice show significantly more laminin positive vessels compared to wild type mice (p-value < 0.005). **(D,E)** Double immunofluorescence analysis for anti-laminin (green) and anti-GFAP (red) shows an increase in total number of astrocytes in mutant mice. **(F)** Quantification of GFAP-positive astrocytes in wild type and β8-/- mice. p-value less than 0.001. **(G,H)** Electron microscopy reveals neurovascular unit pathologies in mutant (H) mice including increased coverage by astrocyte endfeet when compared to wild type (G). **(I)** Quantification of cerebral blood vessel coverage by astrocytes in the cortex of wild type and β8-/- mice. Percentage of laminin expressing blood vessels contacting more than one GFAP positive astrocytes was quantitated. P-value less than 0.002 when compared to the wild type group.

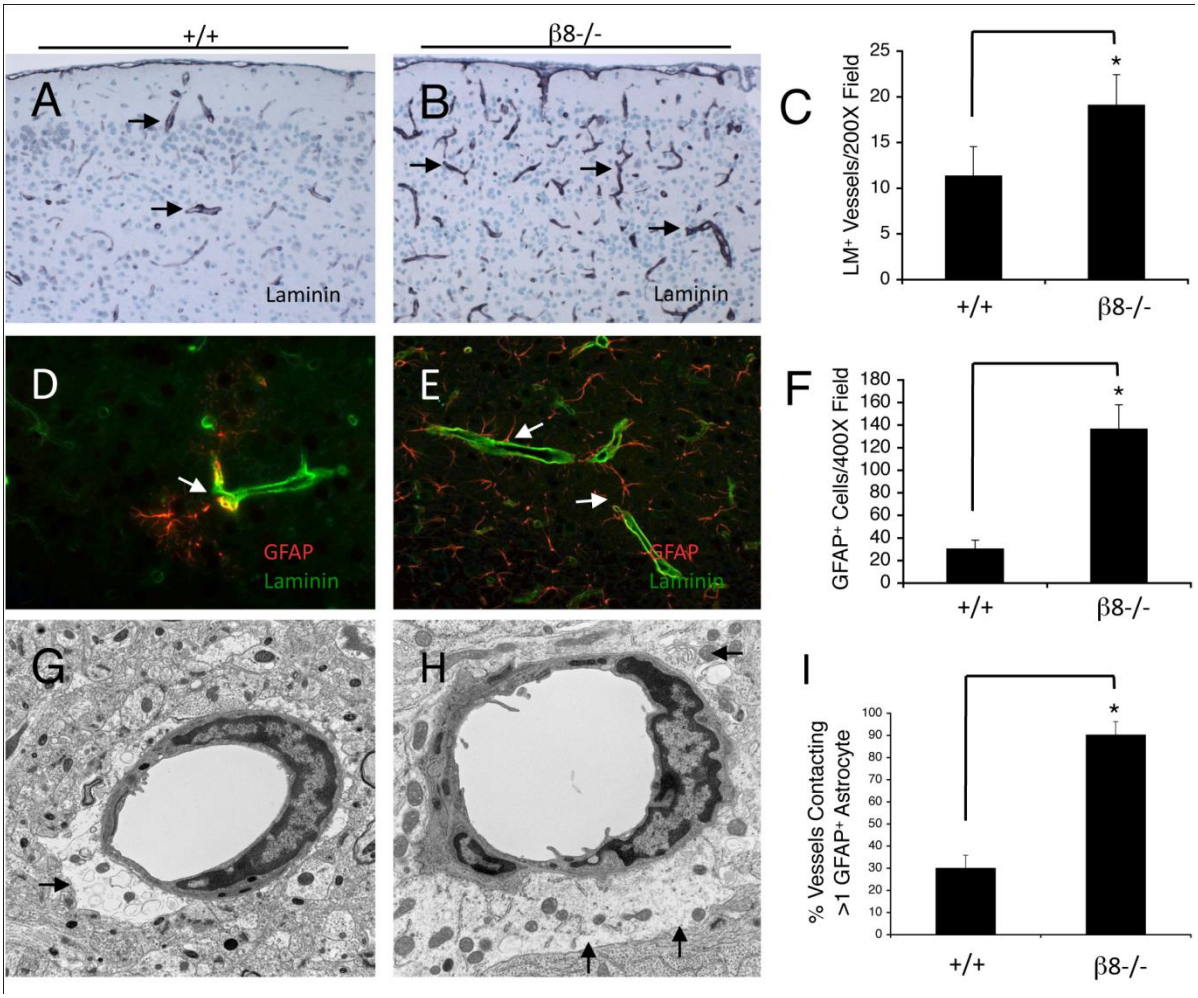
+/+
β8-/-
A
B
Laminin
Laminin
C
LM+ Vessels/200X Field
25
20
15
10
5
0
*
+/+
β8-/-
D
E
GFAP
Laminin
GFAP
Laminin
F
GFAP+ Cells/400X Field
180
160
140
120
100
80
60
40
20
0
*
+/+
β8-/-
G
H
I
% Vessels Contacting
>1 GFAP+ Astrocyte
100
90
80
70
60
50
40
30
20
10
0
*
+/+
β8-/-

Figure 7

Increased reactive astrocyte coverage was possibly due to a compromised blood brain barrier (BBB) in an attempt to correct the defect. Closer examination of the vasculature was necessary to determine if the blood brain barrier was properly regulated in the adult β8-/- brain. Wild type and β8-/- mice were perfused with amine-reactive biotin and brain sections were immunostained with fluorescently labeled streptavidin (Figure 8 A-D). The amine-reactive biotin is a small molecule that binds to free amine groups, and is incapable of crossing the blood brain barrier under normal conditions. However, under pathological conditions in which the BBB is disrupted biotin is seen within the brain parenchyma (108). In both wild type (Figure 8A) and mutant (Figure 8C) cortical brain sections biotin remained in the vessels and showed no signs of leaking out. In contrast, periventricular regions of both wild type and β8-/- mice showed passage of biotin into the brain parenchyma. This finding is consistent with a recent report indicating that vasculature within the periventricular region has increased BBB permeability (42). Further BBB analysis was done with immunostaining for the tight junction protein zona occludin-1 (ZO-1). Similar staining patterns were observed for both wild type (Figure 8E) and β8-/- (Figure 8F) mice. Other tight junction proteins, occludin and claudin-5 were immunoblotted, using wild type and mutant cortical brain lysates (Figure 8G), however, no differences were detected. These results indicate that while there is a vascular defect in the adult β8-/- brain, the BBB is intact.

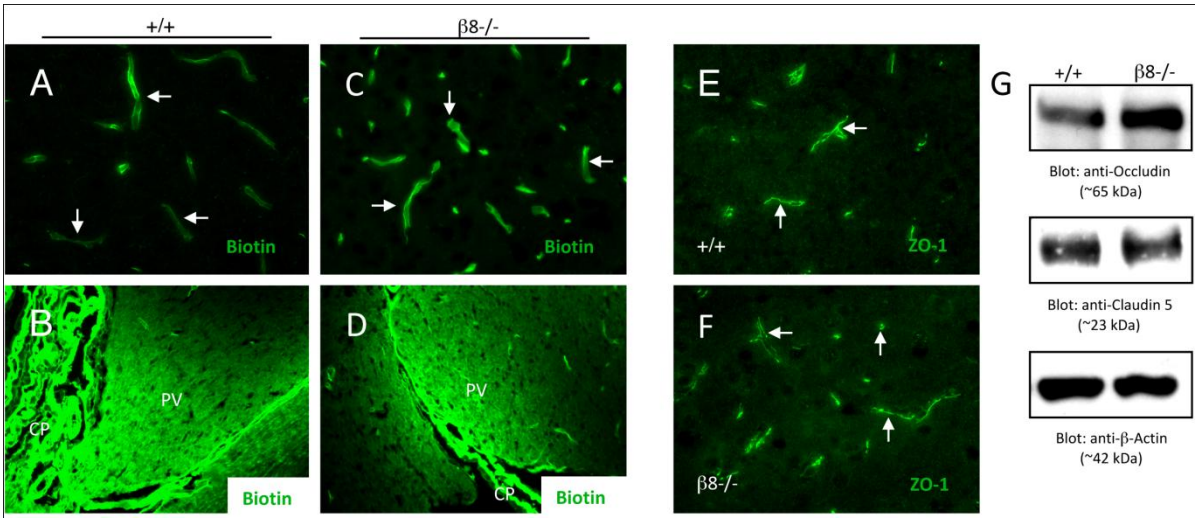

Figure 8: Blood Brain Barrier Intact in Adult β8 -/- Mice

(A-D) Wild type and β8 -/- at P60 were perfused with amine-reactive biotin and brain sections were labeled with fluorescently labeled streptavidin. In both wild type (A) and mutant (C) cortical regions biotin labels endothelial cells (arrows) and did not diffuse out of the blood vessels. However, in the periventricular (PV) region both wild type (B) and mutant (D) mice show equal permeability to the biotin. **(E,F)** Cortical sections of wild type (E) and β8 -/- (F) brains immunostained with anti-zona occluding 1 (ZO1), a tight junction marker. No obvious defects in tight junctions were noticed in the mutant mice. **(G)** Western blotting was performed on cortical lysates from wild type and β8 -/- brains probing with anti-occludin, anti-claudin and anti-actin.

Olfactory Bulbs are Size Reduced in Adult β8-/- Mice

Gross analysis of wild type and β8-/- brains revealed the mutant brain weight was about 15% less than that of the wild type brain. Additional analysis of olfactory bulbs (OB) in wild type (Figure 9A) and mutant (Figure 9B) mice (n=3 for both) revealed approximately 50% smaller OBs in the β8-/- brain. Microscopic analysis of the OB revealed a normal cytoarchitecture in mutants similar to that seen in wild type mice (Figure 9C). However, β8-/- mouse OBs had fewer neuroblasts entering via the RMS (Figure 9E, arrowheads), as detected with anti-DCX immunostaining. Neuroblasts enter the OB after tangential migration along the RMS and then migrate radially to the granule cell layer upon differentiation into interneurons (109). Analysis of granule cell layers did not show any differences between wild type and mutant (Figure 9D, E, arrows).

Figure 9: Olfactory Bulbs in Adult β8 -/- Mice Show Reduced Size.

(A,B) Gross images of wild type (A) and β8 -/- (B) mouse brain at P90 reveals smaller olfactory bulbs in the β8 -/- mice. **(C)** Images of H&E stained sagittal sections of P90 wild type and β8 -/- olfactory bulbs. β8 -/- olfactory bulbs, even though smaller, show normal cytoarchitecture. Abbreviations: GLO, glomerular layer; EPL, external plexiform layer; MCL, mitral cell layer; IPL, internal plexiform layer; GCL, granule cell layer; RMS, rostral migratory stream. **(D,E)** Immunostaining of sagittal sections through wild type and β8 -/- olfactory bulbs (OB) with anti-doublecortin (DCX)(green) to label neuroblasts and neurons, and anti-GFAP (red) to label astrocytes. Arrowheads show decreased DCX-positive cells coming into the OB along the rostral migratory stream (RMS) in β8 -/- mice.

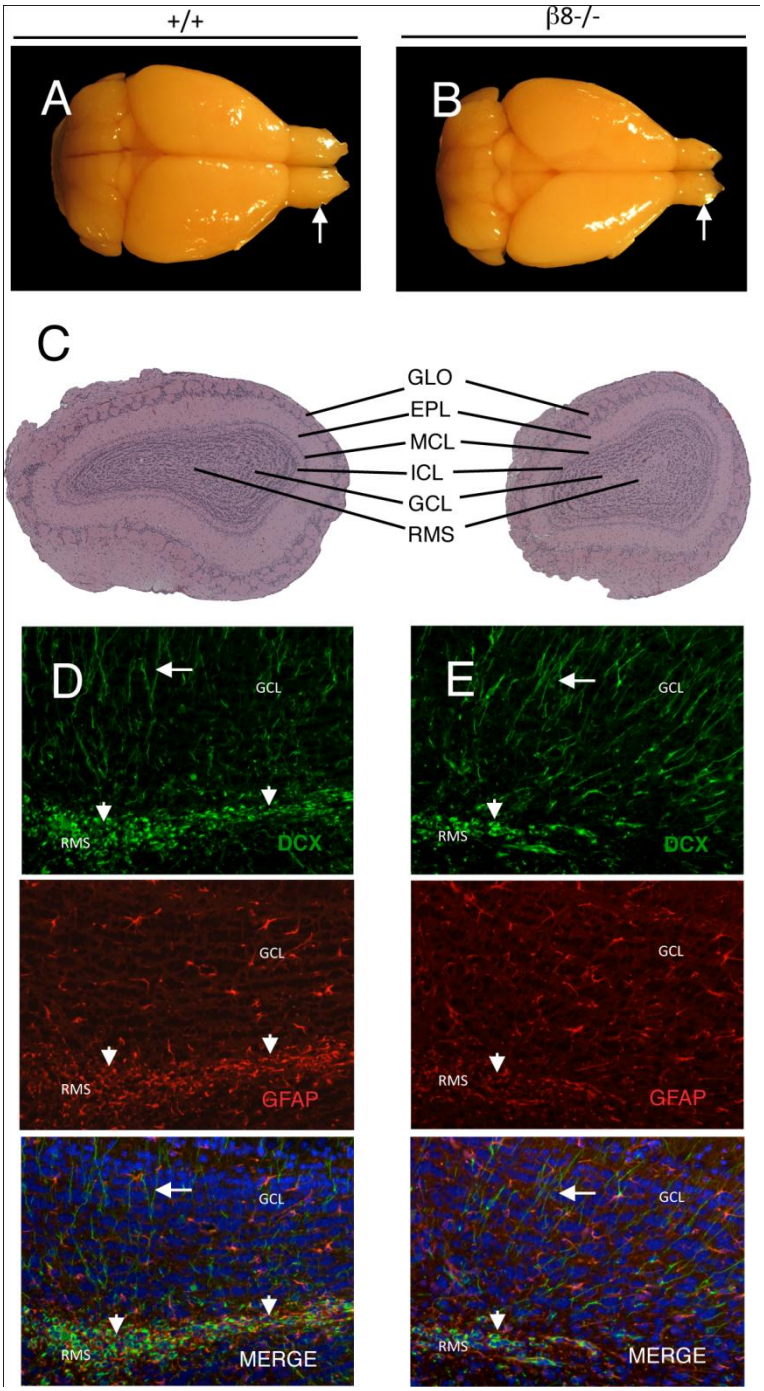
+/+
β8-/-
A
B
C
GLO
EPL
MCL
ICL
GCL
RMS
D
GCL
RMS
DCX
E
GCL
RMS
DCX
GCL
RMS
GFAP
GCL
RMS
GFAP
GCL
RMS
MERGE
GCL
RMS
MERGE

Figure 9

β8-/- Mice Have Defects in the SVZ and RMS.

Small olfactory bulbs have been noted in several mutant mouse models with abnormal SVZ neurogenesis including β1 integrin and neural cell adhesion molecule mutant mouse models (110, 111). Therefore, H&E stained, and DCX and GFAP immunostained sagittal sections from wild type and β8-/- mice were analyzed for SVZ and RMS defects. Analysis of SVZ regions revealed abnormal cytoarchitecture (Figure 10B). Quantitation of DCX positive cells within the SVZ showed a three-fold increase in neuroblasts in the mutant when compared to the wild type SVZ (Figure 10C). DCX positive cells in the SVZ were found mostly in clusters, supporting the integrin dependence of cells in the SVZ. Furthermore, analysis of the RMS in wild type (Figure 10D) and mutant (Figure 10E) mice with H&E staining revealed abnormalities in cells leaving the SVZ in β8 null mice. Width of the RMS was analyzed using immunostaining for neuroblasts and astrocytes (DCX and GFAP, respectively). Mutant mice showed a threefold wider RMS when compared to wild type.

To further analyze the role of αvβ8 integrin in the SVZ, P60 mice were injected with BrdU once per day for two consecutive days. Mice were then perfused and brains were sagittally sectioned and immunostained with anti-BrdU antibody to show proliferating cells within the SVZ. BrdU positive cells in wild type (Figure 11A) and β8-/- (Figure 11B) mice SVZs were quantified revealing a greater than two-fold reduction in proliferating cells within the SVZ in mutant brains (Figure 11C). Interestingly, some BrdU positive cells were noted in the RMS of mutant mice, suggesting that neuroblast migration is not totally defective in β8-/- mice.

Electron microscopy was used to analyze cytoarchitecture of cells within the SVZ. Wild type SVZ showed a normal neurovascular niche made up of clusters of A cells (neuroblasts), with B cells (SVZ astrocytes) and C cells (transit amplifying cells), making up distinct units (Figure 11D). In contrast, these cellular units were rarely seen in the β8-/- SVZ (Figure 11E). Many apoptotic cells were also seen within the mutant SVZ as indicated by the arrows in figure 11E. In order to quantitate apoptotic cells, a TUNEL assay was performed on wild type and β8-/- sagittal sections and TUNEL positive cells were counted. β8-/- brains showed a marked increase in apoptotic cells (Figure 11F).

Figure 10: Subventricular Zone and Rostral Migratory Stream Defects in Adult β8 -/- Mice.

(A,B) Sagittal sections of P90 wild type (A) and β8 -/- (B) brains were H&E stained or immunostained with anti-DCX (green) and anti-GFAP (red) to show SVZ cytoarchitecture and identify neuroblasts and SVZ astrocytes. β8 -/- mice show abnormal SVZ cytoarchitecture (arrow) as well as a increased numbers of DCX positive cells in the SVZ. **(C)** Quantitation of DCX positive cells in the SVZ of wild type and mutant mice. p-value is less than 0.001. **(D,E)** Sagittal sections of P90 wild type (D) and β8 -/- (E) mouse brains were H&E stained to show cytoarchitecture of RMS, or immunostained with anti-DCX (green), to reveal migrating neuroblasts, and anti-GFAP (red) to reveal astrocytes making up the glial sheath. Notice the apparent disorganization of the neuroblasts and glial sheath in the mutant mouse compared to the wild type. **(F)** RMS widths were measured in control and mutant mice sagittal brain sections. P-value less than 0.005. Abbreviations: v, ventricle; SCJ, striatocortical junction; DCX, doublecortin; GFAP, glial fibrillary acidic protein.

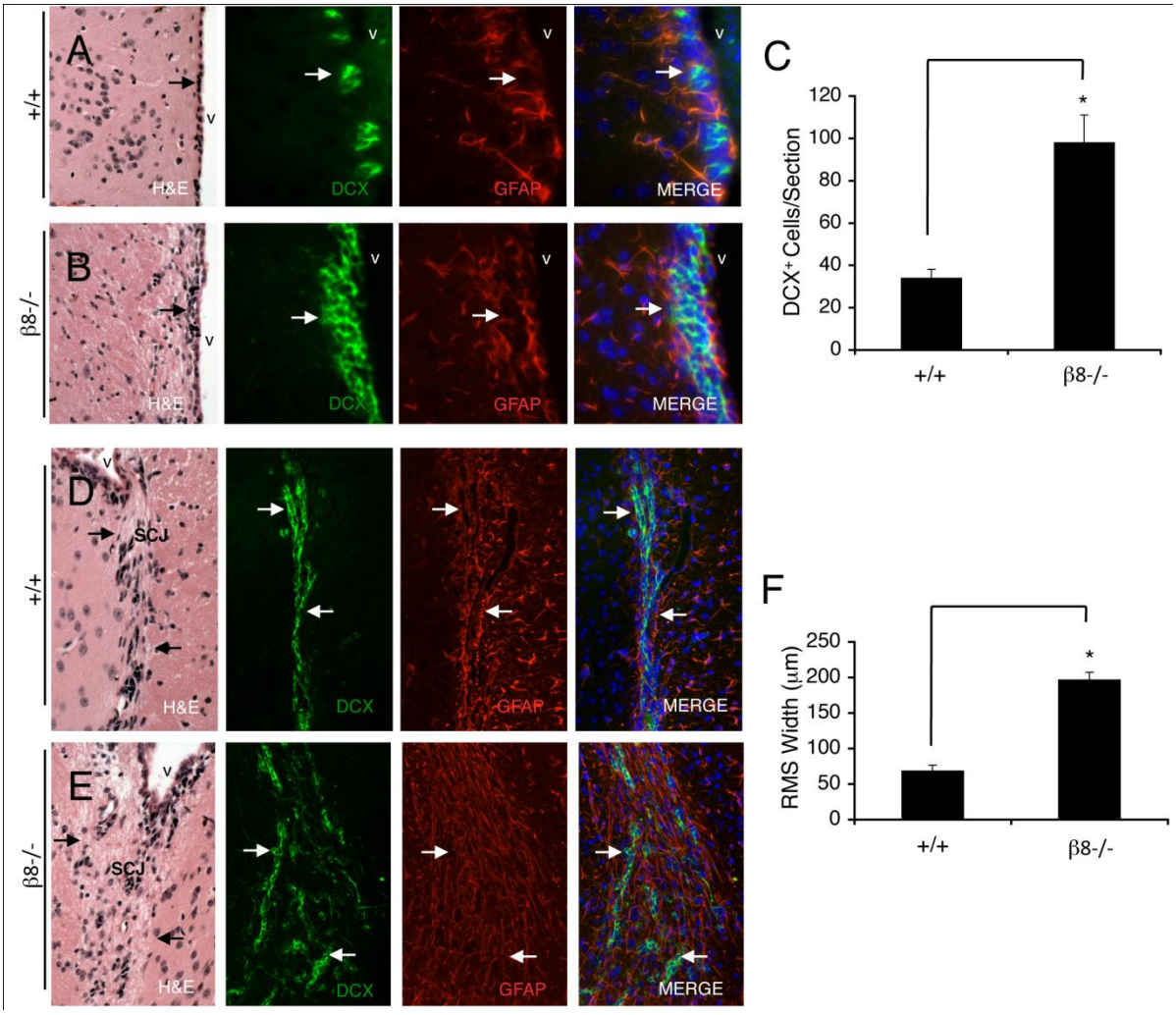
A
B
C
D
E
F
+/+
β8-/-
H&E
DCX
GFAP
MERGE
v
SCJ
DCX+ Cells/Section
RMS Width (μm)
120
100
80
60
40
20
0
250
200
150
100
50
*

Figure 10

Figure 11: Proliferation and Survival Defects in Cells of the SVZ.

(A,B) Sagittal sections of P90 brains from wild type (A) and β8 -/- (B) mice that were injected with BrdU before perfusion. Sections were stained with an anti-BrdU antibody to reveal proliferating cells. Dashed lines show the boundary of the ventricle. **(C)** Quantitation of number of proliferating cells in the SVZ. Note that β8 -/- mice show significant decrease in proliferation of cells within the SVZ. *$p < 0.001$ compared to wild type. **(D,E)** Electron microscopy was used to show cytoarchitecture of P90 wild type (D) and β8 -/- (E) mouse SVZ. Wild type SVZ shows clusters of type a, b and c cells, while the mutant mice show abnormal cytoarchitecture and increased numbers of apoptotic cells. **(F)** Coronal sections of wild type and β8 -/- mouse brains were labeled with TUNEL kit to show apoptotic cells in the SVZ. Increased apoptosis was seen in the mutant mouse SVZ. *$p < 0.001$. Abbreviations: V, ventricle; BrdU, bromodeoxyuridine; a, SVZ type a neuroblast; b; SVZ neural stem cell; c, SVZ transit amplifying cell.

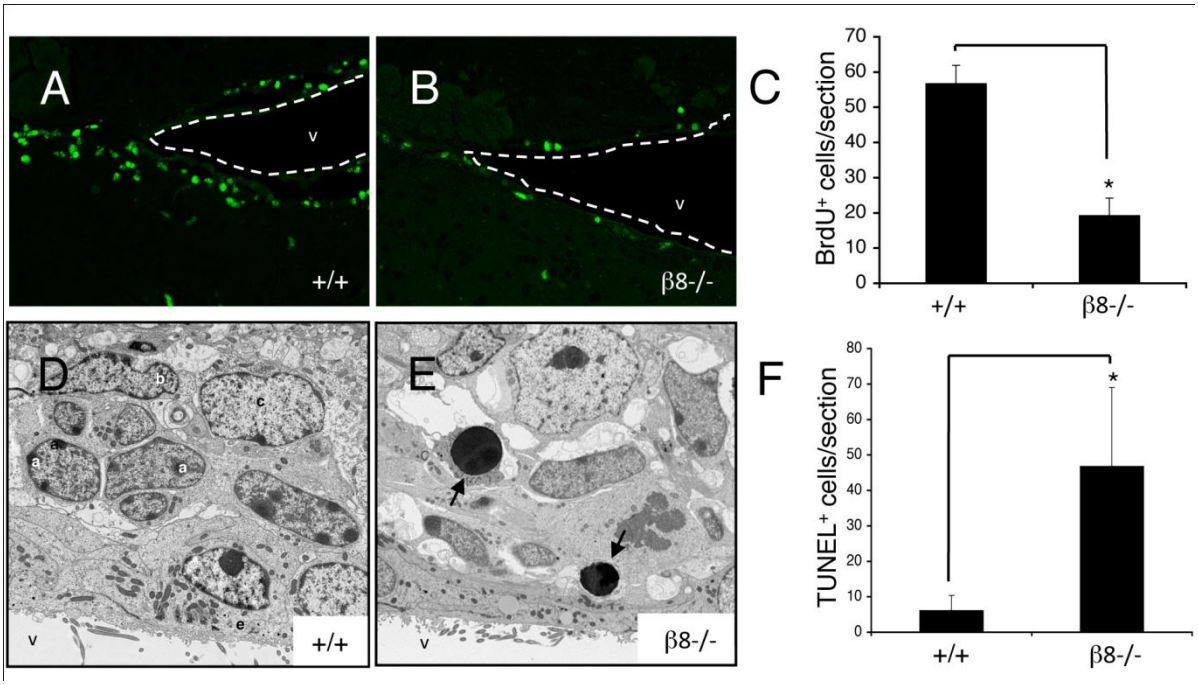
A
v
+/+
B
v
β8-/-
C
BrdU+ cells/section
70
60
50
40
30
20
10
0
*
+/+
β8-/-
D
b
c
a
a
a
e
v
+/+
E
v
β8-/-
F
TUNEL+ cells/section
80
70
60
50
40
30
20
10
0
*
+/+
β8-/-

Figure 11

Inducible Deletion of β8 Integrin in NSCs in the Adult Mouse Shows Similar SVZ Defects to Complete Knockouts

Recently developed transgenic mouse strains, including GLAST-CreERT2 (28) and GFAP-CreERT2 (112), allow for temporal and spatial control of gene deletion through expression of Cre-recombinase coupled to the ligand binding domain of the human estrogen receptor (113). In the absence of tamoxifen, an estrogen derivative, CreERT2 forms a complex with heat shock proteins in the cytosol and recombination cannot occur. When tamoxifen is administered CreERT2 undergoes a conformational change allowing translocation to the nucleus and Cre-recombinase activation followed by gene recombination.

Targeted gene deletion of GLAST-CreERT2 mice was assessed through the use of the reporter Rosa26 mouse strain. This strain expresses β-galactosidase (encoded by bacterial lacZ gene) under control of the Rosa26 promoter. In the absence of Cre expression, lacZ transcription is blocked by an upstream transcription termination codon flanked by a lox-P site (lox-STOP-lox). Cre-mediated excision of the stop codon allows for lacZ expression, which can be analyzed by an enzymatic X-gal assay (114). Alternatively, confocal microscopy can be used to identify the fluorescent product generated from the lacZ/X-gal enzymatic reaction, which fluoresces using the Cy5 channel (633nm).

After X-gal enzyme staining, Cre-positive cells appear blue upon gross examination. Analysis of GLAST-CreERT2+; Rosa+ brains 30 days after tamoxifen injections, revealed Cre-positive cells in both neurogenic regions of the adult brain, the SVZ (Figure 12C) and the DG (Figure 12D). Further analysis of cell specificity

within the SVZ was performed through triple immunostaining. Anti-GFAP and anti-DCX antibodies were used to show expression of type B and type A cells within the SVZ, in brain sections from X-gal stained mice. Colocalization was seen of the LacZ product with GFAP and DCX positive cells indicating the NSC population was properly targeted within the SVZ (Figure 12E).

β8 flox/flox mice, harboring two loxP sites flanking exon four, were crossed to GLAST-CreERT2 mice to generate control (Cre+, β8fl/+) and mutant (Cre+, β8fl/-) mice. IP injections of tamoxifen were administered to P28 mice, twice daily for five consecutive days to allow Cre expression and recombination (Figure 12A, B). Control and mutant mice were sacrificed 30 days after the last injection and brains were analyzed for proliferation, apoptosis and cell markers. Quantitation of Ki67 immunofluorescence revealed a significant decrease in proliferation in mutant mice as compared to controls (Figure 13A). Similarly, TUNEL staining, a method to analyze apoptotic cells, showed an increase in apoptotic cells in the SVZ of mutant mice (Figure 13B). Furthermore, immunofluorescence for markers of the SVZ type A and type B cells showed significantly more DCX-expressing, type A cells within the SVZ of mutant mice (Figure 13C). Similar levels of GFAP-expressing, type B cells were observed in both control and mutant mice (data not shown). These data are consistent with the results seen in the adult complete knockout SVZ indicating that these defects are not secondary to the developmental vascular defects.

Figure 12: Strategy to Delete β8 Integrin Gene Acutely in NSCs and Astroglia.

(A) Transgenic mice expressing the CreERT2 fusion protein under control of the GLAST promoter were bred with mice harboring a conditional (floxed) β8 integrin gene. Under normal conditions Cre-recombinase is inactive but upon IP injection of tamoxifen, Cre-recombinase is activated and subsequently the β8 gene is deleted. **(B)** P29 control and mutant mice are injected twice daily for five consecutive days with tamoxifen. Thirty days after the last tamoxifen injection, mice were sacrificed and brains were analyzed. **(C, D, E)** GLAST-CreERT2; ROSA26 mice were injected with tamoxifen and perfused 30 days after the last injection. (C, D) brains were sections coronally and stained using the X-gal procedure. Sections from the SVZ (C) and Dentate Gyrus (DG) (D) show blue cells indicating Cre expression in the neurogenic regions of the adult brain. (E) Confocal microscopy analysis of the LacZ signal shows cell type specific Cre expression. Sections were stained with GFAP (red) and DCX (blue) with LacZ expression (green). LacZ expression was seen in both GFAP positive and DCX positive cells indicating the NSCs are being targeted.

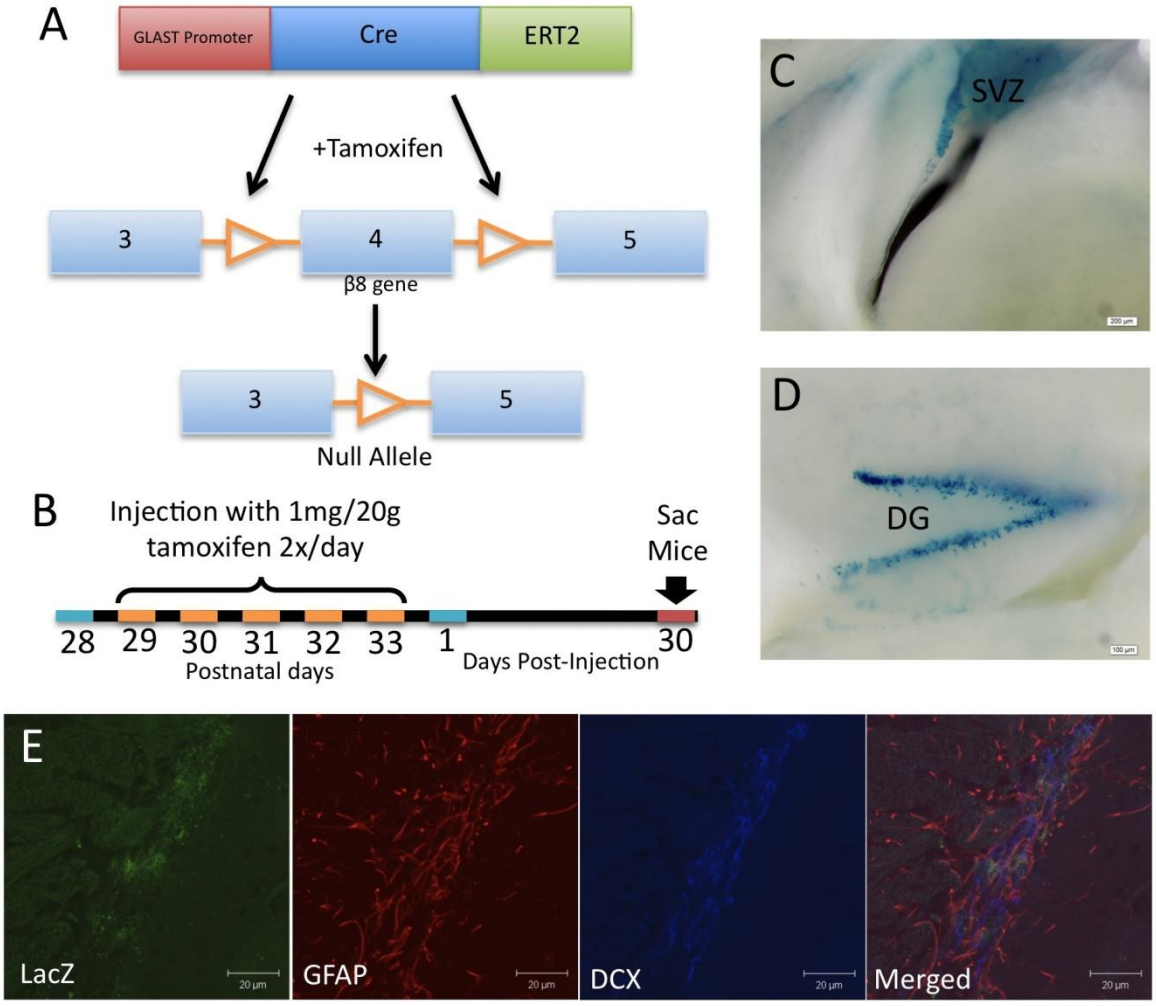
A
GLAST Promoter
Cre
ERT2
+Tamoxifen
3
4
5
β8 gene
3
5
Null Allele
B
Injection with 1mg/20g
tamoxifen 2x/day
Sac
Mice
28 29 30 31 32 33 1 30
Postnatal days
Days Post-Injection
C
SVZ
D
DG
E
LacZ
GFAP
DCX
Merged

Figure 12

Figure 13: Analysis of SVZ Cells in GLAST-CreERT2 Mice Reveal Similar Defects as Those Seen in Complete β8 -/- Mice.

GLAST-CreERT2 control (β8 fl/+; n=4) and mutant (β8 fl/-; n=4) mice were injected with tamoxifen and perfused 30 days after the last injection. **(A)** Coronal sections were immunostained with anti-Ki67 and Ki67 positive cells within the SVZ were quantified. *$p < 0.01$. **(B)** Tunel assay was performed on coronal sections from control and mutant mice to analyze apoptotic cells. Tunel positive cells from the SVZ were quantified. *$p < 0.05$. **(C)** Coronal sections from control and mutant mice were immunostained with anti-DCX to look at neuroblasts within the SVZ. Doublecortin positive neuroblasts were quantified. *$p < 0.001$.

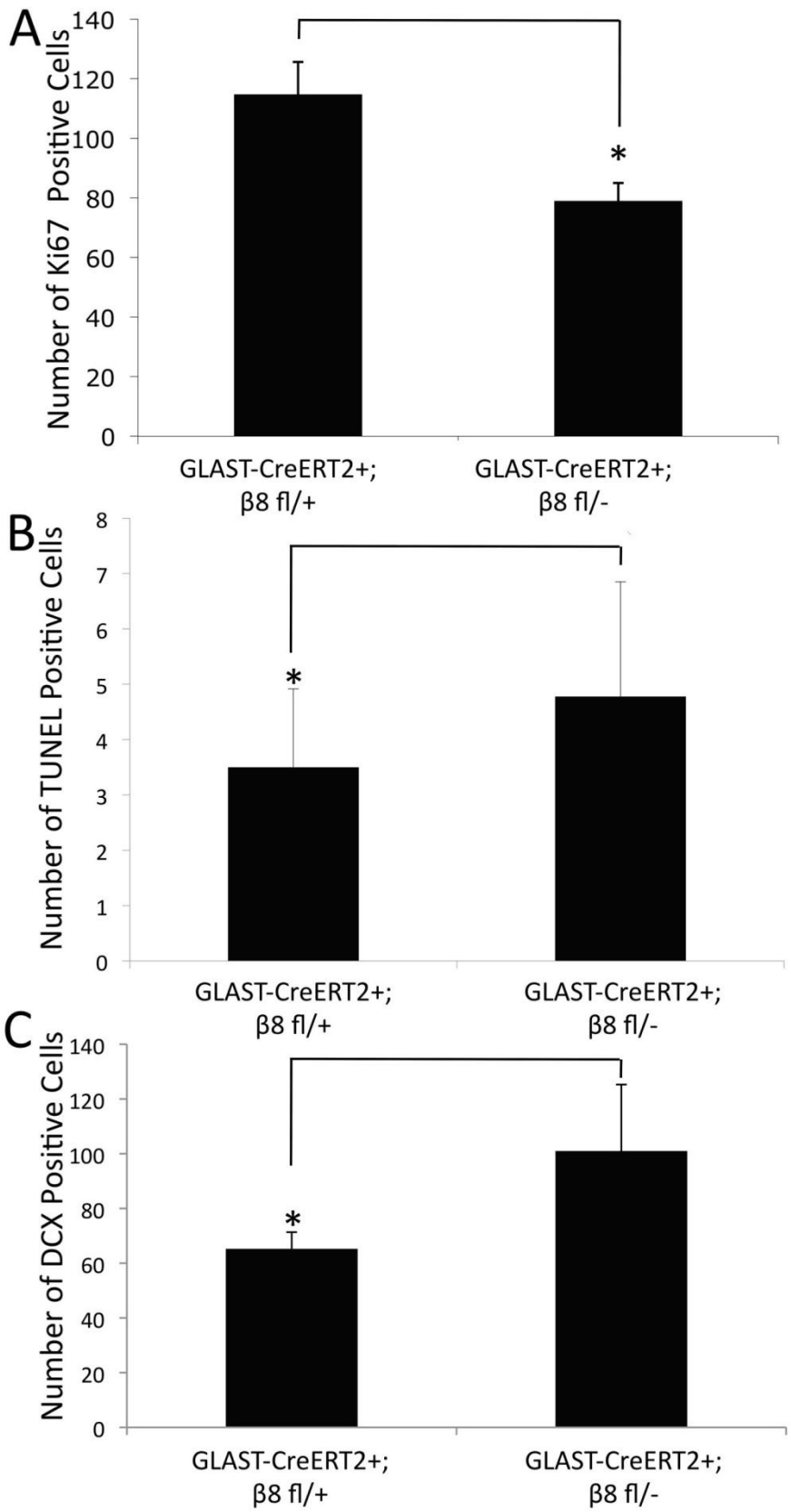
A
Number of Ki67 Positive Cells
140
120
100
80
60
40
20
0
*
GLAST-CreERT2+;
β8 fl/+
GLAST-CreERT2+;
β8 fl/-
B
Number of TUNEL Positive Cells
8
7
6
5
4
3
2
1
0
*
GLAST-CreERT2+;
β8 fl/+
GLAST-CreERT2+;
β8 fl/-
C
Number of DCX Positive Cells
140
120
100
80
60
40
20
0
*
GLAST-CreERT2+;
β8 fl/+
GLAST-CreERT2+;
β8 fl/-

Figure 13

***In Vitro* Neurosphere Analysis Reveals Role for αvβ8 Integrin in Proliferation and Differentiation.**

Neurospheres were cultured from P60 wild type and β8-/- mouse SVZ using methods previously described (96). After culturing neurospheres it was necessary to confirm expression of NSC markers to be certain that the proper cell population was isolated. Many markers have been established in stem cell populations including: CD133 (115), musashi1 (116), sox2 (117) and BMI-1 (118). cDNA was isolated from both wild type and β8-/- neurospheres and semi-quantitative rtPCR was performed to look for these markers (Figure 14A). Expression of integrin αv and the β8 subunits in neurospheres was assessed with immunostaining with anti-αv and anti-β8 integrin antibodies. Wild type neurospheres expressed both αv and β8 integrin, while β8-/- neurospheres only expressed αv as expected (Figure 14B). These results are consistent with previous reports indicating expression of αv and β8 mRNA in embryonic neurospheres (51).

NSCs were isolated from the SVZ of P60 wild type and β8-/- mice, and cultured as free-floating neurospheres. In comparison to wild type neurospheres (Figure 15A), mutant neurospheres (Figure 15B) appeared smaller and less dense. To confirm the difference in size, diameters of both wild type (n=100) and β8-/- neurospheres (n=100) were quantitated (Figure 15C). Short-term proliferation in neurospheres was quantified by allowing single cells from dissociated wild type and mutant neurospheres to adhere to laminin coated coverslips and then pulsing with BrdU-containing media for 1 hour. Quantitation was performed with an anti-BrdU antibody at 24 and 96 hours after the initial BrdU pulse. At both time points β8-/-

NSCs showed decreased proliferation when compared to wild type cells (Figure 15D).

We further assessed proliferation and self-renewal in neurospheres. Wild type and β8-/- neurospheres of similar diameters were selected and dissociated and the ability to self renew was determined over seven passages. Secondary spheres formed after every passage were quantified (Figure 15E). β8 null neurospheres showed a defect in the ability to form secondary spheres, as compared to the wild type neurospheres. This defect was enhanced after several passages and by the seventh passage no spheres reformed in the mutant population. Additionally, proliferation of the NSCs cultured *in vitro* was examined over several passages. $5x10^5$ cells from dissociated wild type or β8-/- neurospheres were plated. After 7 days the spheres were dissociated and the total number of cells was quantified and $5x10^5$ cells were replated. This was repeated for 10 consecutive passages. In comparison to wild type cells, the increase in cell number was significantly less in mutant cells, and the decrease became more pronounced in later passages (Figure 15F). These results indicate β8 plays a significant role in NSC self-renewal and proliferation *in vitro* and correlates with *in vivo* findings.

Differentiation of NSCs was evaluated in wild type and mutant neurospheres. NSCs were plated on laminin-coated glass coverslips and differentiated through addition of 10% FBS to the culture media. Upon differentiation, cells were immunoblotted for neuronal (Tuj1) and glial (GFAP) markers (Figure 16 A,B). Total cells per field were counted and percentage of cells expressing each marker was quantified (Figure 16C). β8-/- NSCs showed more neuronal differentiation as

compared to wild type NSCs. This indicates that β8 integrin has a crucial role in NSC differentiation *in vitro*, similar to the increase in neuroblast differentiation in the SVZ of the β8-/- mouse brain.

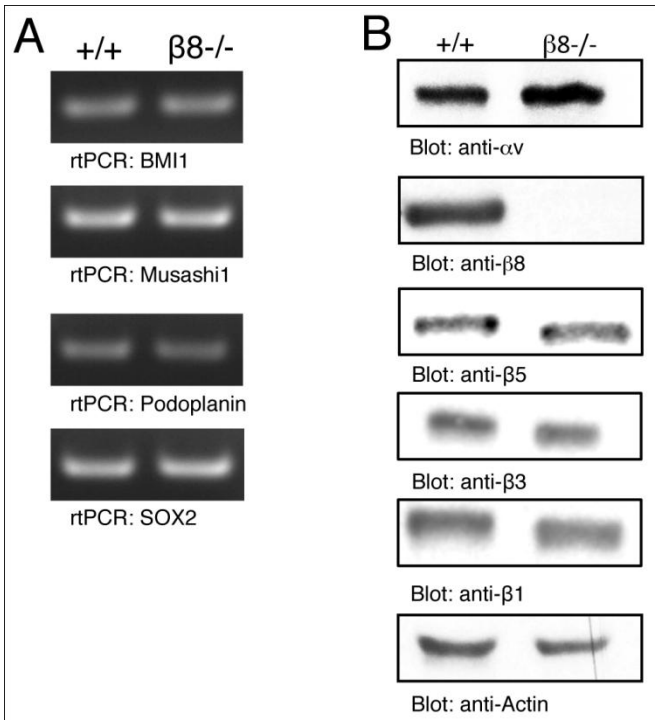

Figure 14: Expression of NSC Markers and Integrin Subunits.

(A) To analyze expression of neural stem cell markers cDNA was isolated from wild type and β8-/- adult neurospheres. Semi-quantitative reverse transcriptase PCR (rtPCR) was performed for BMI-1, musashi1, Podoplanin and SOX2. Both wild type and mutant neurospheres showed similar expression of all markers analyzed, confirming that they are stem cells. **(B)** Expression of αv and the β subunits binding with αv was analyzed. Lysates were made from wild type and β8-/- neurospheres and immunoblotted with; anti-αv, anti-β1, anti-β3, anti-β5, and anti-β8 antibodies. Anti-actin was used as a loading control. Similar expression was seen for αv and all of the β-subunits, with the exception of β8, which showed no expression in the mutant neurospheres as expected.

Figure 15: β8 integrin Regulates NSC Proliferation and Self-Renewal *In Vitro*.

(A,B) Neural stem and progenitor cells were cultured as neurospheres from the SVZ of P60 wild type (A) and β8 -/- (B) mice. **(C)** Diameters of wild type and mutant neurospheres were measured and quantified. Mutant neurospheres were significantly smaller when compared to wild type. *p < 0.001. **(D)** Short term proliferation was analyzed with a 1 hour BrdU pulse in both wild type and β8-/- neurospheres, then washed out with fresh media. Spheres were fixed and stained at 24 or 96 hours after BrdU pulse, and immunostained with an anti-BrdU antibody. β8-/- neurospheres showed a marked decrease in proliferation at both 24 and 96 hour timepoints. *p < 0.05. **(E)** A self-renewal assay was performed in which secondary spheres forming from a single sphere were counted after seven each of seven sequential passages. β8 -/- neurospheres show a progressive decline in the ability to self-renew. *p < 0.001. **(F)** A Proliferation assay was performed in which $5x10^5$ individual NSCs were plated and total cell number minus the starting cell number was quantified through ten sequential passages. Mutant NSCs show a progressive decline in proliferation over time. *p < 0.05.

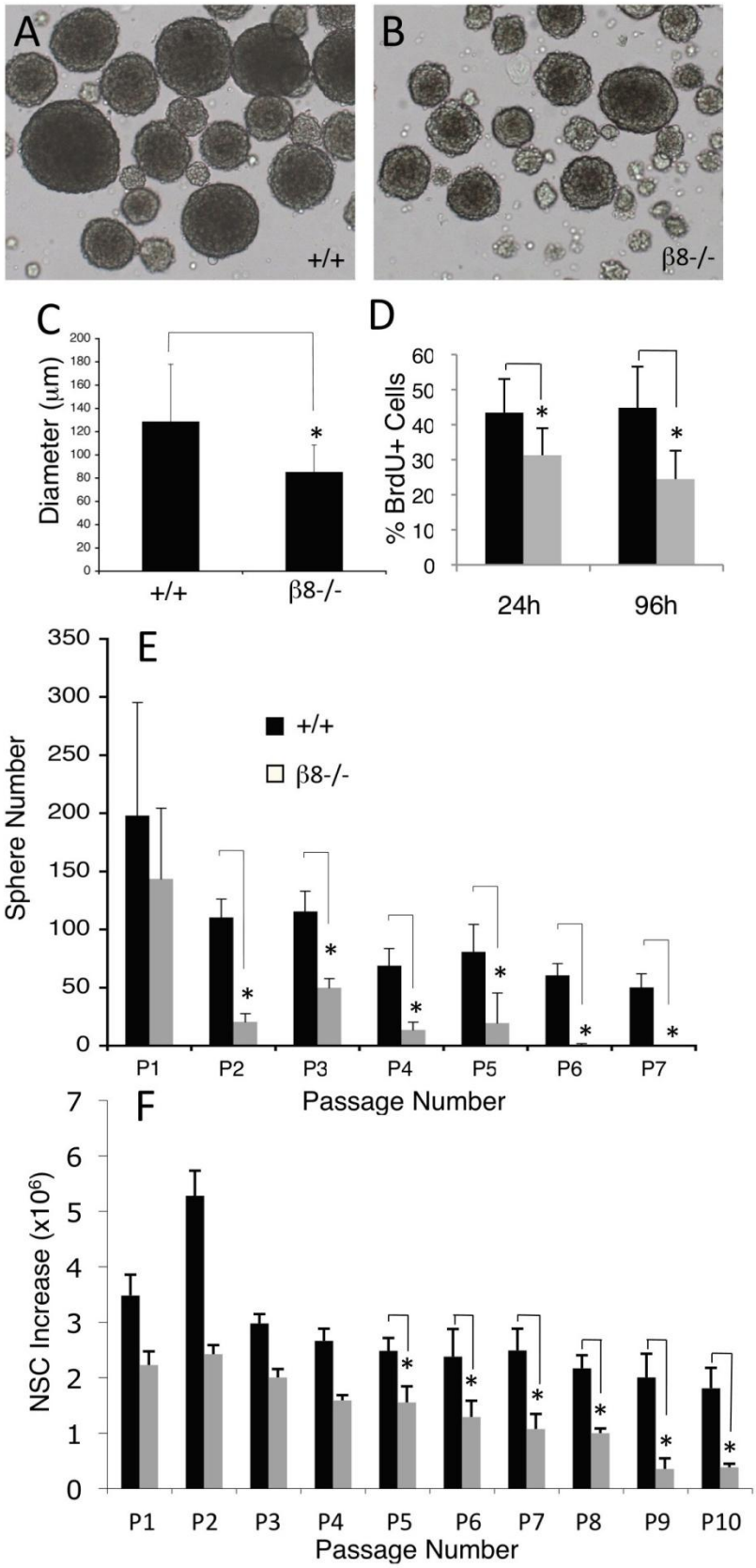
A
+/+
B
β8-/-
C
Diameter (μm)
200
180
160
140
120
100
80
60
40
20
0
*
+/+
β8-/-
D
% BrdU+ Cells
60
50
40
30
20
10
0
*
*
24h
96h
E
Sphere Number
350
300
250
200
150
100
50
0
+/+
β8-/-
*
P1
P2
P3
P4
P5
P6
P7
Passage Number
F
NSC Increase (x10⁶)
7
6
5
4
3
2
1
0
*
P1
P2
P3
P4
P5
P6
P7
P8
P9
P10
Passage Number

Figure 15

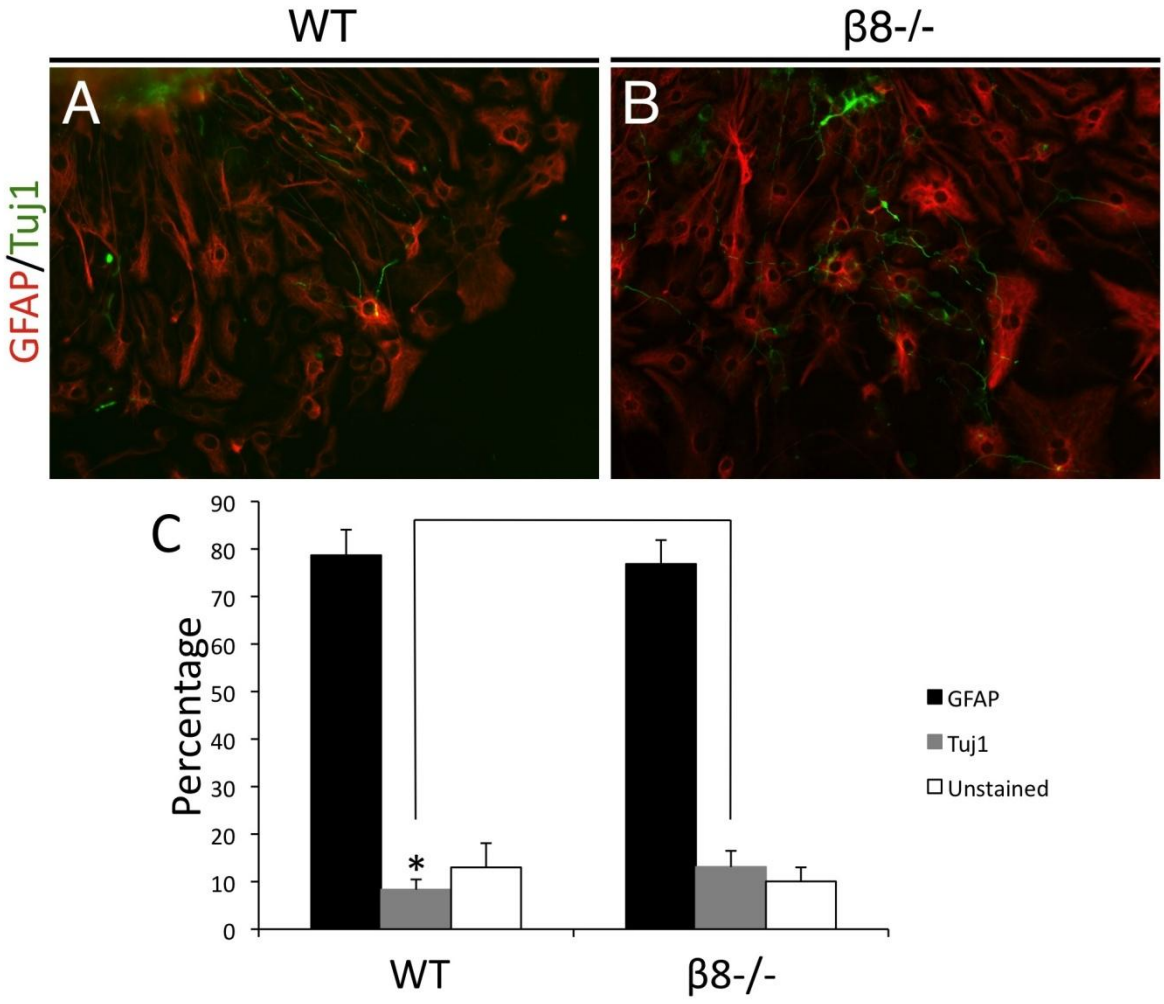

Figure 16: αvβ8 Integrin Regulates NSC Differentiation.

(A,B) Neurospheres from P60 wild type (A) and β8 -/- (B) mice were plated on laminin coated coverslips and differentiated with addition of serum for 5 days. Cells were then stained to visualize astrocytes (GFAP, red) and neurons (Tuj1, green). **(C)** Quantitation of integrin-dependent neurosphere differentiation. *$p < 0.05$.

αvβ8 Integrin Mediated TGFβ Activation in Neurospheres

To address the mechanisms by which αvβ8 integrin regulates NSC proliferation and survival in the adult brain, αvβ8 integrin-dependent latent TGFβ activation was analyzed. αvβ8 integrin is a receptor for the latent forms of TGFβ's 1 and 3 and integrin adhesion leads to the activation of TGFβ's (82, 83). To confirm the ability of αvβ8 integrin to activate TGFβ, 293T cells were stably transfected with a plasmid expressing human β8 integrin fused with a V5 tag (β8V5). Expression of β8 was confirmed with western blot using an anti-β8 antibody (Figure 17A). Exogenous expression of β8 integrin in 293T cells, which express no endogenous β8, made it possible to assess the role β8 plays in activation of TGFβ. A plasmid containing the plasminogen activator inhibitor promoter fused to firefly luciferase (Pai-1 Luc) (97) was transfected into 293T cells with and without β8 expression. Purified latent TGFβ (LAP-TGFβ) (10ng/ml) was added and luciferase activity was read 16 hours later. Indeed 293T cells expressing the β8V5 plasmid showed enhanced activation of TGFβ from its latent form when compared to normal 293T cells (Figure 17B).

While integrin-mediated activation of TGFβ has been confirmed, the significance of the activation has not been analyzed in the adult brain, and more specifically in the neurovascular niche. NSCs isolated from the SVZ of P60 wild type and β8-/- mice were used to study this significance. LAP-TGFβ was added to wild type and β8-/- neurospheres at 10ng/ml and 24 hours later conditioned media (CM) was transferred to PAI-1 luciferase transfected 293T cells and luciferase activity was analyzed. Because of the minimal of β8 expression in 293T cells (figure 17A),

they are an excellent cell line to directly assay TGFβ signaling. Wild type spheres exhibited a great induction of TGFβ signaling, as shown by the increased luciferase activity (Figure 18A). In contrast, CM from β8-/- neurospheres showed a very modest level of luciferase activity, due to the loss of αvβ8 integrin. This modest induction of TGFβ signaling could be due to the fact that neurospheres express other integrins including, αvβ1 αvβ3 and αvβ5 (119), which could be activating LAP-TGFβ. Also of note, was the increase in luciferase activity in CM from wild type and mutant neurospheres that had not been treated with LAP-TGFβ, suggesting that there is some endogenous TGFβ produced by the cells that is being activated in an integrin-independent manner. TGFβ-2, which is not activated by αvβ8 integrin but is expressed in neurospheres (120), could also be responsible for the luciferase activity.

To examine whether integrin mediated-TGFβ signaling was acting in an autocrine manner in neurospheres, active TGFβ (10ng/ml) was added to +/+ neurospheres. Also, in an attempt to 'rescue' the self-renewal and proliferation defects, active TGFβ was added to β8-/- neurospheres. Self-renewal was then analyzed to reveal a remarkable inhibition in both wild type and mutant neurospheres (Figure 18B) with TGFβ addition. Similar results in inhibition were noted with doses ranging from 0.01 to 1ng/ml (data not shown). These results are similar to other reports indicating that TGFβ has a negative impact on NSC self-renewal (121-123). Anti-TGFβ blocking antibody was added to wild type neurospheres to determine if blocking TGFβ signaling would have an effect on wild type NSC self-renewal. No significant effect was seen with addition of anti-TGFβ

when compared to untreated and IgG control (Figure 18C). These data suggest that autocrine TGFβ signaling is not required for NSC self-renewal and proliferation.

Figure 17: β8 Integrin is Involved in Activation LAP-TGFβ

(A) 293T cells were transfected with a plasmid expressing β8 integrin with a V5 tag (β8V5). Negative control and β8V5 transfected cell lysates were immunoblotted with anti-β8 integrin to confirm expression of β8 upon transfection. **(B)** 293T cells stably transfected with β8V5 and normal 293T cells were transfected with PAI-1 luciferase construct. Transfected cells were incubated with or without addition of LAP-TGFβ and luciferase activity was measured. Notice that the addition of β8V5 causes a significant increase in the amount of TGFβ activity.

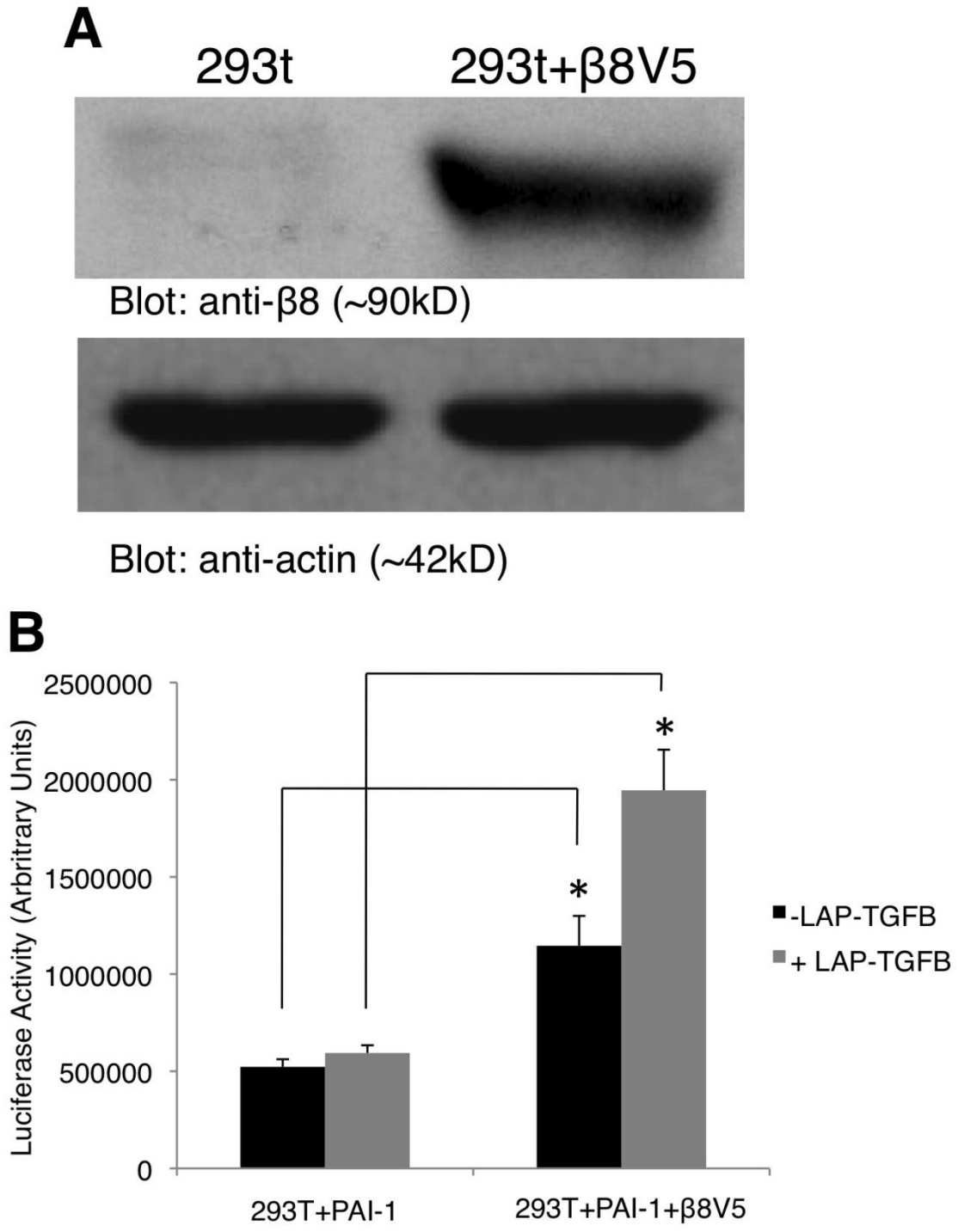
A
293t
293t+β8V5
Blot: anti-β8 (~90kD)
Blot: anti-actin (~42kD)
B
Luciferase Activity (Arbitrary Units)
2500000
2000000
1500000
1000000
500000
0
*
*
-LAP-TGFB
+ LAP-TGFB
293T+PAI-1
293T+PAI-1+β8V5

Figure 17

Figure 18: NSC Proliferation and Self-Renewal are Not Regulated in an Autocrine Fashion Through TGFβ Signaling.

(A) Quantitation of β8 integrin mediated TGFβ activation using a PAI1-luciferase reporter assay. Neurosphere conditioned media from wild type and β8 -/- neurospheres, was transferred to PAI1-luciferase transfected 293T cells and luciferase activity was measured. Wild type neurospheres show a marked increase in activation of TGFβ. In mutant spheres there was significantly less TGFβ activation. *$p < 0.02$, **$p < 0.001$, ***$p < 0.0001$. **(B)** Neurosphere self-renewal and proliferation defects are not rescued by exogenous addition of active TGFβ. Secondary sphere formation from single wild type or mutant neurospheres (with and without TGFβ) was quantified. TGFβ addition inhibited neurosphere formation in both wild type and mutant populations. *$p < 0.001$, **$p < 0.0001$ when compared to wild type untreated neurospheres. **(C)** Inhibition of TGFβ using a blocking antibody does not inhibit NSC self-renewal or proliferation. Wild type neurospheres were treated with IgG control, anti-TGFβ, anti TGFβ in addition to active TGFβ, or active TGFβ alone, and serially passaged for three passages quantifying secondary sphere formation. Only the addition of active TGFβ showed a decrease in neurosphere secondary sphere formation. *$p < 0.0001$ and **$p < 0.001$.

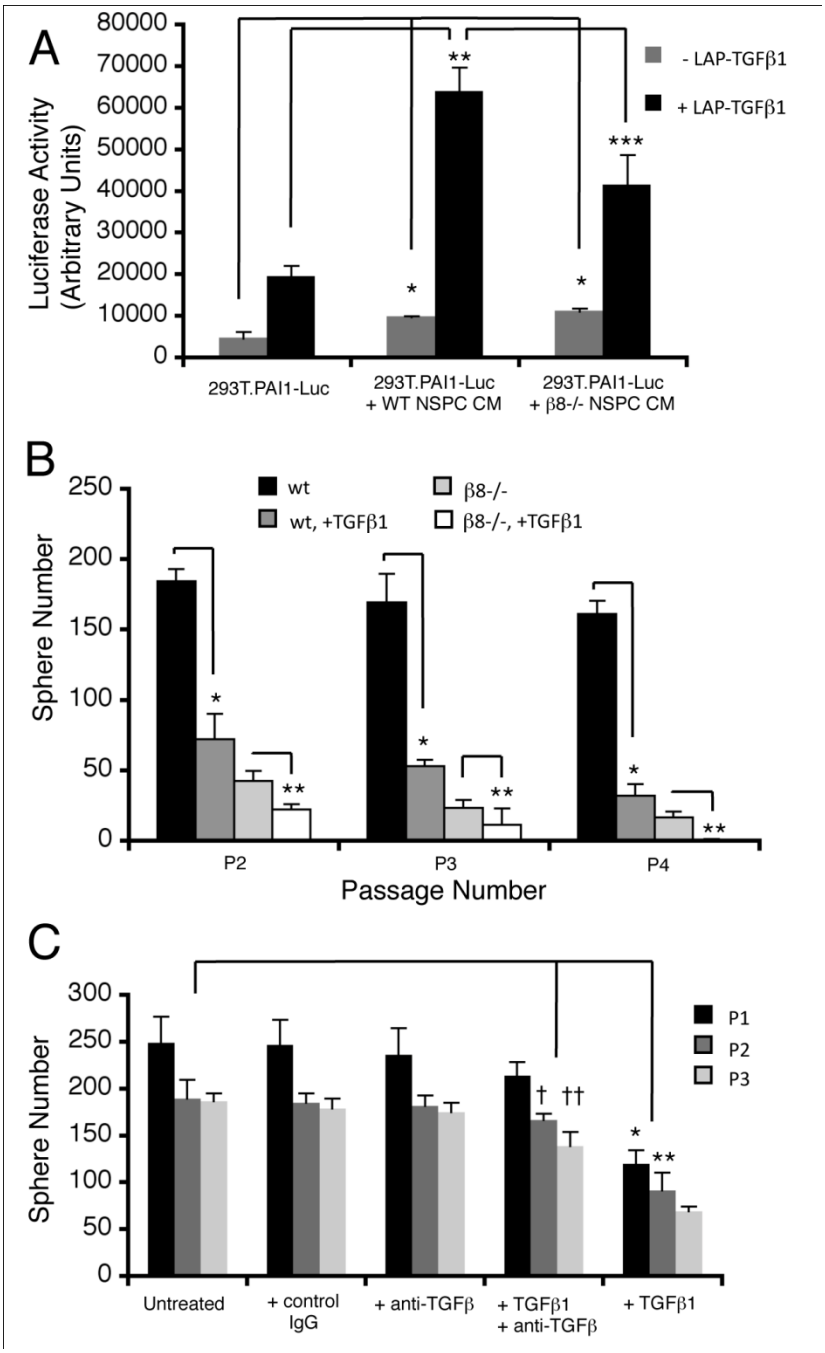
A
Luciferase Activity (Arbitrary Units)
80000
70000
60000
50000
40000
30000
20000
10000
0
- LAP-TGFβ1
+ LAP-TGFβ1
293T.PAI1-Luc
293T.PAI1-Luc + WT NSPC CM
293T.PAI1-Luc + β8-/- NSPC CM
B
Sphere Number
250
200
150
100
50
0
wt
wt, +TGFβ1
β8-/-
β8-/-, +TGFβ1
P2
P3
P4
Passage Number
C
Sphere Number
300
250
200
150
100
50
0
P1
P2
P3
Untreated
+ control IgG
+ anti-TGFβ
+ TGFβ1 + anti-TGFβ
+ TGFβ1

Figure 18

Discussion:

β8 Integrin Regulation of Vascular Niche in Embryonic and Adult Brain

Resolution of hemorrhage in the adult β8-/- brain was unexpected, but consistent with previous reports using conditional knockout strategies (93, 94). Additionally, Munger and colleagues recently reported similar resolution in adult β8-/- mice (89). This finding suggests that αvβ8 integrin is important for neurovascular unit neural cells only during times of active vessel growth or remodeling, most notably during embryonic and neonatal development. Angiogenesis is, for the most part, complete in the brain by P30 (40). However, in neurovascular niches in the adult brain, proliferating endothelial cells were still observed through BrdU pulsing experiments, indicating active angiogenesis in association with neurogenesis (2, 9, 124). This result makes it probable that β8 integrin functions in the adult neurovascular niche, in a similar manner as it does in embryonic angiogenesis.

The phenotype observed in the adult SVZ could be a result of the embryonic neurovascular unit defects, but could also be due to severe hydrocephaly that develops in the lateral ventricles of adult β8-/- mice. Indeed, neurological deficits and hydrocephaly have previously been reported as a result of intracerebral hemorrhage in the human brain (125). Additionally, studies in rats with experimentally induced hydrocephaly, increased reactive gliosis was noted throughout the brain, similar to what was observed in complete β8-/- mice (126). Therefore, the adult β8-/- mouse could potentially be used as a model to study neurodegeneration due to post-hemorrhagic hydrocephaly. However, β8 integrin seems to be necessary for NSC growth and survival in the adult SVZ based on the

following results: (i) β8 integrin is expressed in the SVZ *in vivo* and in cultured NSCs from the SVZ *in vitro* (Figure 6, 14); (ii) mutant neurospheres, grown in a defined culture media that partly mimics the *in vivo* microenvironment, exhibit similar defects in growth and survival (Figure 15); (iii) adult β8-/- mice with or without hydrocephaly display similar NSC defects in the SVZ as those seen in neurospheres; (iv) inducible deletion of β8 integrin in mice shows similar SVZ defects but no sign of hydrocephaly (Figure 13); and (v) abnormal development and/or adult neurogenesis can cause hydrocephaly as a result of cortical atrophy (127).

αvβ8 Integrin-Mediated TGFβ Activation in the Adult SVZ Vascular Niche.

One major ligand for αvβ8 integrin is LAP-TGFβ1 and LAP-TGFβ3. Reduced activation of TGFβ by integrins causes similar pathologies that were observed in αv and β8 null mice (128, 129). Here, significantly less TGFβ signaling was observed in NSCs cultured from P60 β8-/- mice, which display growth and survival defects, suggesting that TGFβ is necessary for NSC regulation. However, while this decrease in TGFβ activation was significant, it was very modest. Also, other experiments using a TGFβ blocking antibody in wild type neurospheres in an attempt to recapitulate the defects observed in the mutant neurospheres was unsuccessful, and an attempt to 'rescue' the defects in β8-/- neurospheres by addition of active TGFβ also failed (Figure 18). It is possible that TGFβ may work in a dose-dependent style, but experiments using doses ranging from 0.01ng/ml to 10ng/ml showed no difference in TGFβ's effect. Additionally, loss of the TGFβ

receptor II on the surface of NSCs using a Nestin-Cre (unpublished data Shin, J and McCarty, JH) or GLAST-CreERT2 (130) transgene showed no defects in SVZ neurogenesis. Taken together, these data suggest that integrin-mediated activation of TGFβ acting in an autocrine fashion in the SVZ plays a minimal role. Therefore, we propose a model showing that integrin-mediated activation of TGFβ acts in a paracrine manner, regulating endothelial cell functions in the neurovascular niche. Signaling in endothelial cells, in turn, leads to the production of cues from the vasculature, which regulate NSCs growth and survival (Figure 19). Similar mechanisms have been proposed indicating TGFβ acting in paracrine fashion for endothelial cell-astrocyte interactions (83, 131). Certainly, other ligands could bind to αvβ8 within the adult neurovascular niche that have not yet been identified.

αvβ8 Integrin May Function in Other Regions of the Brain

Here, we have analyzed in depth the role of αvβ8 integrin in the adult SVZ neurovascular niche. However, αvβ8 could have a similar function in the other major adult NSC neurogenic niche, the dentate gyrus of the hippocampus. Indeed, we observed abnormal development of the hippocampus and the dentate gyrus in adult β8-/- mice (Figure 20D) when compared to wild type (Figure 20C). Closer examination of the mutant hippocampus revealed dendritic projections in the CA3 region of the dentate gyrus (Figure 20 E, F).

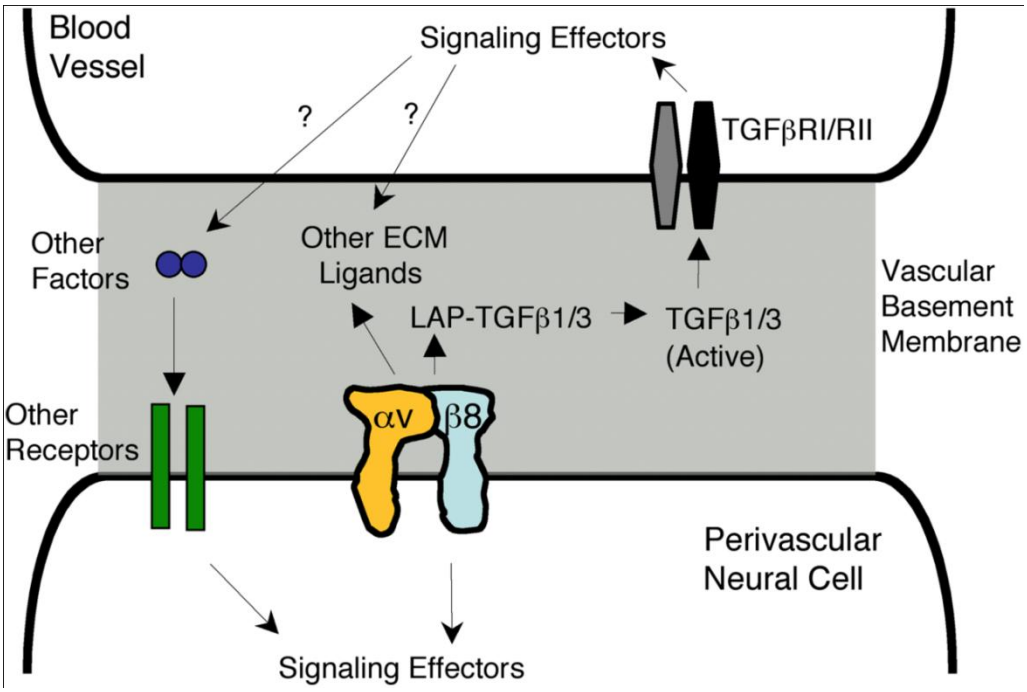

Figure 19: Model for αvβ8 integrin Adhesion and Signaling in the Neurovascular Niche.

αvβ8 expressed on the surface of NSCs interacts with several extracellular matrix ligands, including LAP-TGFβ, which is present in vascular basement membranes. αvβ8 mediated activation of LAP-TGFβ causes the canonical TGFβ signaling pathway to become active, leading to endothelial cell production of growth factors and other cues from the vasculature for survival and NSC regulation. Loss of αvβ8 integrin, through genetic ablation causes loss of αvβ8 adhesion to TGFβ, and thus loss of proper signaling at the NVU and loss of NSC regulation.

Figure 20: β8 Integrin is Necessary for Proper Development of the Corpus Callosum and Hippocampal Dentate Gyrus.

(A-F) Coronal sections through P60 wild type (A, C, E) and β8 -/- (B, D, F) mouse brains. β8 -/- mice show corpus callosum agenesis (arrows, B), which was not seen at all in control mice (arrows, A). **(C,D)** In addition, β8 mutant mice (D) develop an abnormal dentate gyrus and hippocampus, including a thickened hilus (h) and abnormal CA3 cell layer (CA3). **(E,F)** Higher magnification, silver stains, of the hippocampus reveals abnormal dendritic projections (arrows, F) in mutant mice (F) as compared to control (E).

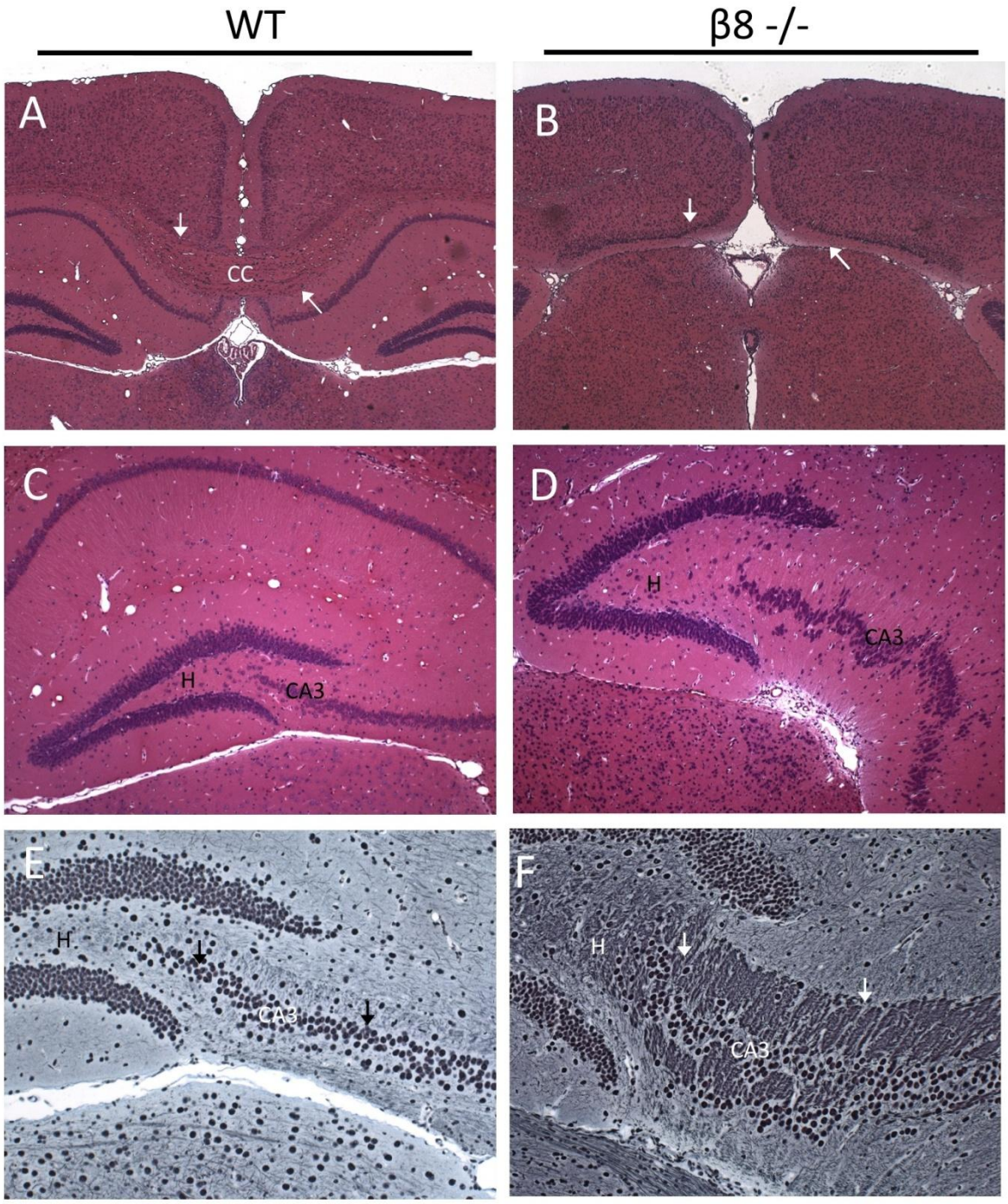

Figure 20

Additionally, we observed abnormal development of the corpus callosum (Figure 20B) in the β8-/- adult mouse. This could be an effect of abnormal migration of axons during development due to glial cells expressing Slit2, a known axonal guidance cue (132). Slit2 knockout mice show a loss of corpus callosum migration across the midline (133), similar to what is seen in β8-/- mice. Also, Slit2 has recently been shown to function in migration of neuroblasts in the RMS from the SVZ (134), which our data indicates β8 integrin plays a key role in. β8 integrin is expressed in glial cells and could potentially have an effect on slit2 expression and/or function in the developing brain.

Oligodendroglial progenitor cells give rise to oligodendrocytes, which myelinate axons in many regions of the brain (135). Nestin-Cre αv mutants develop progressive neurodegenerative defects as a result of axonal demyelination (93). This pathology was not noticed in the complete β8-/- mice, suggesting that a different αv binding β-subunit is responsible for the demyelination. It is possible that β8 integrin could play many other functional roles in the adult brain, which need to be analyzed further.

Chapter 4:

Specific Aim 2

Introduction

In the adult brain, new neurons are continually produced as neuroblasts, which then exit the SVZ and migrate to the olfactory bulb along a pathway called the rostral migratory stream (RMS) (136, 137). As neuroblasts leave the SVZ and enter the RMS greater than 80% migrate rostrally in chains towards the olfactory bulbs while the other 20% migrate between chains or in a circular pattern within the SVZ (138). Chains of neuroblasts move along the RMS in tunnels of GFAP-positive astrocytes, termed the glial tube (38). In several mouse models, disruption of glial tube formation is accompanied with disturbed neuroblast chain migration (110, 111). This suggests that neuroblast migration along the RMS is dependent upon the interactions between neuroblasts and astrocytes in the glial tube. Integrins expressed on neuroblasts interact with the ECM to guide migration in the RMS (139). Indeed, when β1 integrin is deleted CNS neural cells of mice via Nestin-Cre, defects in neuroblast chain formation and glial tube architecture were observed (110). Additionally, in *ex vivo* brain slice studies, using blocking antibodies for β1 and αv integrin, migration along the RMS was greatly reduced. Of the other 4 β-subunits that bind to αv, only a β3-blocking antibody was available, and no inhibition of neuroblast migration was seen (140). However, the role of β5, β6 or β8 integrins has not been assessed in adult RMS migration.

Unlike neuronal migration in the developing brain, which involves migration along scaffolds of radial glial cells, there are no radial scaffolds in the adult RMS. In addition to astrocytes of the glial tube, endothelial cells may play a role in neuroblast migration. Recently, analysis of the vasculature, in the RMS revealed that vessels run parallel to the RMS and neuroblasts are closely associated with the vasculature indicating a probable role for blood vessels in neuroblast migration (49, 141). In the olfactory bulb, neuroblasts also associate with the vasculature, which guides their radial migration (142). Additionally, in stroke models, neuroblasts leave the SVZ and migrate to the site of infarct closely apposed to blood vessels, further indicating that the vasculature is necessary for proper neuroblast migration (143). In the previous chapter, the involvement of αvβ8 integrin in NSC vascular niche homeostasis was analyzed. A similar interaction between β8 integrin and the ECM secreted by the vasculature along the RMS may occur.

While the roles of some integrins have been analyzed within the RMS, the role of αvβ8 integrin has not. In this chapter, complete and conditional β8 knockout mice were used to test the hypothesis that β8 integrin is required for proper neuroblast migration in the RMS. In addition to these models, a mouse model expressing GFP under control of the DCX promoter was employed (DCX-GFP). This model makes it possible to purify neuroblasts using FACS sorting for GFP, as well as track the migration of neuroblasts in the brain. DCX-GFP mice have been crossed to β8+/- mice to generate wild type and β8-/- mutant mice that are DCX-GFP+.

Furthermore, in the last chapter, the importance of integrin-mediated TGFβ activation was analyzed in the NSC vascular niche. TGFβ plays many roles in the brain, including promotion of cell cycle exit in progenitor cells during development (144), neuronal survival (145), and induction of neuronal differentiation in the OB (146). TGFβs and their receptors are expressed in many regions of the CNS. TGFβ2 and 3 are expressed in the DG (147), and TGFβ1 is expressed both in the SVZ and the DG (148). TGFβ receptors' expression on astrocytes and neurons in the adult brain, and radial glial cells in the developing brain indicate a potential role for TGFβ signaling in neuronal polarity and migration (149).TGFβ has also been shown to promote differentiation of immature neurons to axons (150). Recently, SMAD3 knockout mice were shown to have decreased NSC proliferation in the SVZ and defects in neuroblast migration in the RMS (151). While several functions in the developing and adult brain have been identified for TGFβ, including neuroblast migration, the role of integrin-mediated activation of the cytokine in the RMS is not fully understood.

Results:

β8-/- Mice Show Defects in Neuoroblast Migration in the RMS

Initial analysis of complete β8-/- mice revealed defects in DCX+ neuroblasts within the SVZ and along the RMS (Figure 10). Here, sagittal sections from P60 wild type and β8-/- brains were immunostained with anti-DCX antibody to show RMS neuroblasts, and anti-GFAP to show the astrocytes of glial tube (Figure 21). Examination of the wild type RMS revealed tight chains of neuroblasts leaving the SVZ and migrating all the way to the olfactory bulbs (Figure 21A, top panel). GFAP+ astrocytes were detected surrounding the neuroblast chains in an organized glial tube (Figure 21A, bottom panel). However, analysis of the β8-/- RMS revealed many defects. First, we detected clusters of DCX+ cells that were not associated with migrating chains. Second, many of the neuroblasts within the RMS appear to stop abruptly prior to reaching the olfactory bulb (Figure 21B, top panel). Finally, GFAP+ astrocytes were found dispersed throughout the RMS and mixed amongst the neuroblasts, and were not organized into a defined glial tube (Figure 21B, bottom panel).

Previous reports indicate that neuroblasts may migrate using blood vessels as a scaffold (142). To analyze neuroblast association with blood vessels along the RMS, double immunostaining was performed with anti-PSA-NCAM to label migrating neuroblasts, and anti-laminin to label blood vessel basement membranes. Both wild type and β8-/- neuroblasts in the RMS were found closely associated with blood vessels (Figure 22 A, B). Interestingly, in mutant mice, the clusters of

individual cells branching off from the RMS were still associated with blood vessels (Figure 22 B).

Nestin-Cre (N-Cre) hemizygous mice were crossed with β8 flox/flox mice to produce mice that were N-Cre/+; β8 flox/+. These mice were further crossed with β8 +/- mice to produce mice that were N-Cre/+; β8 flox/+ (control) and N-Cre/+; β8 flox/- (mutant). Mutant mice were born with mild hemorrhage, at predicted Mendalian ratios, and survived to adulthood, similar to previous reports (94). To analyze the adult SVZ and RMS in mice with conditional deletion of β8 integrin, mice were sacrificed and cardiac perfused with paraformaldehyde and sagittal brain sections were prepared. Sections from control and mutant mice were immunostained with anti-DCX and anti-GFAP antibodies. In control animals, the SVZ and RMS appeared normal; neuroblasts were seen in migrating chains along the RMS and GFAP+ cells formed the glial tube surrounding them (Figure 23 A, A', A"). In contrast, analysis of the mutant SVZ and RMS revealed increased DCX+ cells within the SVZ as well as abnormal neuroblast migration along the RMS. Several small clusters of neuroblasts were found in the RMS and GFAP+ astrocytes were seen dispersed throughout the neuroblasts (Figure 23 B, B', B"). Additionally, an increase in GFAP+ astrocytes throughout the mutant brain was observed. The results seen here in the conditional β8 integrin knockout model recapitulate the observations made in the complete β8-/- mice.

Figure 21: β8-/- Mice Show Abnormal Neuroblast Migration in the RMS.

(A,B) Sagittal sections from wild type (A) and β8-/- (B) P60 brains were immunostained with an anti-DCX antibody alone (top panels), or in combination with anti-GFAP (bottom panels). **(A)** Normal neuroblast migration was observed in wild type RMS. Notice the defined migratory path of DCX+ neuroblasts and surrounding GFAP+ glial sheath. **(B)** β8-/- neuroblast migration along the RMS is very disorganized, with no defined glial sheath. GFAP+ astrocytes seem to be dispersed amongst the DCX+ neuroblasts, and several individual neuroblasts can be seen. Abbreviations: v, ventricle.

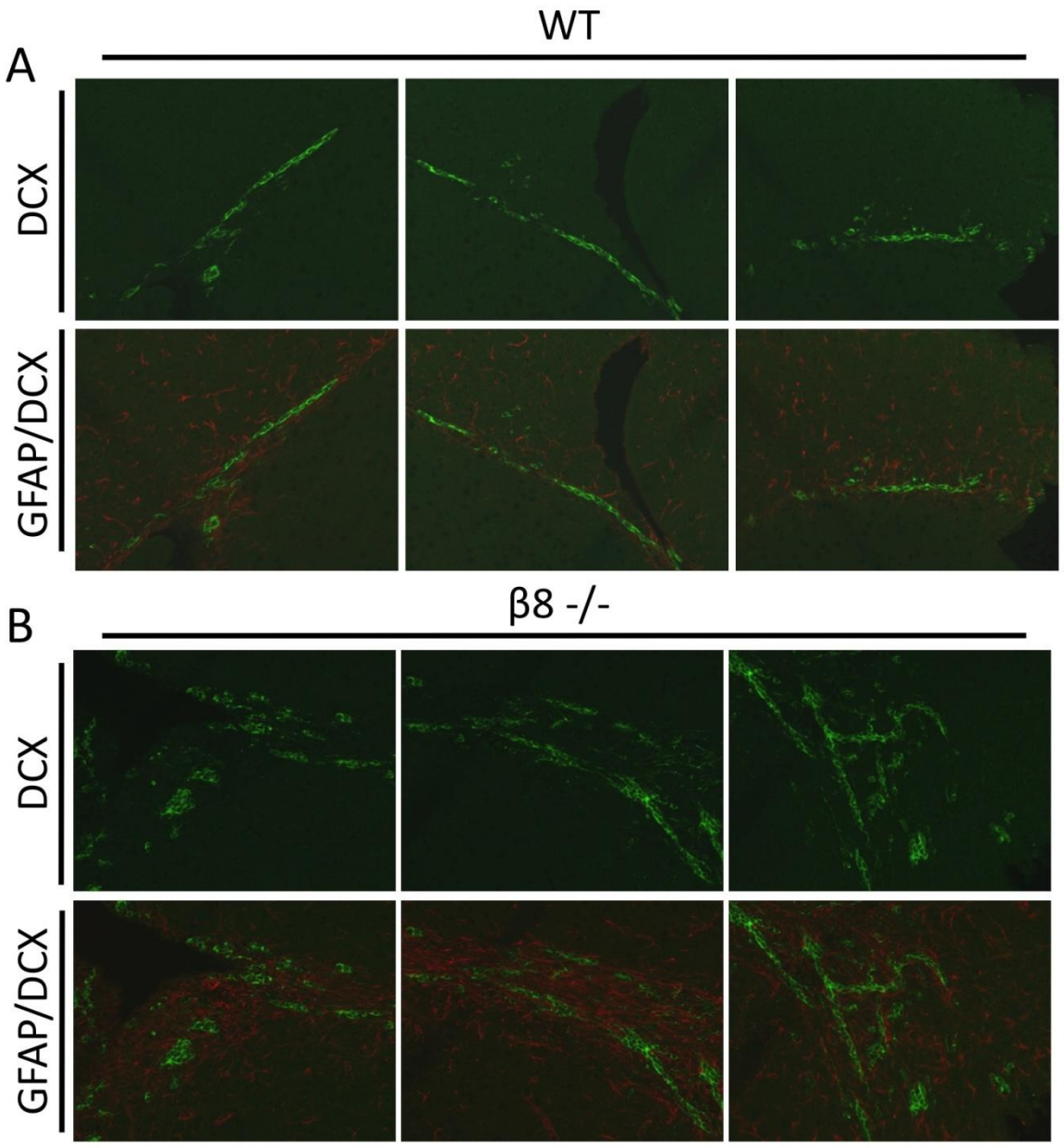

Figure 21

Figure 22: Migrating Neuroblasts are Closely Associated with Blood Vessels

(A,B) P60 Wild type and β8-/- sagittal brain sections were stained with PSA-NCAM to show neuroblasts, and anti-laminin to highlight blood vessels. In both the wild type and knockout RMS, neuroblasts were observed migrating near blood vessels. Blood vessels appeared to be running parallel to the direction of neuroblast migration.

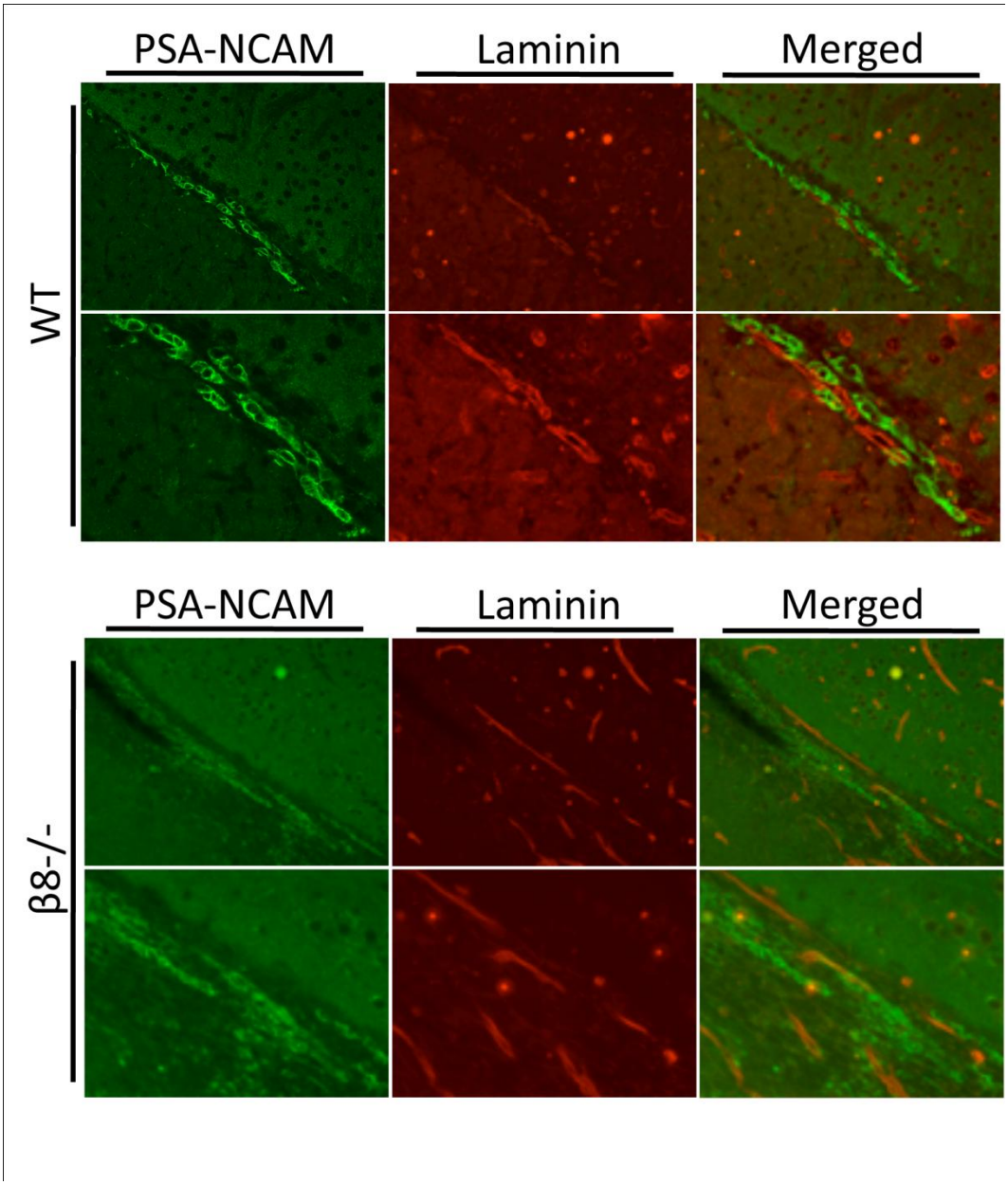

Figure 22

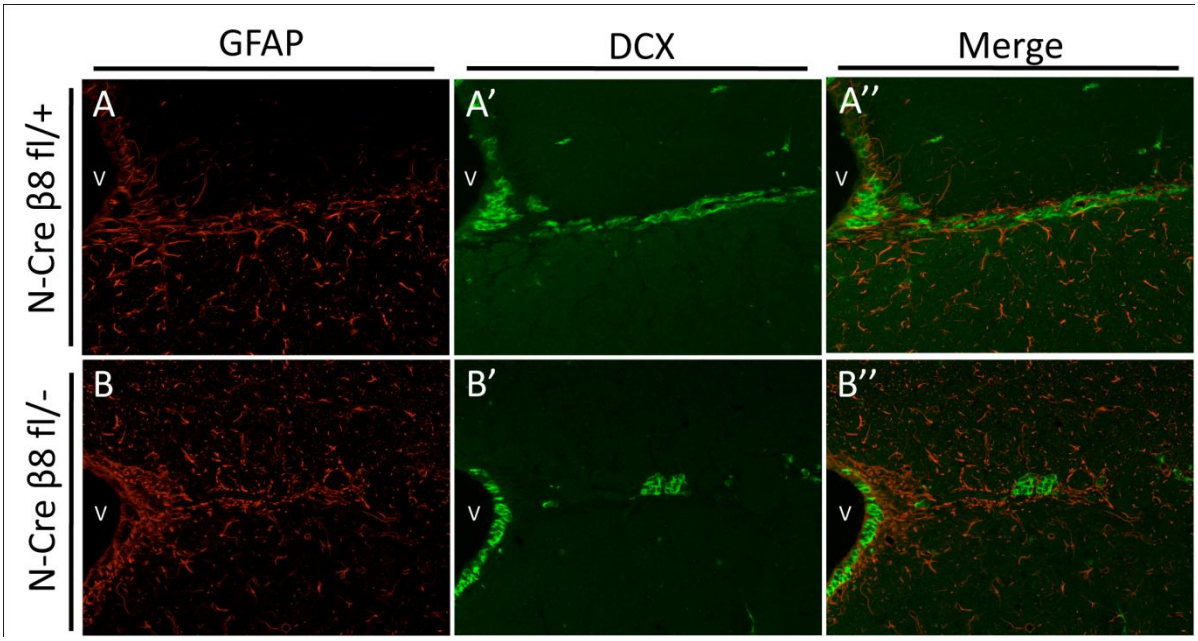

Figure 23: Nestin-Cre Conditional β8 Integrin Mutants Show Similar Neuroblast Defects in the RMS. (A,B) Sagittal brain sections from P60 Nestin-Cre; β8 fl/+ control, A) and Nestin-Cre; β8 fl/- (mutant, B) were immunostained with anti-GFAP (A,B) and anti-DCX (A',B') antibodies. In panels A" and B'' the merged images are shown. Examination of GFAP revealed an increase in GFAP+ astrocytes throughout the mutant brain when compared to control mice (B and A, respectively). DCX analysis in mutant mice shows increased individual cells within, and a more disorganized RMS when compared to controls (B' and A' respectively). These results are similar to observations in the complete β8-/- adult mouse brain. Abbreviations: v, ventricle.

Whole Mount Staining of the SVZ in β8-/- Mice Reveals Abnormal Architecture

A recent study using whole mount staining of the SVZ indicated that the vasculature within the SVZ has a unique cytoarchitecture (152). An elaborate network of vessels running parallel to the surface of the ventricle was observed (153). Here, the vascular plexus and the affiliated SVZ cells were analyzed. Lateral ventricles were dissected from P60 wild type and β8-/- mice, and the SVZ region was isolated. The whole mount staining procedure was performed using double immunofluorescence to show the neuroblasts (anti-DCX) or SVZ astrocytes (anti-GFAP), as well as the vascular plexus (anti-CD31). The vascular plexus of the SVZ appeared normal in both wild type and β8-/- mice, showing parallel vessels with multiple branches throughout the SVZ (Figure 24A'-D' and Figure 25A'-D').

Neuroblasts within the SVZ of wild type mice were organized in chains similar to the organization in the RMS. Many chains were observed and neuroblasts appeared to be migrating in several directions (Figure 24 A, B). In contrast, analysis of neuroblasts in the β8-/- SVZ revealed disorganized chains of neuroblasts as well as several individual DCX+ cells (Figure 24 C, D). Increased total numbers of neuroblasts were also observed in the mutant SVZ when compared to wild type SVZ, consistent with traditional immunostaining analysis of DCX+ cells in the SVZ (Figure 10C).

Figure 24: Whole-Mount immunostaining with anti-DCX Reveals Abnormal Neuroblast Organization Within the SVZ. (A-D) The SVZ was isolated from wild type and β8-/- P60 mice. Immunostaining was performed with anti-DCX (A-D) and anti-CD31 (A'-D') antibodies (merged images are shown in A"-D"). (A,B) Wild type SVZ DCX staining revealed normal chainlike organization of neuroblasts. (C,D) β8-/- SVZ exhibits abnormal neuroblast chain architecture, with several small clusters of cells and individual DCX+ cells that do not appear to be associated with neuroblast chains. In both wild type and mutant SVZs the neuroblasts do not appear to be directly associated with the vasculature (A"-D"). (Magnifications A,C = 70x and B,D = 200x)

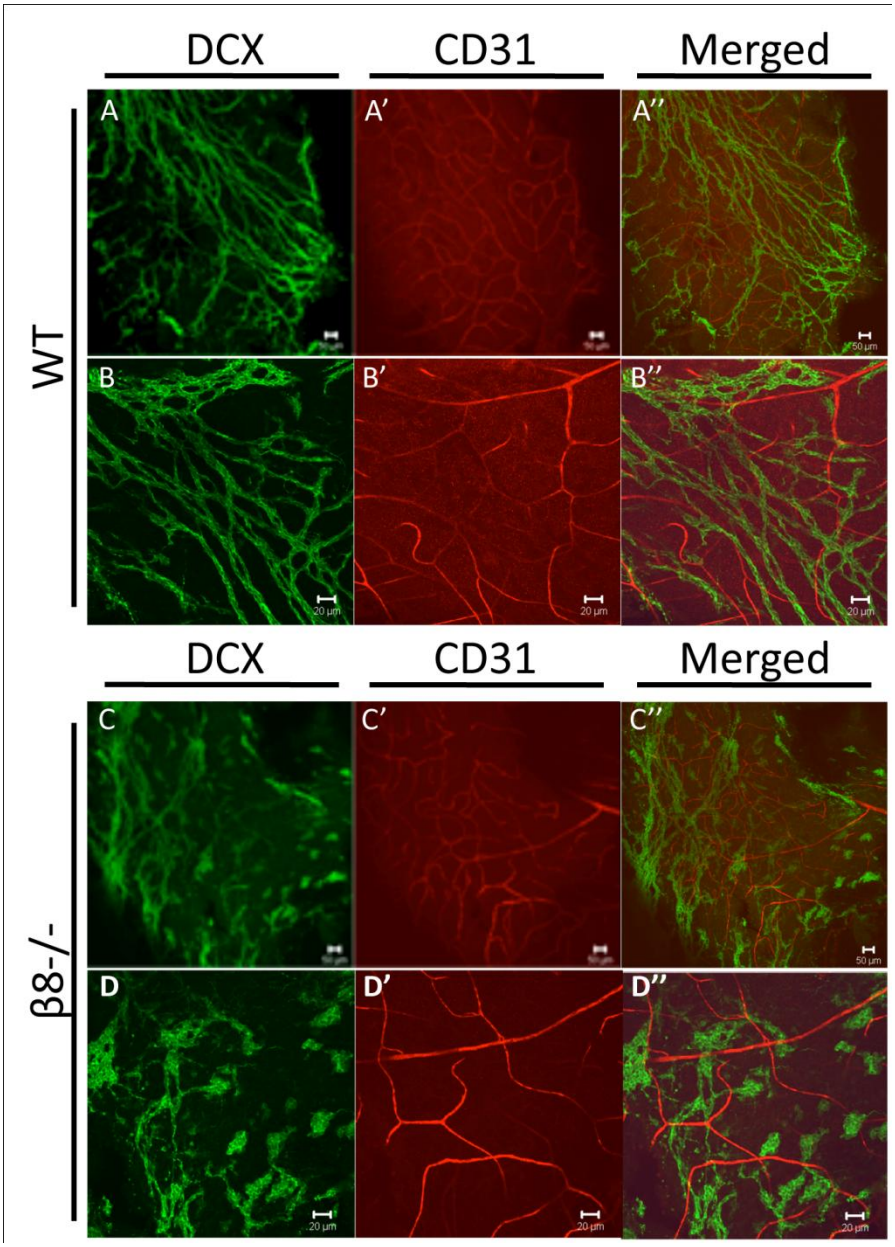

Figure 24

Figure 25: Whole Mount Immunostaining with Anti-GFAP Shows Increased GFAP+ Blood Vessel Coverage Within the SVZ. (A-D) The SVZ was isolated from wild type and β8-/- P60 mice. Immunostaining was performed with anti-GFAP (A-D) and anti-CD31 (A'-D') antibodies (merged images are shown in A"-D"). β8-/- GFAP+ astrocytes within the SVZ show increased endfoot contact with the SVZ vasculature (C", D"), when compared to the wild type (A", B"). Similar increases were observed in the cerebral cortex of the β8-/- mouse. (Magnifications A,C = 200x and B,D = 400x)

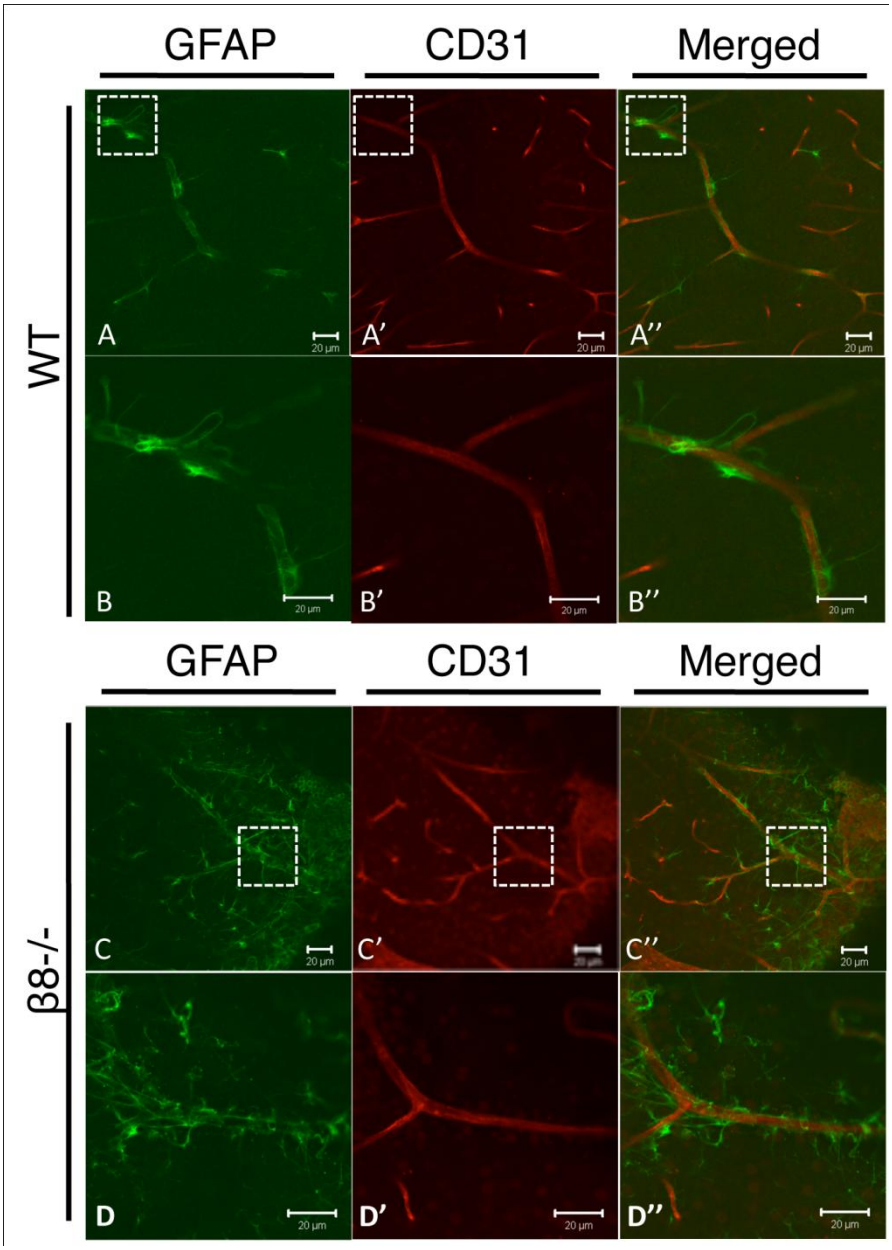

Figure 25

In the wild type SVZ whole mount tissues stained with GFAP, many GFAP+ cells were observed in close proximity to blood vessels (Figure 25 B). Very few cells were noted that were not associated with the vasculature (Figure 25 A). However, examination of β8-/- SVZ revealed more total number of GFAP+ cells (Figure 25 C). Additionally, more GFAP+ astrocytes in contact with blood vessels, as well as increased number of astrocytes not affiliated with the vasculature were noticed (Figure 25 D). These data are consistent with increased GFAP+ astrocytes seen throughout the mutant brain, and increased astrocyte endfoot coverage of blood vessels (Figure 7 B, I).

DCX-GFP Mice Allow for Isolation of Neuroblasts

DCX-GFP+ mice were interbred and their offspring were genotyped to confirm expression of the DCX-GFP transgene. A DCX-GFP+ mouse was then sacrificed and sagittal brain sections were paraffin embedded and immunostained with an anti-GFP antibody to confirm the expression of GFP in the brain (Figure 26 A, C). Double immunostains were performed to confirm colocalization of GFP+ cells with anti-PSA-NCAM, another marker for neuroblasts (anti-DCX antibody was not used due to antibody compatibility issues). Indeed, PSA-NCAM+ cells were also GFP positive showing perfect colocalization (Figure 26 A", C").

A hemizygous DCX-GFP/+ male mouse was crossed with β8+/- female mice, to produce offspring that were DCX-GFP/+; β8+/-. These mice were then crossed again with β8+/- mice to produce DCX-GFP/+; β8+/+ (WT DCX-GFP+), and DCX-GFP+/-; β8-/- (mutant DCX-GFP/+) mice. Upon achieving the proper crosses, wild

type and mutant mice were sacrificed and sagittal brain sections were paraffin embedded. Wild type and β8-/- DCX-GFP+ brain sections were stained with an anti-GFP antibody to show the expression pattern of GFP, in combination with markers for neuroblasts (anti-PSA-NCAM). Colocalization was seen within the SVZ and the RMS in both wild type and mutant mice (Figure 26). Similar to other findings in the β8-/- mice, individual neuroblasts were not associated with the main chain of migrating neuroblasts at both the beginning (Figure 26 B) and the end of the RMS (Figure 26 D). However, as the neuroblasts entered the OB, the chains of cells appeared normal, indicating that perhaps another integrin is the main regulator of radial migration in the OB.

The SVZ from P60 WT DCX-GFP+ and mutant DCX-GFP+ mice and a normal wild type mouse were isolated and digested in tissue dissociation media. After digestion, tissue was triturated to achieve a single cell suspension. A purified GFP+ population was isolated using FACS for GFP, with normal wild type cells as a negative control. FACS plots reveal no GFP+ cells in the negative control (Figure 27 A top panel), while the WT DCX-GFP+ mice showed about 5% GFP positive cells (Figure 27 A, bottom panel). Similar GFP positivity was seen in sorting for β8-/- brains. WT and mutant DCX-GFP+ cells were resuspended in complete neurosphere media and allowed to form free-floating spheres. Immunoblots were performed to analyze neuroblast purity in GFP+ neurospheres. GFP was highly expressed in sorted neurospheres while none was detected in unsorted spheres. The neuroblast marker DCX, and neuronal marker Tuj1 were highly expressed in purified cells as well, while GFAP, a marker for astrocytes and NSCs, was greatly

reduced (Figure 27 B). GFP expression was also confirmed using an inverted fluorescent microscope. Most of the cells within both WT and mutant neurospheres were GFP-positive (Figure 27 C). Also of note was the smaller size of the mutant DCX-GFP+ neurospheres, in comparison to wild type. This slower growth was similar to the growth pattern noticed in unsorted mutant neurospheres (Figure 15 B, C).

Expression of α5β1 and α6β1 was analyzed because laminin receptors, most notably α6β1, have been previously implicated in neuroblast migration (139) Additionally, αv expression was previously shown in the RMS (140), however the status of β8 integrin in adult neuroblasts is unknown. Integrin status in purified neuroblasts was determined using biotinylation/immunoprecipitation of wild type DCX-GFP+ neurospheres. Spheres were allowed to adhere to a laminin substrate for 4 days, followed by biotinylation for 30 minutes. Lysates were then prepared and immunoprecipitations were performed with anti-β8, anti-αv, anti-α5 and anti-α6 antibodies. As expected, expression of α5 and α6 and their binding partner β1, as well as αv and β8, were observed in purified neuroblasts (Figure 27 D).

Figure 26: Confirmation of GFP Expression in DCX-GFP+ Mouse

Wild type and β8-/- mice were crossed to DCX-GFP+ mice to obtain mice that were DCX-GFP+;WT, and DCX-GFP+, β8-/-. DCX-GFP+ WT and mutant mice were then sacrificed and sagittal brain sections were immunostained to show neuroblasts in the RMS with anti-GFP and anti-PSA-NCAM antibodies. **(A, B)** In both wild type (A) and β8-/- (B) mice, neuroblasts at the beginning of the RMS, just caudal to the SVZ, show perfect colocalization for GFP and PSA-NCAM. **(C, D)** At the end of the RMS where neuroblasts begin to enter the olfactory bulb, wild type (C) and mutant (D) neuroblasts stained with GFP and PSA-NCAM colocalize. Note the individual chains of neuroblasts in β8-/- mice (B, D), which were not observed in wild type neuroblasts (A, C). Arrows indicate the direction of neuroblast migration to the OBs.

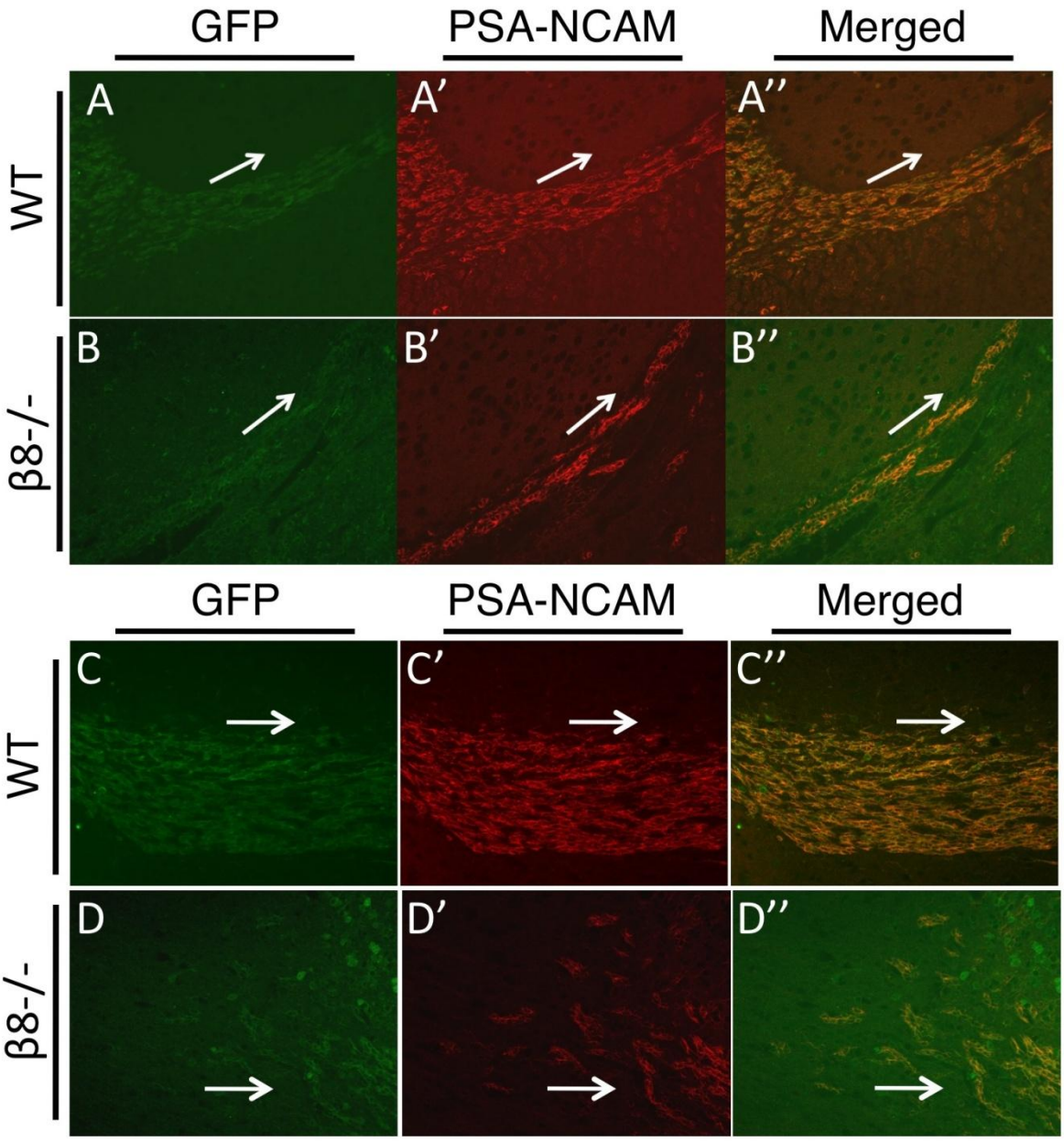
GFP
PSA-NCAM
Merged
WT
β8-/-
A
A'
A''
B
B'
B''
GFP
PSA-NCAM
Merged
WT
β8-/-
C
C'
C''
D
D'
D''

Figure 26

Figure 27: DCX-GFP Mice Allow for *Ex Vivo* Isolation of Purified Neuroblasts.

(A) The SVZ and olfactory bulbs were isolated from wild type and β8-/- DCX-GFP+ mouse brains, as well as from a wild type DCX-GFP- mouse. Tissue was triturated into a single cell suspension. GFP+ neuroblasts were selected using flow cytometry. The GFP- population (top panel) was used to establish gates for the GFP+ population from wild type (bottom panel) and β8-/- mice (not shown). **(B)** Immunoblots were performed to compare unsorted vs. GFP-sorted wild type neurospheres. Expression of GFP was only observed in GFP sorted neurospheres. Additionally, neuronal markers DCX and Tuj1 were expressed at higher levels and one NSC marker, GFAP, exhibited much lower expression in GFP-sorted neurospheres. **(C)** Isolated GFP+ neuroblasts were resuspended in complete neurosphere growth media with EGF and FGF and neurospheres were allowed to form. GFP expression was analyzed in neurospheres from both wild type (top panel) and mutant (bottom panel) mice, both express similar levels of GFP. β8-/- spheres were noticeably smaller and took longer to grow compared to wild type. **(D)** Wild type neurospheres were adhered to a laminin substrate for 4 days before performing a biotinylation and IP. Lysates were made and IP was performed to examine cell surface expression of integrin subunits: β8, αv, α5, α6.

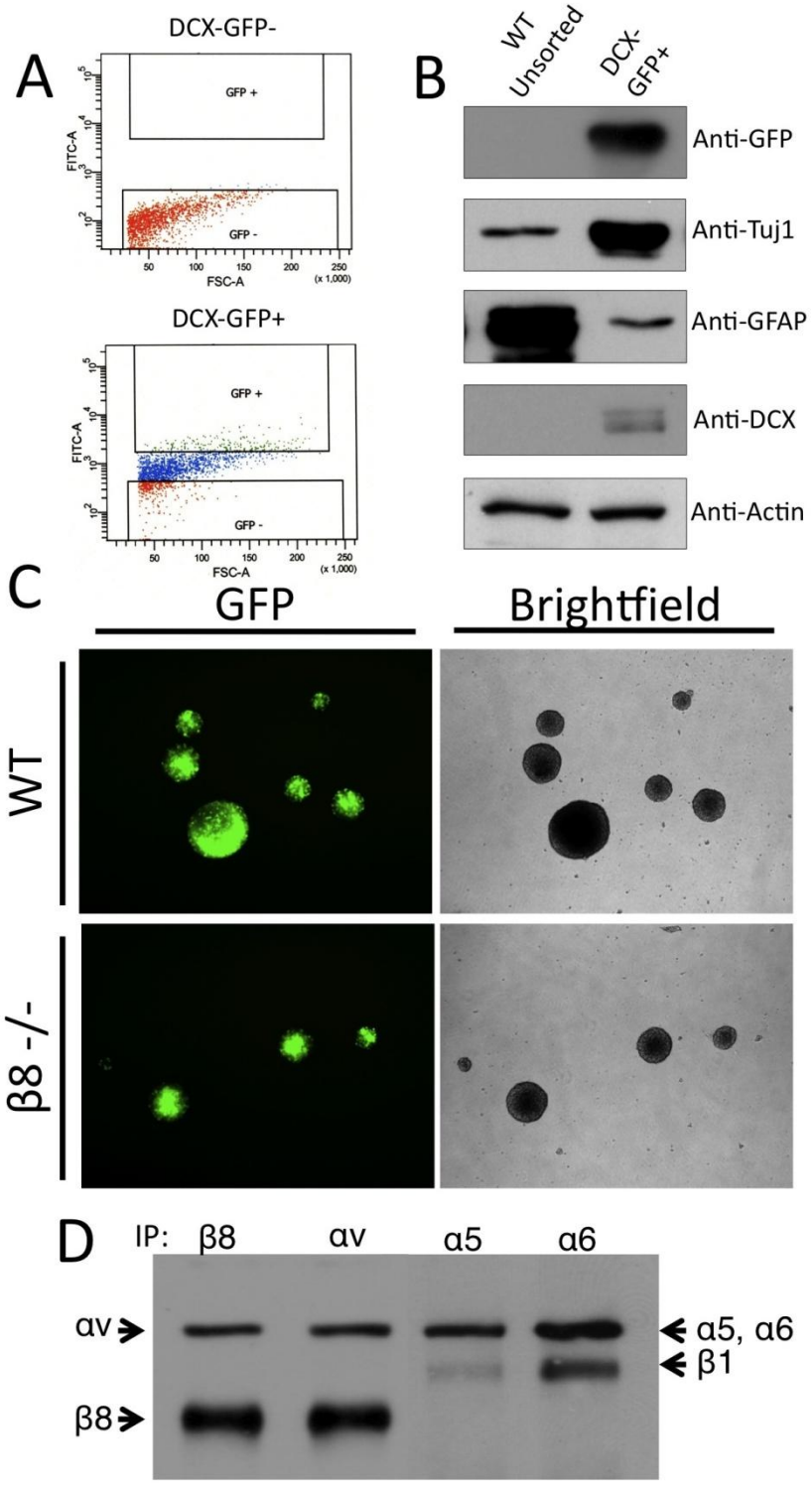
A
DCX-GFP-
GFP +
GFP -
FITC-A
FSC-A
(x 1,000)
DCX-GFP+
GFP +
GFP -
FITC-A
FSC-A
(x 1,000)
B
WT Unsorted
DCX-GFP+
Anti-GFP
Anti-Tuj1
Anti-GFAP
Anti-DCX
Anti-Actin
C
GFP
Brightfield
WT
β8 -/-
D
IP: β8 αv α5 α6
αv
β8
α5, α6
β1

Figure 27

Marker Analysis of GFP+ Purified Neurospheres Reveals Less Differentiated Population in β8-/- Neurospheres.

WT and β8-/- DCX-GFP+ neuroblasts were analyzed for expression of various neural stem and neuronal markers to determine the purity of the isolated population. For western blot analysis, lysates were prepared from neurospheres from WT and mutant mice, which had been GFP sorted. Additionally, immunostaining was performed on neurospheres that were allowed to adhere to a laminin substrate for 5 days, followed by fixation in paraformaldehyde. Commonly used neural stem cell markers, nestin and GFAP, were analyzed by immunoblot. Additionally, GFP expression and αv and β8 expression was further confirmed via western blot. As previously shown, wild type GFP+ purified neurospheres express αv and β8 integrin, but mutant neurospheres express only αv, indicating that other αv binding β subunits are expressed. Equal levels of GFP were also observed. GFAP expression was similar in both wild type and mutant neurospheres, however, expression of nestin was increased in mutant neurospheres (Figure 28 A). The results observed through immunoblots were confirmed with immunostaining for anti-Nestin and anti-GFAP. Indeed, β8-/- mutant neurospheres showed increased expression of nestin when compared to wild type neurospheres (Figure 28 B middle panel), but similar levels of GFP expression were observed (Figure 28 B left panel). Additionally, the morphology of nestin positive cells in the mutant neurospheres appeared more elongated when compared to nestin positive cells in wild type neurospheres. GFAP was similarly expressed in both wild type and β8-/- neurospheres at low levels (Figure 28 C).

Neuronal markers were also analyzed. Anti-PSA-NCAM and anti-DCX were used as neuroblast markers, and anti-Tuj1 and anti-Map2 were used as more differentiated neuronal markers. Western blot analysis for neuroblast markers revealed similar expression of both PSA-NCAM and DCX, in wild type and mutant neurospheres. The anti-Map2 immunoblot showed similar levels of expression in both wild type and β8-/- neurosphere lysates; however, blotting for Tuj1 showed greatly increased levels in wild type cells compared to mutants (Figure 29 A). The diminished Tuj1 expression in combination with increased expression of nestin in β8-/- cells suggests that β8-/- neuroblasts are less differentiated than wild type neuroblasts. Immunostaining for anti-Map2 and anti-PSA-NCAM in wild type and mutant neurosphere attached to a laminin substrate indicate similar expression levels (Figure 29 B,C), confirming results observed in western blots.

While integrin expression was analyzed previously with wild type neuroblasts, comparison of integrin levels between wild type and β8-/- neurospheres was further analyzed. Biotinylation and immunoprecipitation were performed on wild type and mutant neurospheres attached to laminin, for αv, α5 and α6 integrins. Additionally, an immunoblot was performed for β1 integrin. In β8-/- neurospheres, increased expression of three α-integrin subunits was observed as well as increased β1 integrin expression (Figure 30 A). Immunoprecipitation for αv showed a corresponding band at around 100kD that correlates to either β3 or β5 integrin subunits, as well as a very faint band around 125kD corresponding to the β1 subunit, while IP's for α5 and α6 have a lower band showing their β1-binding partners. Immunostaining analysis in wild type and β8-/- neurospheres confirms the

increase in α5 and β1 expression in the mutant (Figure 30 B, lower panels) neurospheres when compared to wild type (Figure 30 B, upper panels). These findings suggest that other integrins may be upregulated in order to compensate for loss of β8 integrin in the RMS of mutant mice, or that β8 integrin functions to regulate levels of other integrins.

Figure 28: Analysis of DCX-GFP+ Neuroblasts for NSC Markers.

(A) Lysates were prepared from wild type and β8-/- GFP+ FACS sorted neurospheres. Immunoblots were performed with anti-αv, anti-β8, anti-nestin, anti-GFAP, anti-GFP, and anti-actin antibodies. As expected, β8-/- spheres show no expression of β8 protein. Interestingly, β8-/- spheres exhibit enhanced nestin positive cells when compared to the wild type cells. **(B,C)** DCX-GFP+ wild type and β8-/- neurospheres were adhered to a laminin substrate and allowed to migrate for 48 hours, followed by fixation and immunostaining with anti-GFP in combination with NSC markers. (B) Cells were immunostained with anti-nestin. Similar levels of GFP expression were observed, however β8-/- spheres showed higher expression of nestin, as observed in western blot. (C) Cells were immunostained with anti-GFAP. Similarly low levels of GFAP were observed in both wild type and β8-/- neuroblasts.

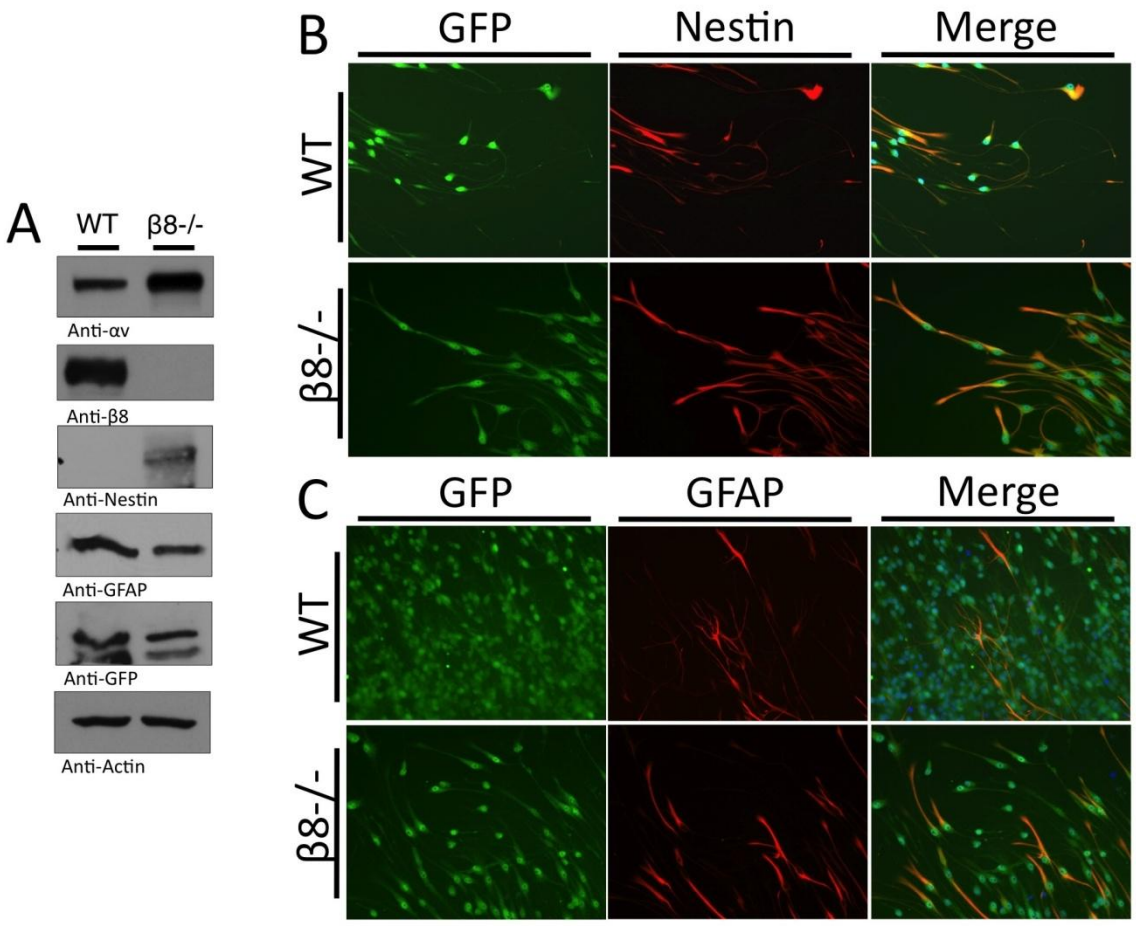
A
WT
β8-/-
Anti-αv
Anti-β8
Anti-Nestin
Anti-GFAP
Anti-GFP
Anti-Actin
B
GFP
Nestin
Merge
WT
β8-/-
C
GFP
GFAP
Merge
WT
β8-/-

Figure 28

Figure 29: Analysis of Neuronal Markers in DCX-GFP+ Neuroblasts.

(A) Lysates were prepared from wild type and β8-/- GFP+ FACS sorted neurospheres. Immunoblots were performed with anti-PSA-NCAM, anti-Tuj1, anti-DCX, antii-MAP2, and anti-actin antibodies. Similar expression levels were seen for all immunoblots except for anti-Tuj1. Increased levels of Tuj1 protein were observed in wild type neurospheres compared to mutant. **(B,C)** DCX-GFP+ wild type and β8-/- neurospheres were adhered to a laminin substrate and allowed to migrate for 48 hours, followed by fixation and immunostaining with anti-GFP in combination with neuronal markers. (B) Immunostaining with anti-DCX and anti-MAP2, neuronal markers, revealed similar expression levels in both populations. (C) Cells from wild type and β8-/- mice were immunostained with an anti-PSA-NCAM antibody. Similar staining patterns were detected in both wild type and β8-/- GFP+ cells.

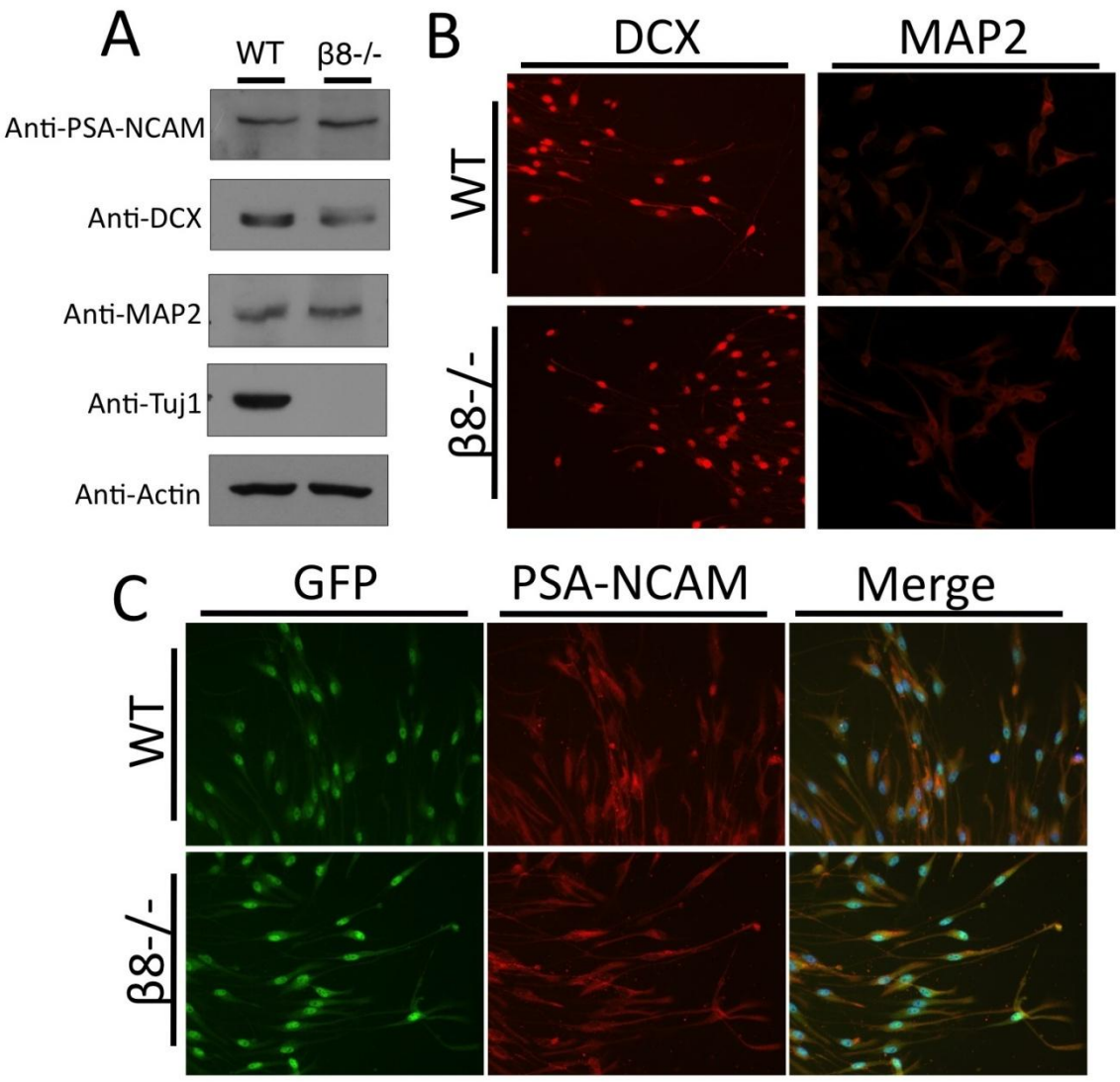
A
WT
β8-/-
Anti-PSA-NCAM
Anti-DCX
Anti-MAP2
Anti-Tuj1
Anti-Actin
B
DCX
MAP2
WT
β8-/-
C
GFP
PSA-NCAM
Merge
WT
β8-/-

Figure 29

Figure 30: Integrin Expression Analysis in WT and β8-/- DCX-GFP+ Neuroblasts.

(A) GFP+ sorted WT and β8-/- neurospheres were allowed to adhere to laminin substrate and 4 days later were biotinylated. Lysates were made and similar levels of protein were used for immunoprecipitation with anti-αv, anti-α5, and anti-α6 antibodies, or immunoblotted with anti-β1 antibody. Increased levels of β1 integrin and all three of the α subunits analyzed were increased in β8-/- neurospheres when compared to wild type. **(B)** DCX-GFP+ wild type and β8-/- neuroblasts adhered to laminin were immunostained with anti-α5 (left panel) and anti-β1 (right panel) antibodies. Increased expression of both was observed in β8-/- cells, which correlates with western data.

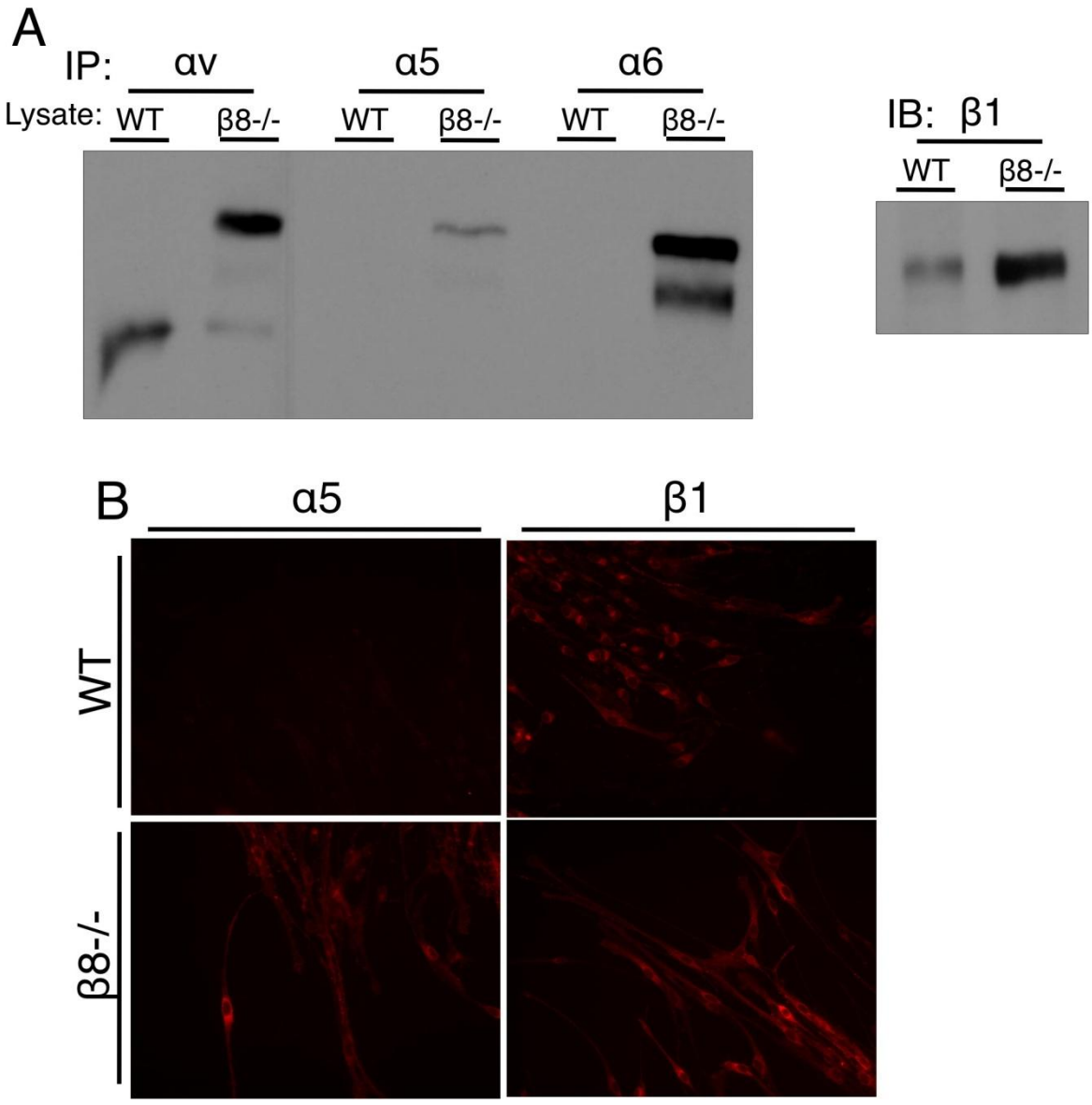

Figure 30

***In vitro* Neurosphere Migration Assay Confirms Migration Defects Observed in the β8-/- Mouse Brain.**

Neurospheres isolated from wild type and β8-/- P60 mouse brains were allowed to adhere to laminin-coated dishes for 30 minutes to allow them to settle and attach. After 30 minutes neurospheres were imaged using an inverted microscope with regulated humidity and CO_2 regulation. Images were taken every 4 hours for 48 hours. Both wild type and mutant neurospheres began to flatten out and cells migrated away from the neurosphere core, however mutant neurospheres migrated much slower than their wild type counterparts (Figure 31A). The migration defect was quantified by calculating the surface area of migrating neurospheres (n=10 for both wild type and β8-/- neurospheres). While neurospheres of similar size were selected for this assay, the difference in sizes was accounted for by normalization to sphere sizes at 0 hours. Indeed the mutant neurospheres migrated significantly less at both the 24hr and 48hr timepoints (Figure 31 B).

Experiments using αv and β1 blocking antibodies in the neurosphere migration assay, confirmed the functional importance of αvβ8 integrin. Wild type and β8-/- neurospheres were incubated in media containing 5μg/ml anti-αv or anti-β1 blocking antibodies or IgG controls, prior to adherence to a laminin-coated dish. Neurospheres were imaged over 48 hours with images taken every 4 hours. Migration was then quantified as described above. Addition of β1 blocking antibody completely inhibited migration in both wild type and β8-/- neurospheres (Figure 32 A white bars). This result was expected based upon previous reports indicating the requirement for β1 integrin for RMS migration (110, 140). Wild type neurosphere

migration was inhibited with the addition of αv integrin blocking antibody. However, mutant neurospheres were not significantly inhibited by the αv-blocking antibody, but IgG control β8-/- neurospheres migrated less that did the wild type neurospheres with αv blockage (Figure 32 A, grey bars), suggesting that not all αvβ8 integrin was blocked with the antibody, or another migratory pathway is operating. This result indicates that both αvβ8 integrin and β1 integrins are necessary for proper migration. In addition to this, the upregulation of β1 integrin seen in β8-/- neurospheres (Figure 30) suggests interplay between αvβ8 and β1 integrins in neuroblasts.

Figure 31: Migration is Defective in β8-/- Neurospheres.

(A) Wild type and β8-/- neurospheres of similar sizes were plated on laminin coated plates and imaged on an inverted light microscope for 48 hours. Images were taken every 6 hours. Representative images from wild type (top panel) and mutant (bottom panel) are shown at 0hr, 24h, and 48h. Periphery of sphere migration is outlined with white dashed lines. **(B)** Quantitation of sphere migration was performed by calculating surface area of sphere migration and normalizing back to 0hr sphere size for wild type (n=12) and mutant (n=12) neurospheres. β8-/- neurospheres exhibited significantly less migration at both 24h and 48h. *$p < 0.01$.

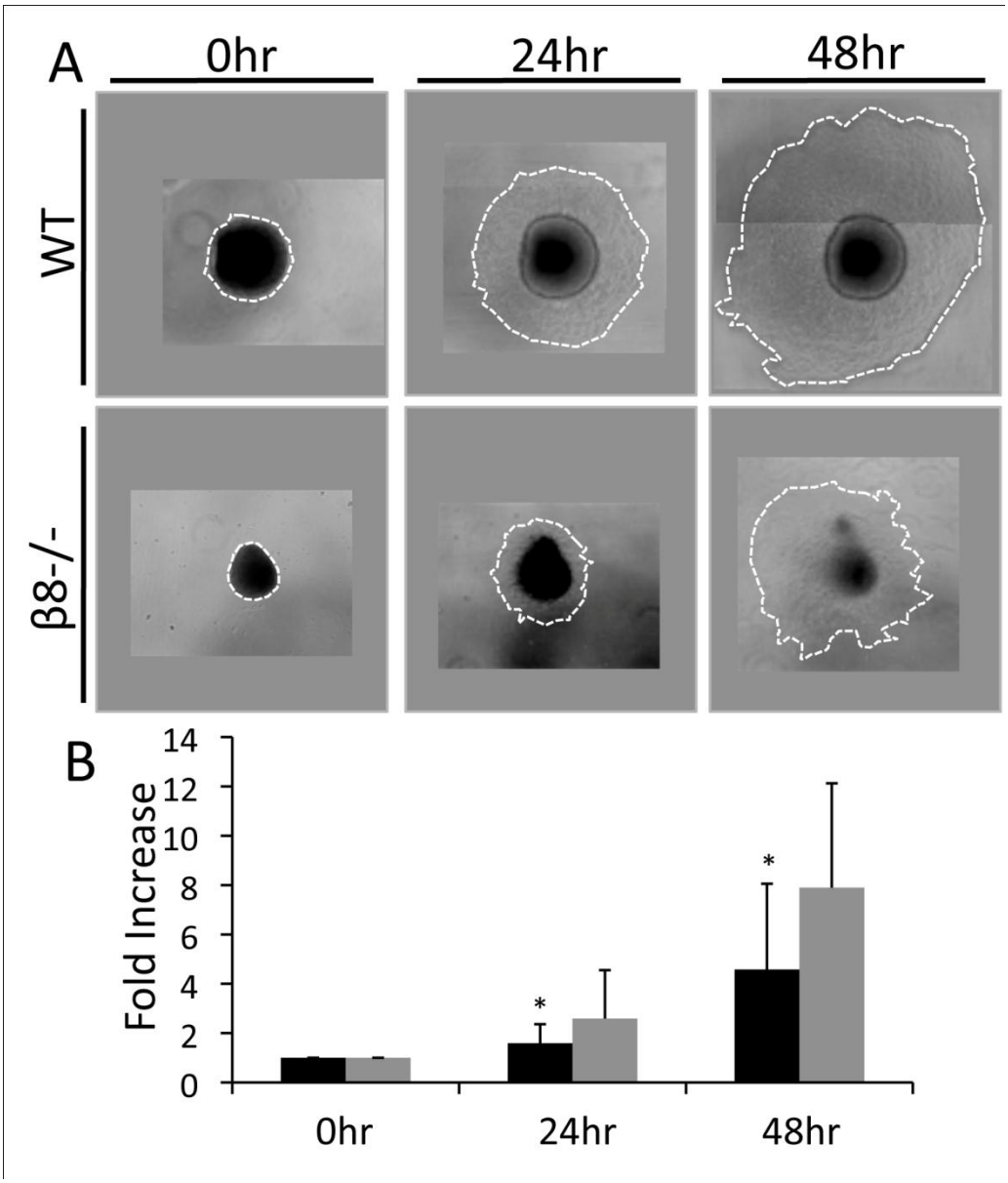
A
0hr
24hr
48hr
WT
β8-/-
B
Fold Increase
14
12
10
8
6
4
2
0
*
*
0hr
24hr
48hr

Figure 31

Analysis of αvβ8 Integrin-Mediated TGFβ Activation in Neuroblast Migration

To explain the neuroblast migration defects observed in the β8-/- mouse brain and *in vitro* neurosphere assays mechanistically, TGFβ signaling was analyzed. A neurosphere migration assay was again utilized. Wild type and β8-/- neurospheres (n=10 for each) were incubated with anti-TGFβ blocking antibody (5μg/ml) or active TGFβ (10ng/ml) for 30 minutes then adhered to laminin-coated dishes. Neurosphere migration was quantified at 12, 24, and 36-hour timepoints using total surface area with 0hr normalization (Figure 32 B). Addition of TGFβ-blocking antibody to wild type neurospheres caused a significant migration decrease at 24 and 36 hours. No significant differences were noticed in mutant neurospheres when TGFβ was blocked at any timepoints analyzed. Exogenous addition of active TGFβ however, did have an effect on β8-/- neurospheres. Migration in mutant neurospheres with the addition of active TGFβ was rescued to near wild type levels by 36 hours. Active TGFβ had very little effect on wild type neurospheres. At later timepoints it seemed to cause a slight, butnot statistically significant, inhibition in migration.

Lysates from wild type and β8-/- DCX-GFP+ neurospheres, attached to a laminin substrate, were prepared and immunoblots were performed to analyze various signaling effectors. TGFβ signaling was examined through immunoblotting for the canonical signaling SMADs. Total SMAD expression levels were similar between wild type and knockout neurospheres. However, western blots for phosphorylated SMAD1,5,8, SMAD2, and SMAD3 revealed decreased canonical TGFβ signaling in β8-/- mice. Decreased levels of phosphoTAK1 and phospho-p38

expression, MAPKs that are phosphorylated by TGFβ receptors, further suggests TGFβs importance. Additionally, ERK signaling was further analyzed with an anti-phospho ERK1/2 antibody; however, no differences in phosphorylated ERK were observed between wild type and mutant lysates. Analysis of AKT1 signaling, using total and phospho AKT antibodies revealed similar levels of the total protein but increased phosphorylated AKT in β8-/- neurospheres (Figure 32 C). Taken together, these results point to a role for integrin mediated activation of TGFβ in neurosphere migration.

Figure 32: *In Vitro* Neurosphere Migration is Integrin and TGFβ Dependent. (A) Neurospheres from wild type and β8-/- P60 mice were incubated with anti-αv, anti-β1, IgG blocking antibodies (A) or anti-TGFβ blocking antibody and recombinant TGFβ1 (B) for 1 hour prior to adherence to laminin substrate. Migration was quantified at 12, 24 and 48 hours, through normalizing the surface area back to the 0 hour timepoint (n=12 for both WT and β8-/-). **(A)** Inhibition of β1 integrin blocked migration completely in both wild type and mutant neurospheres (**$p < 0.001$). αv-blocking antibody produced a significant inhibition of migration in the wild type neurospheres (*$p < 0.05$). In contrast, mutant neurospheres showed very little inhibition of migration with αv blocking. **(B)** Blockage of TGFβ caused a significant reduction in migration in wild type neurospheres at both 24 and 36 hours (*$p < 0.05$). A similar reduction was not seen in mutant neurospheres at any timepoints analyzed. Addition of recombinant TGFβ1 revealed no effect on migration in wild type neurospheres, however in mutant spheres a trend was noticed towards increased migration at 24 and 36 hours, however no significance was noted. **(C)** Lysates from WT and β8-/- sorted neurospheres were immunoblotted for TGFβ and MAPK signaling molecules. Antibodies used were anti-pSMAD2, anti-pSMAD3, anti-pSMAD1,5,8, anti-SMAD, anti-phospho p38, anti-TAK1, anti-pAKT, anti-AKT and anti-pERK.

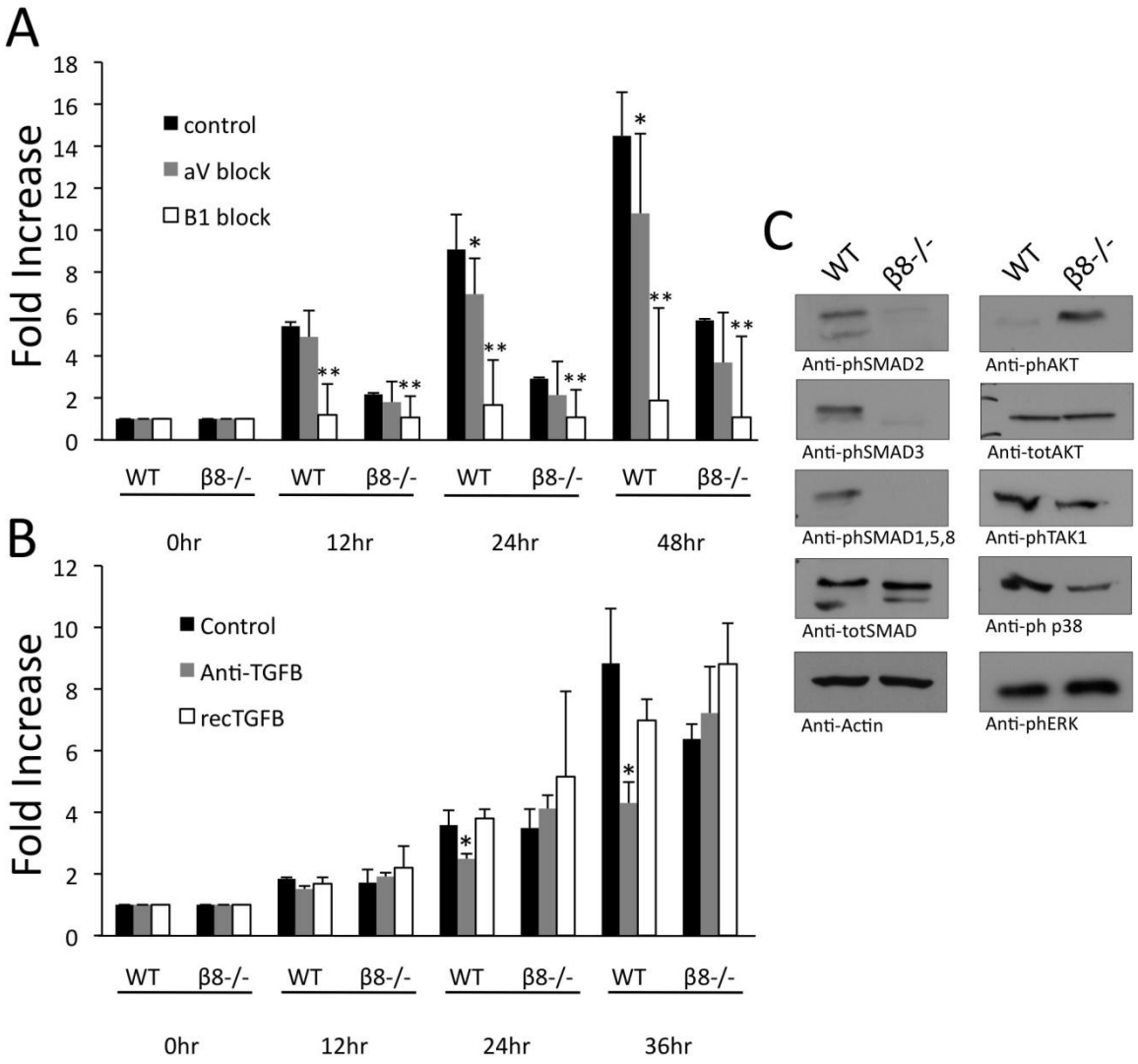
A
Fold Increase
control
aV block
B1 block
WT
β8-/-
0hr
12hr
24hr
48hr
B
Fold Increase
Control
Anti-TGFB
recTGFB
0hr
12hr
24hr
36hr
C
WT
β8-/-
Anti-phSMAD2
Anti-phSMAD3
Anti-phSMAD1,5,8
Anti-totSMAD
Anti-Actin
Anti-phAKT
Anti-totAKT
Anti-phTAK1
Anti-ph p38
Anti-phERK

Figure 32

Discussion:

Here, evidence is provided that β8 integrin is required for proper neuroblast chain formation and directional migration. First, ablation of β8 integrin in the adult brain causes neuroblast chain disorganization in the RMS. Second, the expression of αv and β8 integrin was established in neuroblasts isolated from the SVZ and RMS. Upon loss of β8 integrin, altered expression of other integrin subunits was noted, suggesting a compensatory mechanism or regulation of other integrins by β8 integrin. Finally, integrin-mediated TGFβ activation in the RMS appears to have an autocrine effect on migration of neuroblasts.

αvβ8 Integrin in Neuroblasts is Necessary for Proper Chain Migration in the RMS

Analysis of neuroblast migration in the RMS of β8-/- mice revealed the requirement of β8 integrin for proper chain formation and migration. Loss of β8 integrin causes disorganization in chains of neuroblasts as well as glial tube astrocytes in the RMS (Figure 21 B). Examination of the neuroblast chains in the adult β8-/- RMS revealed that chains do form; however, many clusters of neuroblasts veer off from the RMS, which was not observed in the wild type RMS. Previous studies, using CNS specific β1 knockout mice, have shown a similar defect in chain formation in the RMS when β1 integrin is lost (110). β1 integrin was highly expressed in the β8 mutant brain, and neurospheres isolated from the mutant brain displayed increased levels of α5β1 and α6β1 (Figure 29 A). The increase in

β1 suggests that this integrin may be upregulated to compensate for the loss of β8 integrin. However, it may also reveal that β8 integrin regulates expression of β1 in neuroblasts. Furthermore, *in vitro* studies indicate that complete loss of β8 in combination with a β1-blocking antibody leads to complete inhibition of neurosphere migration. A similar result was seen in wild type neurospheres treated with β1 blocking antibody (Figure 31A). However, when a αv integrin-blocking antibody was used in wild type neurospheres, to block β8 function, a minor, yet significant, decrease in neurosphere migration was noted. These results indicate that while β8 is necessary for migration, it cannot function alone, and likely requires the presence of β1 integrin.

Cues for neuroblast migration likely emanate from astrocytes in the glial tube and the vasculature (141, 154). Neuroblast chains migrate in close association with blood vessels aligned parallel to migrating neuroblasts in the RMS (49, 141). Observations in wild type and mutant mice indicate that neuroblasts migrate associated with blood vessels in both wild type and mutant mice. However, several individual clusters of neuroblasts seen in the β8-/- RMS did not appear to be affiliated with blood vessels, indicating loss of proper signaling. The argument could be made that they are migrating away in a pathological response. However, this is unlikely since in response to stroke, neuroblasts migrate to the site of infarct along blood vessels (143). Further analysis is necessary to determine if the clusters of cells exhibit directional migration. While the association of neuroblasts with blood vessels was not lost, signals coming from the blood vessels may be defective. One important molecule is BDNF, which is expressed by endothelial cells and activates

receptors on neuroblasts to regulate their migration (141). It is likely that αvβ8 integrin-mediated TGFβ signaling could play a role in neuroblast migration as well by regulating migration factors expressed in endothelial cells.

Additionally, β8 integrin is expressed in some GFAP+ astrocytes in the adult brain. Several studies have reported that loss of glial tube organization correlates with disrupted neuroblast chain migration including loss of PSA-NCAM and Slit1 (110, 111, 155). Slit proteins bind to their receptor, Robo, and guide neuronal migration in the developing CNS through chemorepulsion (156, 157). Slit1 is expressed in migrating neuroblasts (155), and a recent report shows expression of Robo on glial tube astrocytes. Signaling between Slit-Robo is necessary for neuroblast migration and glial tube maintenance (134). Collectively, these data suggest that astrocyte-neuroblast direct contact through adhesion molecules, and secreted factors from either neuroblasts or glial tube astrocytes are necessary for neuroblast migration in the adult RMS. Here, abnormal association between migrating neuroblasts and astrocytes of the glial tube was observed in β8-/- mice, likely due to the uncoupling between the two cell types, and loss of TGFβ activation and signaling.

αvβ8 Integrin Mediated Activation of TGFβ in Neuroblast Migration

One potential role for αvβ8-mediated activation of TGFβ was demonstrated in the last chapter in NSC-blood vessel communication. A recent report indicates that loss of SMAD3 reduces proliferation and migration of neuroblasts in the RMS (151). Here, analysis of TGFβ signaling in DCX-GFP+ isolated neuroblasts suggests another potential role. Our model for αvβ8-mediated activation of TGFβ in the SVZ caused upregulation of secreted factors in endothelial cells, which regulate NSCs (Figure 19). The previous aim indicated that TGFβ is indeed activated by αvβ8 integrin in neurospheres (Figure 18 A). Immunoblots of lysates from DCX-GFP/+; β8-/- sorted neurospheres with no exogenous addition of TGFβ, revealed very low levels of SMAD phosphorylation when compared to wild type neurospheres. Furthermore, a TGFβ blocking antibody caused decreased migration in wild type neurospheres and addition of active TGFβ showed a trend towards rescuing mutant neurosphere migration (Figure 31 B). These results indicate that neuroblasts are producing TGFβ and signaling in an autocrine manner. However, even GFP+ sorted neurospheres were not a homogenous population of neuroblasts. GFAP+ astrocytes and nestin positive progenitors were also present within the spheres. Because of the heterogeneity, it is difficult to determine if autocrine TGFβ signals regulate neuroblast migration, or if signaling in another cell type, perhaps glial tube astrocytes or endothelial cells *in vivo*, upregulate various paracrine factors to control neuroblast migration.

Summary

This study was the first to detail specific functions of β8 integrin in the adult neural stem cell vascular niche. The key findings are highlighted below:

1. Many β8-/- mice crossed to ICR/CD1 background survive to adulthood. Hemorrhage was resolved by around 3 weeks of age; however, as mutants age they develop severe neurological phenotypes, including rigid gait, hind limb paresis and seizures (Figure 6).
2. Adult β8-/- mice have increased total vessel numbers throughout the brain, associated with increased coverage by astroglial processes, however the blood brain barrier is likely intact (Figure 8).
3. Abnormal cytoarchitecture in the SVZ of the β8-/- adult brain was observed. Additionally, increased apoptosis, decreased proliferation and increased numbers of DCX+ neuroblasts in the SVZ indicate an important function for β8 integrin in NSC proliferation and survival (Figures 10,11).
4. *In vitro* neurosphere assays indicated self-renewal, proliferation and differentiation defects in NSCs isolated from β8-/- mice, further revealing functions for β8 integrin in NSC regulation (Figures 15,16).
5. αvβ8 integrin mediated activation of TGFβ is responsible for the defects observed in NSC through a paracrine signaling interaction between blood vessels and NSCs in the vascular niche (Figure 18).
6. β8-/- olfactory bulbs are reduced in size, and neuroblasts and glial tube astrocytes in the rostral migratory stream are disorganized, suggesting functional roles for β8 integrin in neuroblast migration (Figures 9, 21).

7. *In vitro* neurosphere migration was significantly reduced in β8-/- mouse neurospheres, further confirming a role for β8 integrin in neurosphere migration (Figure 31).
8. Analysis of integrin expression in purified neuroblasts revealed increased expression of β1 integrins when β8 integrin is absent, suggesting a potential role for β8 integrin in regulation of β1 integrins in migrating neuroblasts (Figure 30), or suggesting that β1 integrins compensate for the loss of β8 integrin.
9. Blocking TGFβ in wild type neurospheres led to decreased migration, and addition of active TGFβ enhanced the migration of β8-/- neurospheres, demonstrating αvβ8 integrin mediated activation of TGFβ functions in neuroblast migration (Figure 32).

Understanding the function of αvβ8 integrin in the adult neural stem cell vascular niche and in migration of neuroblasts in the RMS adds insight as to how NSCs communicate with their niche. Until now, very little was known about specific signaling events that take place between NSCs and the vasculature in the niche. Increasing our understanding about these interactions will not only lead to a better understanding about how β8 functions physiologically, but could also lead to several future studies examining functions for β8 integrin in various CNS pathologies which recruit cells from the NSC vascular niche.

Studies of several brain pathologies, including glioma, stroke and neurodegenerative diseases, have revealed that NSCs migrate toward the insult in normally non-neurogenic regions (158, 159). Aboody and colleagues have shown

that neural stem cell lines implanted into rat brains harboring a glioma are recruited to the site of the tumor and are capable of migrating long distances (159). In a mouse model using middle cerebral artery occlusion (MCAO), chains of neuroblasts from the SVZ were observed migrating in close association with blood vessels toward the injured striatum (143). Cues from angiogenic vessels at the injury site control the migration of neuroblasts from the SVZ and enhance their survival and differentiation (160, 161). Several models of the neurodegenerative disease, Huntington's disease show increased SVZ proliferation and migration toward the striatum, which correlated with severity of the disease (162).

Additional studies using β8 knockout mice could be performed to understand the cellular interactions necessary to accomplish recruitment of NSCs and if β8 integrin plays a similar role in pathological NSC migration. Our lab has shown that it is possible to induce tumors in wild type and β8-/- mice in a syngeneic model using transformed astrocytes from wt or β8-/- P0 neonates. Upon tumor formation, injection of NSCs cultured from wild type or β8 knockout mice and tracking the recruitment of those NSCs to the established tumor could help to identify interactions between normal microenvironment or β8-/- microenvironment and wild type or mutant NSCs. In a similar manner, the migration of wild type and β8-/- neuroblasts towards ischemia could be analyzed with an MCAO model. Endogenous neuroblast migration could be analyzed by tracking the migration of cells from the SVZ and RMS in the ischemic brain, or migration of injected neuroblasts towards the infarct could be analyzed. β8 integrin function in neuroblast differentiation and survival in the ischemic region could also be analyzed.

The GLAST-CreERT2 inducible deletion of β8 integrin was used in this project to further validate the function of β8 integrin in the adult SVZ. Thirty days after tamoxifen injection, mutant mice displayed elevated levels of apoptotic and DCX+ cells, as well as decreased proliferation of cells in the SVZ. However, neuroblast migration in this model was not closely examined. Further examination of the RMS at various timepoints after tamoxifen injection will be needed to further establish β8 integrins function in adult neuroblast migration, and potentially prove that the migration defects in complete β8-/- and N-Cre β8 mutant brains are not a result of the developmental defects.

Additionally, we have identified an important function for αvβ8-mediated activation of TGFβ in both maintenance of the SVZ and in neuroblast migration. While our data indicate that TGFβ is important, there are still several studies that should be done to further understand its function. We have proposed that TGFβ signaling in endothelial cells (EC) controls neural stem cells in the vascular niche in a paracrine manner. To validate this model several additional studies using coculture systems could be performed. We have made several attempts in the past to establish a NSC-EC coculture system, but media compatibility issues were a limiting factor, because neurospheres must be grown in serum free media, while ECs must grow in serum containing media. Our lab recently acquired an early region 4 open reading frame 1 (E4ORF1) adenoviral vector. This vector will enable us to create endothelial cells that proliferate similar to early passage endothelial cells and exhibit long-term survival in the serum free conditions required for neurospheres to grow (163). With these ECs coculture studies can be performed to

look at interactions between ECs and NSCs either in direct contact, or through secreted factors in a transwell assay. This will help us to further identify signaling effectors that regulate NSCs through αvβ8 integrin-mediated TGFβ activation. Furthermore, these cocultures could be used to examine the migration of wild type and β8-/- neuroblasts along blood vessels using timelapse imaging to determine how ECs and NSCs interact in a three-dimensional matrix.

Increased expression of β1 integrins was observed in purified neuroblasts from β8-/- mouse brains. This suggests a possible regulatory function for β8 integrin of other integrins. Here, we have reported increased levels of TGFβ signaling in β8-/- neuroblasts. Previous reports show that TGFβ can control integrin expression. Additional studies could be performed to find a link between αvβ8-mediated TGFβ activation and TGFβ regulation of β1 integrins. Anti-TGFβ blocking antibodies could be added to wild type neuroblasts, and levels of integrins could then be assessed. If TGFβ is indeed regulating β1 integrin expression levels we would expect to see increased β1 expression in wild type neuroblasts when TGFβ signaling is blocked. *In vivo* studies could also be performed looking for colocalization of β1 integrin and phosphorylated SMAD proteins in both wild type and β8-/- mouse brains.

Further analysis of RMS neuroblast migration could increase our knowledge of interactions between neuroblasts and astrocytes of the glial tube. In a similar manner as EC-NSC cocultures, astrocytes and neuroblasts could be co-cultured to directly assess the interactions necessary for neuroblast migration. Studies to determine if β8 integrins expression specifically in astrocytes or in neuroblasts or both is required for proper migration could be accomplished. Also, *in vivo* analyses

could be performed to determine these interactions in the RMS. Determination of which cell type, astrocytes, neuroblasts or both require β8 integrin for proper migration could be performed using GFP+ neuroblasts isolated from wild type and β8-/- mice. Wild type neuroblasts could be injected into the β8-/- RMS to analyze expression of β8 integrin on neuroblasts, or β8-/- neuroblasts could be injected into the wild type RMS to determine the role of β8 integrin in glial tube astrocytes. Brains could then be analyzed with markers for neuroblasts (DCX or PSA-NCAM) and astrocytes (GFAP) as well as GFP to determine where the injected cells have migrated. Together, these experiments would help determine if expression of β8 integrin is required only on neuroblasts or astrocytes, or both cell types for proper neuroblast migration in the RMS.

In addition to the defects observed in the SVZ and RMS, our initial analysis of the adult β8 null mouse brain revealed disorganization in several other areas of the brain. The corpus callosum in the β8-/- brain is incompletely formed likely due to defects in neuronal migration during development. Slit and robo play established roles in directing neuronal migration for corpus callosum development (164). This, along with recent findings indicating a function for slit/robo in neuroblast migration in the RMS (134), suggests an additional function for β8 integrin in regulation of either slit or robo. The RMS and the corpus callosum could be studied to decipher this role.

Analysis of β8 integrins' function in the other major adult neurogenic region, the subgranular zone of the dentate gyrus, should also be done. Our analysis of adult β8 knockout mice revealed abnormal architecture in the hippocampus,

including increased thickness of the hilus and abnormal dendritic projections in the CA3 region of the dentate gyrus. These findings indicate further roles for β8 integrin in the dentate gyrus. Simliar analysis of NSCs in this region using both *in vivo* as well as *in vitro* neurosphere assays could be used to determine if β8 plays a similar functional role in NSC regulation and migration.

Collectively, my thesis project has identified a novel function for β8 integrin in adult neurogenesis and neurovascular homeostasis using complete, conditional and inducible β8 integrin knockout mouse models. More detailed examination of the β8-/- mouse model will identify several other functions beyond the novel functions demonstrated here.

References

1. McCarty, J. H. 2005. Cell biology of the neurovascular unit: implications for drug delivery across the blood-brain barrier. Assay Drug Dev Technol 3:89-95.
2. Mercier, F., J. T. Kitasako, and G. I. Hatton. 2002. Anatomy of the brain neurogenic zones revisited: fractones and the fibroblast/macrophage network. J Comp Neurol 451:170-188.
3. Ballabh, P., A. Braun, and M. Nedergaard. 2004. The blood-brain barrier: an overview: structure, regulation, and clinical implications. Neurobiol Dis 16:1-13.
4. Mulligan, S. J., and B. A. MacVicar. 2004. Calcium transients in astrocyte endfeet cause cerebrovascular constrictions. Nature 431:195-199.
5. Kriegstein, A., and A. Alvarez-Buylla. 2009. The glial nature of embryonic and adult neural stem cells. Annu Rev Neurosci 32:149-184.
6. Marin-Padilla, M. 1985. Early vascularization of the embryonic cerebral cortex: Golgi and electron microscopic studies. J Comp Neurol 241:237-249.
7. Mi, H., H. Haeberle, and B. A. Barres. 2001. Induction of astrocyte differentiation by endothelial cells. J Neurosci 21:1538-1547.
8. Zerlin, M., and J. E. Goldman. 1997. Interactions between glial progenitors and blood vessels during early postnatal corticogenesis: blood vessel contact represents an early stage of astrocyte differentiation. J Comp Neurol 387:537-546.

9. Palmer, T. D., A. R. Willhoite, and F. H. Gage. 2000. Vascular niche for adult hippocampal neurogenesis. J Comp Neurol 425:479-494.

10. Song, H., C. F. Stevens, and F. H. Gage. 2002. Astroglia induce neurogenesis from adult neural stem cells. Nature 417:39-44.

11. Goldberg, J. S., and K. K. Hirschi. 2009. Diverse roles of the vasculature within the neural stem cell niche. Regen Med 4:879-897.

12. Louissaint, A., Jr., S. Rao, C. Leventhal, and S. A. Goldman. 2002. Coordinated interaction of neurogenesis and angiogenesis in the adult songbird brain. Neuron 34:945-960.

13. Iadecola, C., and M. Nedergaard. 2007. Glial regulation of the cerebral microvasculature. Nat Neurosci 10:1369-1376.

14. Hawkins, B. T., and T. P. Davis. 2005. The blood-brain barrier/neurovascular unit in health and disease. Pharmacol Rev 57:173-185.

15. Abbott, N. J., L. Ronnback, and E. Hansson. 2006. Astrocyte-endothelial interactions at the blood-brain barrier. Nat Rev Neurosci 7:41-53.

16. Gould, D. B., F. C. Phalan, G. J. Breedveld, S. E. van Mil, R. S. Smith, J. C. Schimenti, U. Aguglia, M. S. van der Knaap, P. Heutink, and S. W. John. 2005. Mutations in Col4a1 cause perinatal cerebral hemorrhage and porencephaly. Science 308:1167-1171.

17. Ozduman, K., B. R. Pober, P. Barnes, J. A. Copel, E. A. Ogle, C. C. Duncan, and L. R. Ment. 2004. Fetal stroke. Pediatr Neurol 30:151-162.

18. Deane, R., R. D. Bell, A. Sagare, and B. V. Zlokovic. 2009. Clearance of amyloid-beta peptide across the blood-brain barrier: implication for therapies in Alzheimer's disease. CNS Neurol Disord Drug Targets 8:16-30.

19. Bailey, T. L., C. B. Rivara, A. B. Rocher, and P. R. Hof. 2004. The nature and effects of cortical microvascular pathology in aging and Alzheimer's disease. Neurol Res 26:573-578.

20. Grammas, P., M. Yamada, and B. Zlokovic. 2002. The cerebromicrovasculature: a key player in the pathogenesis of Alzheimer's disease. J Alzheimers Dis 4:217-223.

21. del Zoppo, G. J. The neurovascular unit in the setting of stroke. J Intern Med 267:156-171.

22. Petty, M. A., and J. G. Wettstein. 2001. Elements of cerebral microvascular ischaemia. Brain Res Brain Res Rev 36:23-34.

23. Lee, J., C. Lund-Smith, A. Borboa, A. M. Gonzalez, A. Baird, and B. P. Eliceiri. 2009. Glioma-induced remodeling of the neurovascular unit. Brain Res 1288:125-134.

24. Tchaicha, J. H., A. K. Mobley, M. G. Hossain, K. D. Aldape, and J. H. McCarty. A mosaic mouse model of astrocytoma identifies alphavbeta8 integrin as a negative regulator of tumor angiogenesis. Oncogene.

25. Gilbertson, R. J., and J. N. Rich. 2007. Making a tumour's bed: glioblastoma stem cells and the vascular niche. Nat Rev Cancer 7:733-736.

26. Schofield, R. 1978. The relationship between the spleen colony-forming cell and the haemopoietic stem cell. Blood Cells 4:7-25.

27. Doetsch, F. 2003. The glial identity of neural stem cells. Nat Neurosci 6:1127-1134.

28. Mori, T., K. Tanaka, A. Buffo, W. Wurst, R. Kuhn, and M. Gotz. 2006. Inducible gene deletion in astroglia and radial glia--a valuable tool for functional and lineage analysis. Glia 54:21-34.

29. Voigt, T. 1989. Development of glial cells in the cerebral wall of ferrets: direct tracing of their transformation from radial glia into astrocytes. J Comp Neurol 289:74-88.

30. Doetsch, F., and C. Scharff. 2001. Challenges for brain repair: insights from adult neurogenesis in birds and mammals. Brain Behav Evol 58:306-322.

31. Ming, G. L., and H. Song. 2005. Adult neurogenesis in the mammalian central nervous system. Annu Rev Neurosci 28:223-250.

32. Seri, B., J. M. Garcia-Verdugo, B. S. McEwen, and A. Alvarez-Buylla. 2001. Astrocytes give rise to new neurons in the adult mammalian hippocampus. J Neurosci 21:7153-7160.

33. Kempermann, G., H. G. Kuhn, and F. H. Gage. 1997. More hippocampal neurons in adult mice living in an enriched environment. Nature 386:493-495.

34. Parent, J. M., T. W. Yu, R. T. Leibowitz, D. H. Geschwind, R. S. Sloviter, and D. H. Lowenstein. 1997. Dentate granule cell neurogenesis is increased by seizures and contributes to aberrant network reorganization in the adult rat hippocampus. J Neurosci 17:3727-3738.

35. Eisch, A. J., M. Barrot, C. A. Schad, D. W. Self, and E. J. Nestler. 2000. Opiates inhibit neurogenesis in the adult rat hippocampus. Proc Natl Acad Sci U S A 97:7579-7584.

36. Lois, C., and A. Alvarez-Buylla. 1993. Proliferating subventricular zone cells in the adult mammalian forebrain can differentiate into neurons and glia. Proc Natl Acad Sci U S A 90:2074-2077.

37. Doetsch, F., J. M. Garcia-Verdugo, and A. Alvarez-Buylla. 1997. Cellular composition and three-dimensional organization of the subventricular germinal zone in the adult mammalian brain. J Neurosci 17:5046-5061.

38. Lois, C., J. M. Garcia-Verdugo, and A. Alvarez-Buylla. 1996. Chain migration of neuronal precursors. Science 271:978-981.

39. Doetsch, F. 2003. A niche for adult neural stem cells. Curr Opin Genet Dev 13:543-550.

40. Plate, K. H. 1999. Mechanisms of angiogenesis in the brain. J Neuropathol Exp Neurol 58:313-320.

41. Shen, Q., S. K. Goderie, L. Jin, N. Karanth, Y. Sun, N. Abramova, P. Vincent, K. Pumiglia, and S. Temple. 2004. Endothelial cells stimulate self-renewal and expand neurogenesis of neural stem cells. Science 304:1338-1340.

42. Tavazoie, M., L. Van der Veken, V. Silva-Vargas, M. Louissaint, L. Colonna, B. Zaidi, J. M. Garcia-Verdugo, and F. Doetsch. 2008. A specialized vascular niche for adult neural stem cells. Cell Stem Cell 3:279-288.

43. Breton-Provencher, V., M. Lemasson, M. R. Peralta, 3rd, and A. Saghatelyan. 2009. Interneurons produced in adulthood are required for the

normal functioning of the olfactory bulb network and for the execution of selected olfactory behaviors. J Neurosci 29:15245-15257.

44. Jankovski, A., and C. Sotelo. 1996. Subventricular zone-olfactory bulb migratory pathway in the adult mouse: cellular composition and specificity as determined by heterochronic and heterotopic transplantation. J Comp Neurol 371:376-396.

45. Wichterle, H., J. M. Garcia-Verdugo, and A. Alvarez-Buylla. 1997. Direct evidence for homotypic, glia-independent neuronal migration. Neuron 18:779-791.

46. Ghashghaei, H. T., C. Lai, and E. S. Anton. 2007. Neuronal migration in the adult brain: are we there yet? Nat Rev Neurosci 8:141-151.

47. Kojima, T., Y. Hirota, M. Ema, S. Takahashi, I. Miyoshi, H. Okano, and K. Sawamoto. Subventricular zone-derived neural progenitor cells migrate along a blood vessel scaffold toward the post-stroke striatum. Stem Cells 28:545-554.

48. Thomas, L. B., M. A. Gates, and D. A. Steindler. 1996. Young neurons from the adult subependymal zone proliferate and migrate along an astrocyte, extracellular matrix-rich pathway. Glia 17:1-14.

49. Whitman, M. C., W. Fan, L. Rela, D. J. Rodriguez-Gil, and C. A. Greer. 2009. Blood vessels form a migratory scaffold in the rostral migratory stream. J Comp Neurol 516:94-104.

50. Carleton, A., L. T. Petreanu, R. Lansford, A. Alvarez-Buylla, and P. M. Lledo. 2003. Becoming a new neuron in the adult olfactory bulb. Nat Neurosci 6:507-518.

51. Hall, P. E., J. D. Lathia, N. G. Miller, M. A. Caldwell, and C. ffrench-Constant. 2006. Integrins are markers of human neural stem cells. Stem Cells 24:2078-2084.

52. Hynes, R. O. 2002. Integrins: bidirectional, allosteric signaling machines. Cell 110:673-687.

53. Wegener, K. L., A. W. Partridge, J. Han, A. R. Pickford, R. C. Liddington, M. H. Ginsberg, and I. D. Campbell. 2007. Structural basis of integrin activation by talin. Cell 128:171-182.

54. Giancotti, F. G., and E. Ruoslahti. 1999. Integrin signaling. Science 285:1028-1032.

55. Takada, Y., X. Ye, and S. Simon. 2007. The integrins. Genome Biol 8:215.

56. Burke, R. D. 1999. Invertebrate integrins: structure, function, and evolution. Int Rev Cytol 191:257-284.

57. Hynes, R. O. 1992. Integrins: versatility, modulation, and signaling in cell adhesion. Cell 69:11-25.

58. Meyer, A., J. Auernheimer, A. Modlinger, and H. Kessler. 2006. Targeting RGD recognizing integrins: drug development, biomaterial research, tumor imaging and targeting. Curr Pharm Des 12:2723-2747.

59. Barczyk, M., S. Carracedo, and D. Gullberg. Integrins. Cell Tissue Res 339:269-280.

60. Eble, J. A. 2005. Collagen-binding integrins as pharmaceutical targets. Curr Pharm Des 11:867-880.

61. Harris, E. S., T. M. McIntyre, S. M. Prescott, and G. A. Zimmerman. 2000. The leukocyte integrins. J Biol Chem 275:23409-23412.

62. Shimamura, N., G. Matchett, H. Yatsushige, J. W. Calvert, H. Ohkuma, and J. Zhang. 2006. Inhibition of integrin alphavbeta3 ameliorates focal cerebral ischemic damage in the rat middle cerebral artery occlusion model. Stroke 37:1902-1909.

63. Delannet, M., F. Martin, B. Bossy, D. A. Cheresh, L. F. Reichardt, and J. L. Duband. 1994. Specific roles of the alpha V beta 1, alpha V beta 3 and alpha V beta 5 integrins in avian neural crest cell adhesion and migration on vitronectin. Development 120:2687-2702.

64. Hirsch, E., D. Gullberg, F. Balzac, F. Altruda, L. Silengo, and G. Tarone. 1994. Alpha v integrin subunit is predominantly located in nervous tissue and skeletal muscle during mouse development. Dev Dyn 201:108-120.

65. Breuss, J. M., J. Gallo, H. M. DeLisser, I. V. Klimanskaya, H. G. Folkesson, J. F. Pittet, S. L. Nishimura, K. Aldape, D. V. Landers, W. Carpenter, and et al. 1995. Expression of the beta 6 integrin subunit in development, neoplasia and tissue repair suggests a role in epithelial remodeling. J Cell Sci 108 (Pt 6):2241-2251.

66. Brooks, P. C., R. A. Clark, and D. A. Cheresh. 1994. Requirement of vascular integrin alpha v beta 3 for angiogenesis. Science 264:569-571.

67. Bader, B. L., H. Rayburn, D. Crowley, and R. O. Hynes. 1998. Extensive vasculogenesis, angiogenesis, and organogenesis precede lethality in mice lacking all alpha v integrins. Cell 95:507-519.

68. Fassler, R., M. Pfaff, J. Murphy, A. A. Noegel, S. Johansson, R. Timpl, and R. Albrecht. 1995. Lack of beta 1 integrin gene in embryonic stem cells affects morphology, adhesion, and migration but not integration into the inner cell mass of blastocysts. J Cell Biol 128:979-988.

69. Hodivala-Dilke, K. M., K. P. McHugh, D. A. Tsakiris, H. Rayburn, D. Crowley, M. Ullman-Cullere, F. P. Ross, B. S. Coller, S. Teitelbaum, and R. O. Hynes. 1999. Beta3-integrin-deficient mice are a model for Glanzmann thrombasthenia showing placental defects and reduced survival. J Clin Invest 103:229-238.

70. Tronik-Le Roux, D., V. Roullot, C. Poujol, T. Kortulewski, P. Nurden, and G. Marguerie. 2000. Thrombasthenic mice generated by replacement of the integrin alpha(IIb) gene: demonstration that transcriptional activation of this megakaryocytic locus precedes lineage commitment. Blood 96:1399-1408.

71. Huang, X., M. Griffiths, J. Wu, R. V. Farese, Jr., and D. Sheppard. 2000. Normal development, wound healing, and adenovirus susceptibility in beta5-deficient mice. Mol Cell Biol 20:755-759.

72. Nandrot, E. F., Y. Kim, S. E. Brodie, X. Huang, D. Sheppard, and S. C. Finnemann. 2004. Loss of synchronized retinal phagocytosis and age-related blindness in mice lacking alphavbeta5 integrin. J Exp Med 200:1539-1545.

73. Huang, X. Z., J. F. Wu, D. Cass, D. J. Erle, D. Corry, S. G. Young, R. V. Farese, Jr., and D. Sheppard. 1996. Inactivation of the integrin beta 6 subunit gene reveals a role of epithelial integrins in regulating inflammation in the lung and skin. J Cell Biol 133:921-928.

74. Zhu, J., K. Motejlek, D. Wang, K. Zang, A. Schmidt, and L. F. Reichardt. 2002. beta8 integrins are required for vascular morphogenesis in mouse embryos. Development 129:2891-2903.

75. Moyle, M., M. A. Napier, and J. W. McLean. 1991. Cloning and expression of a divergent integrin subunit beta 8. J Biol Chem 266:19650-19658.

76. Lein, E. S., M. J. Hawrylycz, N. Ao, M. Ayres, A. Bensinger, A. Bernard, A. F. Boe, M. S. Boguski, K. S. Brockway, E. J. Byrnes, L. Chen, T. M. Chen, M. C. Chin, J. Chong, B. E. Crook, A. Czaplinska, C. N. Dang, S. Datta, N. R. Dee, A. L. Desaki, T. Desta, E. Diep, T. A. Dolbeare, M. J. Donelan, H. W. Dong, J. G. Dougherty, B. J. Duncan, A. J. Ebbert, G. Eichele, L. K. Estin, C. Faber, B. A. Facer, R. Fields, S. R. Fischer, T. P. Fliss, C. Frensley, S. N. Gates, K. J. Glattfelder, K. R. Halverson, M. R. Hart, J. G. Hohmann, M. P. Howell, D. P. Jeung, R. A. Johnson, P. T. Karr, R. Kawal, J. M. Kidney, R. H. Knapik, C. L. Kuan, J. H. Lake, A. R. Laramee, K. D. Larsen, C. Lau, T. A. Lemon, A. J. Liang, Y. Liu, L. T. Luong, J. Michaels, J. J. Morgan, R. J. Morgan, M. T. Mortrud, N. F. Mosqueda, L. L. Ng, R. Ng, G. J. Orta, C. C. Overly, T. H. Pak, S. E. Parry, S. D. Pathak, O. C. Pearson, R. B. Puchalski, Z. L. Riley, H. R. Rockett, S. A. Rowland, J. J. Royall, M. J. Ruiz, N. R. Sarno, K. Schaffnit, N. V. Shapovalova, T. Sivisay, C. R. Slaughterbeck, S.

C. Smith, K. A. Smith, B. I. Smith, A. J. Sodt, N. N. Stewart, K. R. Stumpf, S. M. Sunkin, M. Sutram, A. Tam, C. D. Teemer, C. Thaller, C. L. Thompson, L. R. Varnam, A. Visel, R. M. Whitlock, P. E. Wohnoutka, C. K. Wolkey, V. Y. Wong, M. Wood, M. B. Yaylaoglu, R. C. Young, B. L. Youngstrom, X. F. Yuan, B. Zhang, T. A. Zwingman, and A. R. Jones. 2007. Genome-wide atlas of gene expression in the adult mouse brain. Nature 445:168-176.

77. Nishimura, S. L., K. P. Boylen, S. Einheber, T. A. Milner, D. M. Ramos, and R. Pytela. 1998. Synaptic and glial localization of the integrin alphavbeta8 in mouse and rat brain. Brain Res 791:271-282.

78. Calderwood, D. A., B. Yan, J. M. de Pereda, B. G. Alvarez, Y. Fujioka, R. C. Liddington, and M. H. Ginsberg. 2002. The phosphotyrosine binding-like domain of talin activates integrins. J Biol Chem 277:21749-21758.

79. McCarty, J. H., A. A. Cook, and R. O. Hynes. 2005. An interaction between {alpha}v{beta}8 integrin and Band 4.1B via a highly conserved region of the Band 4.1 C-terminal domain. Proc Natl Acad Sci U S A 102:13479-13483.

80. Nishimura, S. L., D. Sheppard, and R. Pytela. 1994. Integrin alpha v beta 8. Interaction with vitronectin and functional divergence of the beta 8 cytoplasmic domain. J Biol Chem 269:28708-28715.

81. Venstrom, K., and L. Reichardt. 1995. Beta 8 integrins mediate interactions of chick sensory neurons with laminin-1, collagen IV, and fibronectin. Mol Biol Cell 6:419-431.

82. Mu, D., S. Cambier, L. Fjellbirkeland, J. L. Baron, J. S. Munger, H. Kawakatsu, D. Sheppard, V. C. Broaddus, and S. L. Nishimura. 2002. The

integrin alpha(v)beta8 mediates epithelial homeostasis through MT1-MMP-dependent activation of TGF-beta1. J Cell Biol 157:493-507.

83. Cambier, S., S. Gline, D. Mu, R. Collins, J. Araya, G. Dolganov, S. Einheber, N. Boudreau, and S. L. Nishimura. 2005. Integrin alpha(v)beta8-mediated activation of transforming growth factor-beta by perivascular astrocytes: an angiogenic control switch. Am J Pathol 166:1883-1894.

84. Annes, J. P., J. S. Munger, and D. B. Rifkin. 2003. Making sense of latent TGFbeta activation. J Cell Sci 116:217-224.

85. Sato, Y., and D. B. Rifkin. 1989. Inhibition of endothelial cell movement by pericytes and smooth muscle cells: activation of a latent transforming growth factor-beta 1-like molecule by plasmin during co-culture. J Cell Biol 109:309-315.

86. Yu, Q., and I. Stamenkovic. 2000. Cell surface-localized matrix metalloproteinase-9 proteolytically activates TGF-beta and promotes tumor invasion and angiogenesis. Genes Dev 14:163-176.

87. Schultz-Cherry, S., and J. E. Murphy-Ullrich. 1993. Thrombospondin causes activation of latent transforming growth factor-beta secreted by endothelial cells by a novel mechanism. J Cell Biol 122:923-932.

88. Munger, J. S., X. Huang, H. Kawakatsu, M. J. Griffiths, S. L. Dalton, J. Wu, J. F. Pittet, N. Kaminski, C. Garat, M. A. Matthay, D. B. Rifkin, and D. Sheppard. 1999. The integrin alpha v beta 6 binds and activates latent TGF beta 1: a mechanism for regulating pulmonary inflammation and fibrosis. Cell 96:319-328.

89. Aluwihare, P., Z. Mu, Z. Zhao, D. Yu, P. H. Weinreb, G. S. Horan, S. M. Violette, and J. S. Munger. 2009. Mice that lack activity of alphavbeta6- and alphavbeta8-integrins reproduce the abnormalities of Tgfb1- and Tgfb3-null mice. J Cell Sci 122:227-232.

90. Yang, Z., Z. Mu, B. Dabovic, V. Jurukovski, D. Yu, J. Sung, X. Xiong, and J. S. Munger. 2007. Absence of integrin-mediated TGFbeta1 activation in vivo recapitulates the phenotype of TGFbeta1-null mice. J Cell Biol 176:787-793.

91. Dickson, M. C., J. S. Martin, F. M. Cousins, A. B. Kulkarni, S. Karlsson, and R. J. Akhurst. 1995. Defective haematopoiesis and vasculogenesis in transforming growth factor-beta 1 knock out mice. Development 121:1845-1854.

92. Mu, Z., Z. Yang, D. Yu, Z. Zhao, and J. S. Munger. 2008. TGFbeta1 and TGFbeta3 are partially redundant effectors in brain vascular morphogenesis. Mech Dev 125:508-516.

93. McCarty, J. H., A. Lacy-Hulbert, A. Charest, R. T. Bronson, D. Crowley, D. Housman, J. Savill, J. Roes, and R. O. Hynes. 2005. Selective ablation of alphav integrins in the central nervous system leads to cerebral hemorrhage, seizures, axonal degeneration and premature death. Development 132:165-176.

94. Proctor, J. M., K. Zang, D. Wang, R. Wang, and L. F. Reichardt. 2005. Vascular development of the brain requires beta8 integrin expression in the neuroepithelium. J Neurosci 25:9940-9948.

95. Tronche, F., C. Kellendonk, O. Kretz, P. Gass, K. Anlag, P. C. Orban, R. Bock, R. Klein, and G. Schutz. 1999. Disruption of the glucocorticoid receptor gene in the nervous system results in reduced anxiety. Nat Genet 23:99-103.

96. Rietze, R. L., and B. A. Reynolds. 2006. Neural stem cell isolation and characterization. Methods Enzymol 419:3-23.

97. Abe, M., J. G. Harpel, C. N. Metz, I. Nunes, D. J. Loskutoff, and D. B. Rifkin. 1994. An assay for transforming growth factor-beta using cells transfected with a plasminogen activator inhibitor-1 promoter-luciferase construct. Anal Biochem 216:276-284.

98. Alvarez-Buylla, A., and J. M. Garcia-Verdugo. 2002. Neurogenesis in adult subventricular zone. J Neurosci 22:629-634.

99. Lledo, P. M., M. Alonso, and M. S. Grubb. 2006. Adult neurogenesis and functional plasticity in neuronal circuits. Nat Rev Neurosci 7:179-193.

100. Pardal, R., A. V. Molofsky, S. He, and S. J. Morrison. 2005. Stem cell self-renewal and cancer cell proliferation are regulated by common networks that balance the activation of proto-oncogenes and tumor suppressors. Cold Spring Harb Symp Quant Biol 70:177-185.

101. Morrison, S. J., and A. C. Spradling. 2008. Stem cells and niches: mechanisms that promote stem cell maintenance throughout life. Cell 132:598-611.

102. Wurmser, A. E., T. D. Palmer, and F. H. Gage. 2004. Neuroscience. Cellular interactions in the stem cell niche. Science 304:1253-1255.

103. Le Bras, B., M. J. Barallobre, J. Homman-Ludiye, A. Ny, S. Wyns, T. Tammela, P. Haiko, M. J. Karkkainen, L. Yuan, M. P. Muriel, E. Chatzopoulou, C. Breant, B. Zalc, P. Carmeliet, K. Alitalo, A. Eichmann, and J. L. Thomas. 2006. VEGF-C is a trophic factor for neural progenitors in the vertebrate embryonic brain. Nat Neurosci 9:340-348.

104. Li, Q., M. C. Ford, E. B. Lavik, and J. A. Madri. 2006. Modeling the neurovascular niche: VEGF- and BDNF-mediated cross-talk between neural stem cells and endothelial cells: an in vitro study. J Neurosci Res 84:1656-1668.

105. Ramirez-Castillejo, C., F. Sanchez-Sanchez, C. Andreu-Agullo, S. R. Ferron, J. D. Aroca-Aguilar, P. Sanchez, H. Mira, J. Escribano, and I. Farinas. 2006. Pigment epithelium-derived factor is a niche signal for neural stem cell renewal. Nat Neurosci 9:331-339.

106. Ward, N. L., and J. C. Lamanna. 2004. The neurovascular unit and its growth factors: coordinated response in the vascular and nervous systems. Neurol Res 26:870-883.

107. McCarty, J. H., R. A. Monahan-Earley, L. F. Brown, M. Keller, H. Gerhardt, K. Rubin, M. Shani, H. F. Dvorak, H. Wolburg, B. L. Bader, A. M. Dvorak, and R. O. Hynes. 2002. Defective associations between blood vessels and brain parenchyma lead to cerebral hemorrhage in mice lacking alphav integrins. Mol Cell Biol 22:7667-7677.

108. Nitta, T., M. Hata, S. Gotoh, Y. Seo, H. Sasaki, N. Hashimoto, M. Furuse, and S. Tsukita. 2003. Size-selective loosening of the blood-brain barrier in claudin-5-deficient mice. J Cell Biol 161:653-660.

109. Sawamoto, K., H. Wichterle, O. Gonzalez-Perez, J. A. Cholfin, M. Yamada, N. Spassky, N. S. Murcia, J. M. Garcia-Verdugo, O. Marin, J. L. Rubenstein, M. Tessier-Lavigne, H. Okano, and A. Alvarez-Buylla. 2006. New neurons follow the flow of cerebrospinal fluid in the adult brain. Science 311:629-632.

110. Belvindrah, R., S. Hankel, J. Walker, B. L. Patton, and U. Muller. 2007. Beta1 integrins control the formation of cell chains in the adult rostral migratory stream. J Neurosci 27:2704-2717.

111. Chazal, G., P. Durbec, A. Jankovski, G. Rougon, and H. Cremer. 2000. Consequences of neural cell adhesion molecule deficiency on cell migration in the rostral migratory stream of the mouse. J Neurosci 20:1446-1457.

112. Hirrlinger, P. G., A. Scheller, C. Braun, J. Hirrlinger, and F. Kirchhoff. 2006. Temporal control of gene recombination in astrocytes by transgenic expression of the tamoxifen-inducible DNA recombinase variant CreERT2. Glia 54:11-20.

113. Branda, C. S., and S. M. Dymecki. 2004. Talking about a revolution: The impact of site-specific recombinases on genetic analyses in mice. Dev Cell 6:7-28.

114. Soriano, P. 1999. Generalized lacZ expression with the ROSA26 Cre reporter strain. Nat Genet 21:70-71.

115. Uchida, N., D. W. Buck, D. He, M. J. Reitsma, M. Masek, T. V. Phan, A. S. Tsukamoto, F. H. Gage, and I. L. Weissman. 2000. Direct isolation of human central nervous system stem cells. Proc Natl Acad Sci U S A 97:14720-14725.

116. Kaneko, Y., S. Sakakibara, T. Imai, A. Suzuki, Y. Nakamura, K. Sawamoto, Y. Ogawa, Y. Toyama, T. Miyata, and H. Okano. 2000. Musashi1: an evolutionally conserved marker for CNS progenitor cells including neural stem cells. Dev Neurosci 22:139-153.

117. Zappone, M. V., R. Galli, R. Catena, N. Meani, S. De Biasi, E. Mattei, C. Tiveron, A. L. Vescovi, R. Lovell-Badge, S. Ottolenghi, and S. K. Nicolis. 2000. Sox2 regulatory sequences direct expression of a (beta)-geo transgene to telencephalic neural stem cells and precursors of the mouse embryo, revealing regionalization of gene expression in CNS stem cells. Development 127:2367-2382.

118. Molofsky, A. V., S. He, M. Bydon, S. J. Morrison, and R. Pardal. 2005. Bmi-1 promotes neural stem cell self-renewal and neural development but not mouse growth and survival by repressing the p16Ink4a and p19Arf senescence pathways. Genes Dev 19:1432-1437.

119. Jacques, T. S., J. B. Relvas, S. Nishimura, R. Pytela, G. M. Edwards, C. H. Streuli, and C. ffrench-Constant. 1998. Neural precursor cell chain migration and division are regulated through different beta1 integrins. Development 125:3167-3177.

120. Roussa, E., M. Wiehle, N. Dunker, S. Becker-Katins, O. Oehlke, and K. Krieglstein. 2006. Transforming growth factor beta is required for differentiation of mouse mesencephalic progenitors into dopaminergic neurons in vitro and in vivo: ectopic induction in dorsal mesencephalon. Stem Cells 24:2120-2129.

121. Battista, D., C. C. Ferrari, F. H. Gage, and F. J. Pitossi. 2006. Neurogenic niche modulation by activated microglia: transforming growth factor beta increases neurogenesis in the adult dentate gyrus. Eur J Neurosci 23:83-93.

122. Falk, S., H. Wurdak, L. M. Ittner, F. Ille, G. Sumara, M. T. Schmid, K. Draganova, K. S. Lang, C. Paratore, P. Leveen, U. Suter, S. Karlsson, W. Born, R. Ricci, M. Gotz, and L. Sommer. 2008. Brain area-specific effect of TGF-beta signaling on Wnt-dependent neural stem cell expansion. Cell Stem Cell 2:472-483.

123. Wachs, F. P., B. Winner, S. Couillard-Despres, T. Schiller, R. Aigner, J. Winkler, U. Bogdahn, and L. Aigner. 2006. Transforming growth factor-beta1 is a negative modulator of adult neurogenesis. J Neuropathol Exp Neurol 65:358-370.

124. Kerever, A., J. Schnack, D. Vellinga, N. Ichikawa, C. Moon, E. Arikawa-Hirasawa, J. T. Efird, and F. Mercier. 2007. Novel extracellular matrix structures in the neural stem cell niche capture the neurogenic factor fibroblast growth factor 2 from the extracellular milieu. Stem Cells 25:2146-2157.

125. Roland, E. H., and A. Hill. 2003. Germinal matrix-intraventricular hemorrhage in the premature newborn: management and outcome. Neurol Clin 21:833-851, vi-vii.

126. Del Bigio, M. R., and Y. W. Zhang. 1998. Cell death, axonal damage, and cell birth in the immature rat brain following induction of hydrocephalus. Exp Neurol 154:157-169.

127. Tomita, S., M. Ueno, M. Sakamoto, Y. Kitahama, M. Ueki, N. Maekawa, H. Sakamoto, M. Gassmann, R. Kageyama, N. Ueda, F. J. Gonzalez, and Y. Takahama. 2003. Defective brain development in mice lacking the Hif-1alpha gene in neural cells. Mol Cell Biol 23:6739-6749.

128. Travis, M. A., B. Reizis, A. C. Melton, E. Masteller, Q. Tang, J. M. Proctor, Y. Wang, X. Bernstein, X. Huang, L. F. Reichardt, J. A. Bluestone, and D. Sheppard. 2007. Loss of integrin alpha(v)beta8 on dendritic cells causes autoimmunity and colitis in mice. Nature 449:361-365.

129. Lacy-Hulbert, A., A. M. Smith, H. Tissire, M. Barry, D. Crowley, R. T. Bronson, J. T. Roes, J. S. Savill, and R. O. Hynes. 2007. Ulcerative colitis and autoimmunity induced by loss of myeloid alphav integrins. Proc Natl Acad Sci U S A 104:15823-15828.

130. Colak, D., T. Mori, M. S. Brill, A. Pfeifer, S. Falk, C. Deng, R. Monteiro, C. Mummery, L. Sommer, and M. Gotz. 2008. Adult neurogenesis requires Smad4-mediated bone morphogenic protein signaling in stem cells. J Neurosci 28:434-446.

131. Garcia, C. M., D. C. Darland, L. J. Massingham, and P. A. D'Amore. 2004. Endothelial cell-astrocyte interactions and TGF beta are required for induction of blood-neural barrier properties. Brain Res Dev Brain Res 152:25-38.

132. Nguyen Ba-Charvet, K. T., K. Brose, V. Marillat, T. Kidd, C. S. Goodman, M. Tessier-Lavigne, C. Sotelo, and A. Chedotal. 1999. Slit2-Mediated chemorepulsion and collapse of developing forebrain axons. Neuron 22:463-473.

133. Bagri, A., O. Marin, A. S. Plump, J. Mak, S. J. Pleasure, J. L. Rubenstein, and M. Tessier-Lavigne. 2002. Slit proteins prevent midline crossing and determine the dorsoventral position of major axonal pathways in the mammalian forebrain. Neuron 33:233-248.

134. Kaneko, N., O. Marin, M. Koike, Y. Hirota, Y. Uchiyama, J. Y. Wu, Q. Lu, M. Tessier-Lavigne, A. Alvarez-Buylla, H. Okano, J. L. Rubenstein, and K. Sawamoto. New neurons clear the path of astrocytic processes for their rapid migration in the adult brain. Neuron 67:213-223.

135. Menn, B., J. M. Garcia-Verdugo, C. Yaschine, O. Gonzalez-Perez, D. Rowitch, and A. Alvarez-Buylla. 2006. Origin of oligodendrocytes in the subventricular zone of the adult brain. J Neurosci 26:7907-7918.

136. Doetsch, F., and A. Alvarez-Buylla. 1996. Network of tangential pathways for neuronal migration in adult mammalian brain. Proc Natl Acad Sci U S A 93:14895-14900.

137. Lois, C., and A. Alvarez-Buylla. 1994. Long-distance neuronal migration in the adult mammalian brain. Science 264:1145-1148.

138. Bolteus, A. J., and A. Bordey. 2004. GABA release and uptake regulate neuronal precursor migration in the postnatal subventricular zone. J Neurosci 24:7623-7631.

139. Emsley, J. G., and T. Hagg. 2003. alpha6beta1 integrin directs migration of neuronal precursors in adult mouse forebrain. Exp Neurol 183:273-285.

140. Murase, S., and A. F. Horwitz. 2002. Deleted in colorectal carcinoma and differentially expressed integrins mediate the directional migration of neural precursors in the rostral migratory stream. J Neurosci 22:3568-3579.

141. Snapyan, M., M. Lemasson, M. S. Brill, M. Blais, M. Massouh, J. Ninkovic, C. Gravel, F. Berthod, M. Gotz, P. A. Barker, A. Parent, and A. Saghatelyan. 2009. Vasculature guides migrating neuronal precursors in the adult mammalian forebrain via brain-derived neurotrophic factor signaling. J Neurosci 29:4172-4188.

142. Bovetti, S., Y. C. Hsieh, P. Bovolin, I. Perroteau, T. Kazunori, and A. C. Puche. 2007. Blood vessels form a scaffold for neuroblast migration in the adult olfactory bulb. J Neurosci 27:5976-5980.

143. Yamashita, T., M. Ninomiya, P. Hernandez Acosta, J. M. Garcia-Verdugo, T. Sunabori, M. Sakaguchi, K. Adachi, T. Kojima, Y. Hirota, T. Kawase, N. Araki, K. Abe, H. Okano, and K. Sawamoto. 2006. Subventricular zone-derived neuroblasts migrate and differentiate into mature neurons in the post-stroke adult striatum. J Neurosci 26:6627-6636.

144. Siegenthaler, J. A., and M. W. Miller. 2005. Transforming growth factor beta 1 promotes cell cycle exit through the cyclin-dependent kinase inhibitor p21 in the developing cerebral cortex. J Neurosci 25:8627-8636.

145. Brionne, T. C., I. Tesseur, E. Masliah, and T. Wyss-Coray. 2003. Loss of TGF-beta 1 leads to increased neuronal cell death and microgliosis in mouse brain. Neuron 40:1133-1145.

146. Newman, M. P., F. Feron, and A. Mackay-Sim. 2000. Growth factor regulation of neurogenesis in adult olfactory epithelium. Neuroscience 99:343-350.

147. Bravo, J. A., C. S. Parra, S. Arancibia, S. Andres, P. Morales, M. Herrera-Marschitz, L. Herrera, H. E. Lara, and J. L. Fiedler. 2006. Adrenalectomy promotes a permanent decrease of plasma corticoid levels and a transient increase of apoptosis and the expression of Transforming Growth Factor beta1 (TGF-beta1) in hippocampus: effect of a TGF-beta1 oligo-antisense. BMC Neurosci 7:40.

148. Miller, M. W. 2003. Expression of transforming growth factor-beta in developing rat cerebral cortex: effects of prenatal exposure to ethanol. J Comp Neurol 460:410-424.

149. Bottner, M., K. Krieglstein, and K. Unsicker. 2000. The transforming growth factor-betas: structure, signaling, and roles in nervous system development and functions. J Neurochem 75:2227-2240.

150. Yi, J. J., A. P. Barnes, R. Hand, F. Polleux, and M. D. Ehlers. TGF-beta signaling specifies axons during brain development. Cell 142:144-157.

151. Wang, Y., and A. J. Symes. Smad3 deficiency reduces neurogenesis in adult mice. J Mol Neurosci 41:383-396.

152. Mirzadeh, Z., F. Doetsch, K. Sawamoto, H. Wichterle, and A. Alvarez-Buylla. The subventricular zone en-face: wholemount staining and ependymal flow. J Vis Exp.

153. Shen, Q., Y. Wang, E. Kokovay, G. Lin, S. M. Chuang, S. K. Goderie, B. Roysam, and S. Temple. 2008. Adult SVZ stem cells lie in a vascular niche: a quantitative analysis of niche cell-cell interactions. Cell Stem Cell 3:289-300.

154. Mason, H. A., S. Ito, and G. Corfas. 2001. Extracellular signals that regulate the tangential migration of olfactory bulb neuronal precursors: inducers, inhibitors, and repellents. J Neurosci 21:7654-7663.

155. Nguyen-Ba-Charvet, K. T., N. Picard-Riera, M. Tessier-Lavigne, A. Baron-Van Evercooren, C. Sotelo, and A. Chedotal. 2004. Multiple roles for slits in the control of cell migration in the rostral migratory stream. J Neurosci 24:1497-1506.

156. Andrews, W., A. Liapi, C. Plachez, L. Camurri, J. Zhang, S. Mori, F. Murakami, J. G. Parnavelas, V. Sundaresan, and L. J. Richards. 2006. Robo1 regulates the development of major axon tracts and interneuron migration in the forebrain. Development 133:2243-2252.

157. Andrews, W. D., M. Barber, and J. G. Parnavelas. 2007. Slit-Robo interactions during cortical development. J Anat 211:188-198.

158. Okano, H., and K. Sawamoto. 2008. Neural stem cells: involvement in adult neurogenesis and CNS repair. Philos Trans R Soc Lond B Biol Sci 363:2111-2122.

159. Aboody, K. S., A. Brown, N. G. Rainov, K. A. Bower, S. Liu, W. Yang, J. E. Small, U. Herrlinger, V. Ourednik, P. M. Black, X. O. Breakefield, and E. Y. Snyder. 2000. Neural stem cells display extensive tropism for pathology in adult brain: evidence from intracranial gliomas. Proc Natl Acad Sci U S A 97:12846-12851.

160. Sun, Y., K. Jin, L. Xie, J. Childs, X. O. Mao, A. Logvinova, and D. A. Greenberg. 2003. VEGF-induced neuroprotection, neurogenesis, and angiogenesis after focal cerebral ischemia. J Clin Invest 111:1843-1851.

161. Taguchi, A., T. Soma, H. Tanaka, T. Kanda, H. Nishimura, H. Yoshikawa, Y. Tsukamoto, H. Iso, Y. Fujimori, D. M. Stern, H. Naritomi, and T. Matsuyama. 2004. Administration of CD34+ cells after stroke enhances neurogenesis via angiogenesis in a mouse model. J Clin Invest 114:330-338.

162. Curtis, M. A., B. Connor, and R. L. Faull. 2003. Neurogenesis in the diseased adult human brain--new therapeutic strategies for neurodegenerative diseases. Cell Cycle 2:428-430.

163. Seandel, M., J. M. Butler, H. Kobayashi, A. T. Hooper, I. A. White, F. Zhang, E. L. Vertes, M. Kobayashi, Y. Zhang, S. V. Shmelkov, N. R. Hackett, S. Rabbany, J. L. Boyer, and S. Rafii. 2008. Generation of a functional and durable vascular niche by the adenoviral E4ORF1 gene. Proc Natl Acad Sci U S A 105:19288-19293.

164. Shu, T., and L. J. Richards. 2001. Cortical axon guidance by the glial wedge during the development of the corpus callosum. J Neurosci 21:2749-2758.

Vitae

Aaron Kyle Mobley was born in Sedalia, Missouri on March 30, 1982, the son of Charles Eugene Mobley and Vicki Diane Mobley. Upon graduating from Caldwell High School in Caldwell, TX, Aaron enrolled at Texas A&M University in College Station, Texas. A Bachelor of Science degree in Biology was granted to him in December 2004. After receiving his degree, Aaron worked as a technician in the lab of Dr. George Davis at the Texas A&M University Health Science Center. In August 2005, Aaron enrolled in the Ph.D. program at the University of Texas Health Science Center at Houston Graduate School of Biomedical Sciences. In May 2006, Aaron joined the lab of Dr. Joseph McCarty at the University of Texas MD Anderson Cancer Center, where he examined the role of αvβ8 integrin in the neural-vascular adhesion and communication in the brain.